A Lamb-Shift Polarimeter for a Molecular Beam Source and Further Applications

Inaugural-Dissertation

zur Erlangung des Doktorgrades
der Mathematisch-Naturwissenschaftlichen Fakultät
der Heinrich-Heine-Universität Düsseldorf

vorgelegt von

Lukas Huxold
aus Köln

Köln, Mai 2021

aus dem Institut für Laser- und Plasmaphysik
der Heinrich-Heine-Universität Düsseldorf

Gedruckt mit der Genehmigung der
Mathematisch-Naturwissenschaftlichen Fakultät der
Heinrich-Heine-Universität Düsseldorf

Berichterstatter:

1. Prof. Dr. Markus Büscher

2. Prof. Dr. Axel Görlitz

Tag der mündlichen Prüfung: 02.12.2021
(bitte bei der Abgabe Ihrer Dissertation noch offenlassen)

Declaration of Authorship

I declare under oath that I have produced my inaugural dissertation

**"A Lamb-Shift Polarimeter for a Molecular
Beam Source and Further Applications"**

independently and without any undue assistance by third parties under consideration of the "Principles for the Safeguarding of Good Scientific Practice at Heinrich Heine University Düsseldorf".

Ich versichere an Eides Statt, dass die Dissertation

**„A Lamb-Shift Polarimeter for a Molecular
Beam Source and Further Applications"**

von mir selbstständig und ohne unzulässige fremde Hilfe unter Beachtung der „Grundsätze zur Sicherung guter wissenschaftlicher Praxis an der Heinrich-Heine-Universität Düsseldorf" erstellt worden ist.

_____   _____
        Lukas Huxold   Place, Date

Für meine wundervolle Ehefrau, Laura, die ich so sehr liebe
und unser Kind, das wir beide mit großer Freude erwarten.

Abstract

For decades, Lamb-shift polarimeters have been used successfully to measure the nuclear spin polarization of hydrogen and deuterium atomic beams as well as proton and deuteron beams. In particular, they are used for polarized atomic beam sources, which in turn are used as sources for accelerators or as internal gas targets in collision experiments. In previous experiments it has been shown that Lamb-shift polarimeters are also suitable for measuring the nuclear spin polarization of hydrogen and deuterium molecules and molecular ions. Since polarized atomic beam sources are largely exhausted in terms of their intensity and since nuclear spin-polarized molecules are advantageous in various applications, the development of a polarized molecular beam source was started at the Budker Institute for Nuclear Physics in Novosibirsk. It has already been demonstrated that with a prototype of such a source, parts of the molecular beam can be focused, which is an indirect proof of successful polarization of the beam.

In order to confirm this result through direct polarization measurements and to determine the degree of nuclear-spin polarization of the bound atoms, a Lamb-shift polarimeter was build at the research center Jülich, in a cooperation of the Peter-Grünberg Institute (PGI), the Institute for Nuclear Physics (IKP) and the Institute for Laser and Plasma-Physics (ILPP) of the Heinrich-Heine University Düsseldorf. After checking the components and optimizing the magnetic field homogeneity of the spin filter in Jülich, the Lamb-shift polarimeter was sent to Novosibirsk and connected to the source. The functionality of the polarimeter has been shown through first measurements with atomic beams.

In addition, a Lamb-shift polarimeter setup in Jülich was supplemented by a second spin filter and two coils to carry out experiments with Sona transitions in the $2S_{1/2}$ state of hydrogen atoms. The setup is capable of performing spectroscopy with quantum energies in the order of $10\,\text{neV}$.

Zusammenfassung

Lambshift-Polarimeter werden seit Jahrzehnten erfolgreich genutzt um die Kernspin-Polarisation sowohl von Wasserstoff- und Deuterium-Atomstrahlen, als auch von Proton- und Deuteronstrahlen zu messen. Insbesondere wird es bei polarisierten Atomstrahlquellen eingesetzt, die wiederum als Ionenquellen für Beschleuniger oder als interne Gastargets in Kollisionsexperimenten genutzt werden. In vorhergehenden Experimenten konnte gezeigt werden, dass sich Lambshift-Polarimeter auch für die Messung der Kernspin-Polarisation von Wasserstoff- und Deuterium-Molekülen und Molekülionen eignen. Da polarisierte Atomstrahlquellen hinsichtlich ihrer Intensität weitestgehend ausgereizt sind und da kernspin-polarisierte Moleküle für eine Reihe von Anwendungen vorteilhaft sind, wurde die Entwicklung einer polarisierten Molekülstrahlquelle am Budker Institut für Kernphysik in Nowosibirsk begonnen. Es konnte bereits gezeigt werden, dass mit einem Prototyp einer solchen Quelle Teile des Molekülstrahls fokussiert werden können, was ein indirekter Nachweis einer erfolgreichen Polarisierung des Strahls ist.

Um dieses Ergebnis durch eine direkte Polarisationsmessung zu bestätigen und den Grad der Kernspin-Polarisation der gebundenen Atome zu bestimmen wurde im Forschungszentrum Jülich – in Zusammenarbeit des Peter Grünberg Instituts (PGI), des Instituts für Kernphysik (IKP) und des Instituts für Laser- und Plasmaphysik (ILPP) der Heinrich-Heine Universität Düsseldorf – ein Lambshift-Polarimeter gebaut. Nach Überprüfung der Komponenten und Optimierung der Magnetfeldhomogenität des Spinfilters in Jülich wurde das Lambshift-Polarimeter nach Nowosibirsk versandt und mit der Quelle verbunden. Durch erste Messungen mit Atomstrahlen konnte die Funktionsfähigkeit des Polarimeters gezeigt werden.

Außerdem wurde ein Lambshift-Polarimeter Aufbau in Jülich um einen zweiten Spinfilter und zwei Spulen ergänzt um Experimente mit Sona-Übergängen im $2S_{1/2}$ Zustand von Wasserstoff-Atomen durchzuführen. Dabei zeigte sich, dass ein solcher Aufbau geeignet ist um Spektroskopie mit Quantenenergien in der Größenordnung von $10\,\mathrm{neV}$ durchzuführen.

Contents

Contents

List of Figures

List of Tables

1. Introduction

Nuclear spin-polarized hydrogen and deuterium atoms and ions are used in a variety of experiments around the world. Especially, experiments at particle accelerators with polarized projectiles and/or polarized targets are of great interest in experimental nuclear physics. By measuring polarization observables – such as the analyzing power (either beam or target are polarized), the polarization transfer coefficients (beam or target are polarized and the ejectiles' polarization is measured) or the spin-correlation parameters (beam and target are polarized) – additional independent observable quantities are obtained. With these observables, deeper insights into the physics of nuclear reactions are possible than with cross-sections alone [Alt+00]. To allow this kind of measurements sources and targets of nuclear spin polarized atoms, molecules and/or ions are required. Today, there are more than 20 sources for polarized atoms or ions, which follow three different working principles [Bel13]:

- Atomic Beam Sources (ABS), which utilize electron spin dependent beam separation (Stern-Gerlach) and radio-frequency transitions between hyperfine states (Breit-Rabi),

- Optically Pumped Polarized Ion Sources (OPPIS), which use optically pumped alkali atoms in charge exchange reactions with unpolarized protons (deuterons) to produce electron spin-polarized atoms and hyperfine transitions to convert the electron-spin polarization into nuclear-spin polarization, and

- Lamb-shift Sources, which utilize a spin filter for selective quenching of metastable atoms and ionization of remaining metastable atoms.

While Lamb-shift Sources are rarely used today, the underlying method is still used for the Lamb-shift polarimeter.
In order to tune an atomic beam source, it is helpful, if not mandatory, to be able to

measure the polarization of its beam – ideally without using an accelerator and nuclear reactions with known analyzing power. If an acceleration stage is ought to be avoided, the usual options are Breit-Rabi or Lamb-shift polarimeters.

With Breit-Rabi polarimeters, the principle of operation of atomic beam sources is reversed. Thus, they are able to determine the relative occupation numbers of all hyperfine states of hydrogen and deuterium atoms – usually of the ground states, but with a different tuning also metastable states could be measured. However, polarization measurements of atomic ions, molecules, or molecular ions are not possible unless the ions are converted into neutral atoms through a polarization conserving process (neutralization, dissociation, or neutralization and dissociation, respectively). Examples of the use of Breit-Rabi polarimeters are the HERMES [BH98], EDDA [HR00], and PAX [Ciu+11] experiments.

Lamb-shift polarimeters use the fact that the metastable $2S_{1/2}$ state is energetically separated from the short-lived $2P_{1/2}$ state by the Lamb-shift, but can be coupled with combinations of static electric, static magnetic and radio-frequency fields. This takes place in a spin filter which – in its original form – was first proposed by McKibben et al. [MLO68]. Under certain conditions only a single hyperfine substate of the metastable $2S_{1/2}$ state remains populated in the beam, which then can be detected. If the nuclear-spin polarization is conserved during the formation of the metastable atoms from ground state atoms, molecules, atomic ions and molecular ions, their polarization can be measured. Lamb-shift polarimeters have been successfully used at various facilities around the world. A few examples are TUNL in Durham [Lem+93], BNL in Brookhaven [Zel+02], and three at IKP in Jülich. Here, one is used for polarization measurements at the COSY ion source [Fel+13]. Another one was exploited at the internal target of ANKE [Eng02] and is now primarily used in recombination experiments [Eng+14; Eng+20b]. The third one is used in several experiments including a proof of concept for a new type of laser driven polarized ion source [Kan+19], hydrogen spectroscopy with a Sona transition [Eng+20a] (also part of this work), and studies of the production of metastable atoms from molecular ions (this work). With the Lamb-shift polarimeter at the ANKE atomic beam source the polarization of the direct beam can be measured within a few seconds. Over the years it proved to be a reliable device which is capable not only of measuring relative polarizations for the optimization of atomic beam sources, but also of measuring the absolute polarization with an uncertainty of about 1% [Eng+03].

Recently, the possibility of producing nuclear spin-polarized hydrogen molecules received more attention. Some reasons for this are:

- The beam intensity of atomic beam sources has largely been exhausted, but with polarized molecules the target density in storage cells could be increased further.

- HD, D_2 and DT molecules can be frozen out and, if their nuclear polarization is conserved, highly polarized solid targets with minimal amounts of impurities could be produced.

- The D_2 or DT ice could be used as fuel for polarized fusion.

- In combination with a stripping injection, molecular ion-beam sources could serve as sources of polarized protons and deuterons for accelerators which would be easier to handle, since the orientation of the polarization vector of molecular ions is not changed in Wienfilters or similar deflection devices in beam lines[1]. In addition, a H_2^+ (D_2^+) beam would provide twice the number of protons (deuterons) after the stripping for the same charge density before the injection.

- Polarized molecules could serve as targets for laser-driven acceleration of polarized protons and deuterons.

In Jülich the production of polarized molecules by recombination of polarized atoms has already been demonstrated [Eng+15]. A major advantage of this approach is that different combinations of nuclear spin orientations in HD molecules can be achieved [Eng+20b]. Due to the similarities of hydrogen and tritium the same should be possible for DT molecules. Since extended safety measures, however, are needed for the handling of tritium, this has not been done yet. The major disadvantage is that it does still rely on an atomic beam source and, therefore, a scaling for higher intensities is very limited. In Novosibirsk, a different approach is being pursued to generate beams of polarized molecules [Top+17]. Here the polarization of the molecules is achieved – directly – by separating the molecules by their nuclear spin orientations in a Stern-Gerlach-like setup. A dedicated molecular beam source, involving a superconducting magnet with 60 poles, has been proposed [Yur+17]. To prove the concept and gain experience, a prototype of such a molecular beam source was built by modifying an existing atomic beam source

---

[1]This is explained in Sect. 2.4.2.

comprising sextupole magnets. By measuring the flux of molecules into a compression tube behind the prototype, while the magnets are switched on and off, indications for a successful Stern-Gerlach separation of the molecules were observed [She+19]. In order to verify these findings and measure the polarization of the molecules directly, a suitable polarimeter is needed. Since a Lamb-shift polarimeter has been successfully used with polarized molecules in the recombination experiments mentioned earlier, a polarimeter of this kind was taken into consideration for these measurements. With an estimated detection limit of about 10^{11} molecules/s, polarization measurements of beams with about 10^{12} molecules/s should be challenging but possible with a Lamb-shift polarimeter. Building a Lamb-shift polarimeter in collaboration of the groups in Novosibirsk and Jülich (IKP and PGI) and in support of the Heinrich-Heine Universität Düsseldorf was proposed to and granted by the German Research Foundation (project no. BU 2227/1-1) and the Russian Science Foundation (project no.16-42-01009). In addition to its intended use for measurement with molecules, the Lamb-shift polarimeter can also be used with the atomic beam source.

Remarks:

- In the following the phrases "magnetic field" and "magnetic field strength" are used as synonyms for "magnetic flux density" for more convenient reading. Since the magnetic flux density vector $\boldsymbol{B}$ is related to the magnetic field strength vector $\boldsymbol{H}$ and the magnetization vector $\boldsymbol{M}$ via $\boldsymbol{B} = \mu_0(\boldsymbol{H} + \boldsymbol{M})$, and since $\boldsymbol{M} = 0$ in vacuum, the magnetic flux density and magnetic field strength are proportional, with the proportionality factor $\mu_0 \approx 4\pi \cdot 10^{-6} \, \frac{\mathrm{T\,m}}{\mathrm{A}}$ (vacuum permeability).

- Although only the isotopes hydrogen and deuterium are mentioned here, polarization measurements of tritium are possible, too. Since tritium also possesses a nuclear spin of $I = 1/2$, it behaves very similarly to hydrogen in a Lamb-shift polarimeter. The difference in mass is primarily only noticeable in the Wienfilter.

2. Theory

2.1. Atomic Theory

The concept of the atom is one of the most important and successful approaches to describe nature. Originally, atoms were considered as indivisible or "uncuttable" (Greek: ατομος) particles, of which everything is made of. From its first occurrences, in ancient Greece and India, the concept of atoms has changed drastically.

In the early 1800s, first evidences for the existence of atoms were found, for example by John Dalton with his "law of multiple proportions" and by Robert Brown, in the random motion of dust particles in water, called "Brownian motion" [Bro28]. In 1897, J. J. Thomson's discovery of the electron [Tho97], as part of the atom, gave rise to the first model to describe atoms, which, despite the fact they could no longer considered "uncuttable", kept their name. In this so called "plum pudding model", the atom is described as a sphere of positive charge, throughout which the light and negatively charged electrons are distributed. The next milestone was set by Ernest Rutherford in 1909 by proving the existence of a small but heavy nucleus, in which the positive charge of the atom is contained, and which is widely surrounded by the electrons [Rut11]. A few years later – 1913 – Niels Bohr proposed his famous model [Boh13], the first model, that included the quatization of energy and angular momentum and, thus, was the starting point of quantum-mechanical atomic theory. With the progress in quantum theory, also the atomic theory advanced. After Louis de Broglie postulated the wave-like character of particles [Bro24], Erwin Schrödinger published his famous equation [Sch26], which is the starting point for a new mathematical language of quantum mechanics. Unlike before, as in the theories of Bohr and Sommerfeld, electrons do no longer describe defined trajectories around the nucleus. Instead, only probabilities of finding electrons in a volume can be specified. In quantum mechanics, observables are described by operators. Since

then, quantum mechanics has been steadily improved. With Paul Dirac, relativity was integrated into the quantum mechanics of Schrödinger. Shortly afterwards, the development of quantum-field theories began with quantum electrodynamics. Very few theories agree so well with experimental measurements and have been tested as intensively as these quantum-field theories. With the new Sona transition spectroscopy, which will be discussed in Sects. 2.6 and 2.6, another tool is available to experimentally access the quantum electrodynamics corrections of the Breit-Rabi theory.

2.1.1. Quantum Mechanics of Angular Momenta

Generally, an angular momentum $\boldsymbol{L}$ is defined as the cross product of the distance to the rotational axis $\boldsymbol{r}$ and the linear momentum $\boldsymbol{p}$ of a point-like particle: $\boldsymbol{L} = \boldsymbol{r} \times \boldsymbol{p}$. As, in the language of quantum mechanics, all observable quantities are expressed by operators, the angular momentum operator $\hat{\boldsymbol{L}}$ is the cross product of position operator $\hat{\boldsymbol{r}}$ and momentum operator $\hat{\boldsymbol{p}}$. Using the canonical commutation relation for position and momentum operator, which is a representation of Heisenberg's uncertainty principle,

$$[\hat{r}_l, \hat{p}_m] = i\,\hbar\,\delta_{lm} \;\;,\tag{2.1}$$

the commutation relation for angular momenta result in

$$\left[\hat{L}_l, \hat{L}_m\right] = i\,\hbar\,\epsilon_{lmn}\hat{L}_n \;\;.\tag{2.2}$$

Consequently, only a single component of an angular momentum can be observed at the same time. For the magnitude $\hat{\boldsymbol{L}}^2 = \hat{L}_x^2 + \hat{L}_y^2 + \hat{L}_z^2$ one can calculate, that

$$\left[\hat{\boldsymbol{L}}^2, \hat{L}_x\right] = \left[\hat{\boldsymbol{L}}^2, \hat{L}_y\right] = \left[\hat{\boldsymbol{L}}^2, \hat{L}_z\right] = 0 \;\;,\tag{2.3}$$

meaning, that the magnitude $\hat{\boldsymbol{L}}^2$ and a single component (as conventional in literature the z-component $\hat{L}_z$ is used here) of a generic angular momentum can be defined

simultaneously. With the eigenfunctions $|l, m\rangle$, the relation holds:

$$\hat{\boldsymbol{L}}^2 |l, m\rangle = \hbar^2 \, l \, (l+1) |l, m\rangle \tag{2.4}$$

$$\hat{L}_z |l, m\rangle = \hbar \, m \, |l, m\rangle \quad . \tag{2.5}$$

By using ladder operators $\hat{L}_{\pm} = \hat{L}_x \pm i \, \hat{L}_y$, it can be derived, that l is always a multiple of $^1\!/_2$ and m can take values from $m = -l$ to $m = l$ in steps of one.

$$l = 0, 1, 2, ... \quad \text{or} \quad l = ^1\!/_2, ^3\!/_2, ... \tag{2.6}$$

$$m = -l, -(l-1), ... , l-1, l \tag{2.7}$$

The spin s (discussed in Sect. 2.1.2) can take integer (bosons) or half-integer (fermions) values. Protons, neutrons and electrons are all fermions with $s = ^1\!/_2$. In atoms, the quantum number for orbital angular momentum ℓ[1] can only take integer values. By j, the coupling of orbital angular momentum and electron spin – the total electron angular momentum – is denoted. The nuclear spin I is composed from the spins of protons and neutrons in the nucleus. And the coupling of nuclear spin and total angular electron momentum is denoted by F.

2.1.2. Stern Gerlach Experiment and the Spin

The Stern-Gerlach experiment is a famous experiments in modern physics. It was proposed by Otto Stern in 1921, conducted and published by him and Walther Gerlach in 1922 [GS22]. Essentially, the experiment comprised a silver evaporating furnace, a strong magnetic field, and a glass slide on which the silver atoms condensate after passing the magnet. By means of a small hole in the furnace and subsequent apertures, a beam of silver atoms is formed. The magnetic field, through which the beam is passing, is oriented perpendicular to the beam axis with a strong gradient in the direction, labeled as z-axis. A scheme of the setup is shown in Fig. 2.1. Since the potential V of a magnetic

---

[1]Note the different notation of a generic angular momentum number l and the specific orbital angular momentum number ℓ.
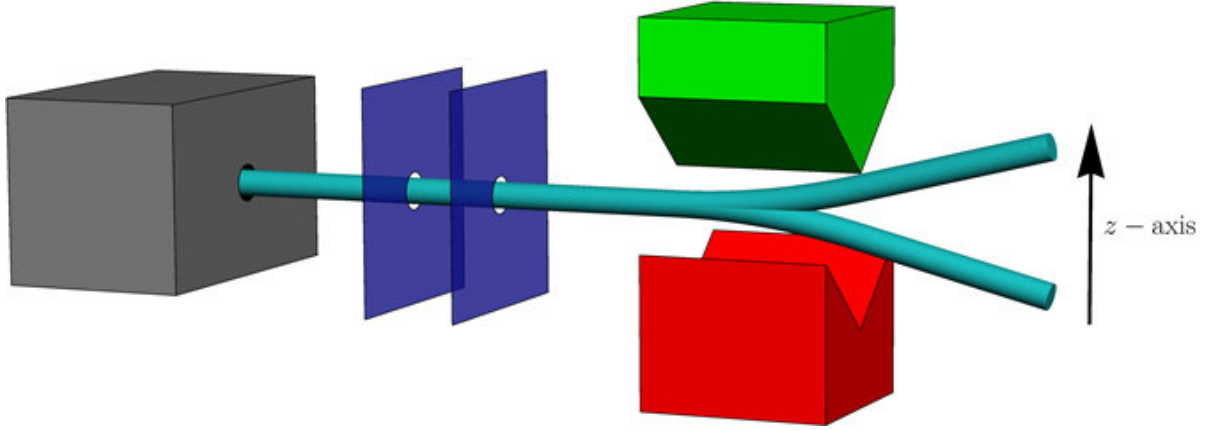
Figure 2.1.: Scheme of the Stern-Gerlach experiment setup.

moment $\boldsymbol{\mu}$ inside a magnetic field $\boldsymbol{B} = B(z)\,\hat{\boldsymbol{e}}_{\boldsymbol{z}}$ is given by

$$V = -\boldsymbol{\mu} \cdot \boldsymbol{B} \ , \tag{2.8}$$

a force $\boldsymbol{F}$ acts on the magnetic moment in the direction of the magnetic field gradient $\frac{\partial B_z}{\partial z}$, given by

$$\boldsymbol{F} = -\nabla\,V = \mu_z \frac{\partial B_z}{\partial z}\,\hat{\boldsymbol{e}}_{\boldsymbol{z}} \ . \tag{2.9}$$

In classical physics the projections of the magnetic moments to the z-axis μ_z would have continuous values, and thus, the silver atoms would be evenly distributed along the z-axis on the glass screen. Contrarily to this classical expectation a discrete separation into two parts was found. Although the experiment confirmed the quantization of angular momenta and a value of about one Bohr magneton ($\mu_B = \frac{e\,\hbar}{2\,m_e}$) for the magnetic moment of silver atoms, it was still a surprising outcome even for those, who supported the hypothesis of angular momentum quantization. According to the Bohr-Sommerfeld model, which was the most prevalent atomic model at that time, the only quantum number accountable for the magnetic moment of an atom was the magnetic quantum number, also called secondary orbital angular momentum number m_ℓ, with: $\mu_{\mathrm{BS\ atom}} = \mu_B\,m_\ell$. However, m_ℓ can only take values from $-\ell$ to ℓ, in steps of one (see Eq. (2.7)). As ℓ in turn can only take integer values from zero to $(n-1)$, only odd numbers $(2\ell + 1)$ of projection quantum numbers $\ell_z = m_\ell\,\hbar$ onto a quantization axis z were thought possible. In particular, for a silver atom it was assumed that, in the ground state, the angular

momenta of electrons would cancel for all but one electron, and that for this electron the angular momentum quantum number would be $\ell = 1$. Therefore, a splitting of the beam into three branches was expected.

The explanation for this observation was provided in 1925 by Samuel Goudsmit and George Uhlenbeck, by introducing the spin quantum number s for the electron, which can be regarded as an intrinsic angular momentum [UG26]. As it turned out later, the spin is a fundamental property of particles and can take values as multiple of $^1/_2$, while particles with integer spin ($s = 0, 1, 2, ...$) are called bosons, whereas particles with half-integer spin ($s = ^1/_2, ^3/_2, ...$) are referred to as fermions. Since the spin mathematically behaves like an angular momentum, projections onto a quantization axis are defined by the secondary spin quantum number m_s, which, analogous to the secondary orbital angular momentum quantum number m_ℓ, can take values from $-s$ to s in steps of one ($m_s = -s, -(s-1), ..., (s-1), s$). In case of fermions the number of possible m_s-states is even, and therefore, also the number of projections onto the quantization axis z, given by $s_z = m_s \hbar$, is even.

An electron, a fermion with spin $s = ^1/_2$, therefore, has two possible orientations in a magnetic field, which are also referred to as "spin up" ($m_s = +^1/_2$) and "spin down" ($m_s = -^1/_2$). Thus the two projection onto the quantization axis z are $s_z = \pm ^1/_2 \hbar$. The magnetic moment, caused by the spin of an electron is $\mu_s = -g_s \mu_B m_s$, with g_s being the g-factor for the electron spin. When now $\ell = 0$ is assigned to the ground state of silver atoms, the spin of the single unpaired electron is responsible for the magnetic moment of the silver atom and the beam will be separated into atoms with "spin up" and "spin down" in the gradient field. With $m_s = \pm ^1/_2$ and $g_s \approx 2$, the absolute value of the silver atom's magnetic moment is about one Bohr magneton.

2.1.3. Zeeman and Paschen-Back Effect

The potential energy of a magnetic moment in a magnetic field (Eq. (2.8)) contributes to the Hamiltonian of an atom, or in other words, the binding energy of any atomic state with a magnetic moment varies, if an external field is applied. Thus, the energy difference between states with different magnetic moments changes as function of the magnetic field. These changes to atomic spectra were first observed by Pieter Zeeman

in 1896 [Zee97]. In his honor the phenomenon is called Zeeman effect. A theoretical explanation were provided by Hendrik Antoon Lorentz two years later [Lor99]. In 1902, both were rewarded with a Nobel prize. In weak magnetic fields, where the spin-orbit interaction is stronger than their interaction with the external field, the additional energy can be expressed by:

$$\Delta E_{\text{Zee}} = \mu_{\text{B}} g_J m_j B_{\text{ext}} \ , \tag{2.10}$$

with g_J being the Landé g-factor, which for an atom with a single electron simplifies to $g_J \approx 1 \pm (2\ell + 1)^{-1}$. In stronger magnetic fields, the spin-orbit coupling breaks and the magnetic moments of spin and orbital angular momentum, get oriented separately in the external magnetic field. This effect is named Paschen-Back effect, after Friedrich Paschen and Ernst Back, who discovered it in 1921 [PB21]. The energy difference is given by:

$$\Delta E_{\text{PB}} = \mu_{\text{B}} \left(m_\ell + g_s m_s \right) B_{\text{ext}} \ , \tag{2.11}$$

with the electron g-factor $g_s \approx 2$.

2.1.4. Fine and Hyperfine Structure

Already in 1887 A.A. Michelson and E.W. Morley discovered a splitting of the red spectral line of hydrogen into two components [MM87]. This fine structure could first be explained by Sommerfeld, without the knowledge of the spin [Som16]. Since the discovery of the electron spin, the fine structure is explained by the interaction of the magnetic moments created by the spin and the orbital angular momentum of the electron. The potential energy of this interaction, combined with relativistic effects and the so called Darwin[2] term gives the energy splitting of the fine structure as

$$\Delta E_{n,j} = E_n \left(\frac{\alpha}{n} \right)^2 \left(\frac{n}{j + \frac{1}{2}} - \frac{3}{4} \right) \ , \tag{2.12}$$

---

[2]Named after Charles Galton Darwin, not to be mistaken with Charles Robert Darwin, his possibly more famous grandfather.

where $\alpha \approx 1/137$ is the fine-structure constant.

When the nuclear magnetic moment μ_N, created by the nuclear spin I, is considered, another energy splitting occurs, which is called hyperfine structure. In a simplified version it can be expressed as:

$$\Delta E_{\mathrm{HFS}} = \frac{1}{2}\hat{A}\left(F\left(F+1\right) - I\left(I+1\right) - J\left(J+1\right)\right) \ , \tag{2.13}$$

where $\hat{A}$ is a parameter, which has to be determined experimentally, and is called hyperfine-structure constant. The total spin F is composed of the total electron angular momentum J and nuclear spin I with $|I - J| \leqslant F \leqslant I + J$.

2.1.5. The Lamb-shift

Several measurements of the hydrogen and deuterium spectrum around the year 1937 showed another splitting ([Hou37], [Pas38], [Wil38]), which could not be explained by the Dirac theory alone. To confirm these findings Willis Lamb and Robert Retherford came up with a new method to measure the $2S_{1/2}$ and $2P_{1/2}$ levels of hydrogen and deuterium. By utilizing the Zeeman effect, they were able to observe microwave transitions of the $2S_{1/2}$ to the $2P_{1/2}$ and $2P_{3/2}$ states, at different magnetic field strength. By extrapolation of the obtained data to $B = 0$ they found an energy difference between the $2S_{1/2}$ and the $2P_{1/2}$ state of about $1000\,\mathrm{MHz}$, i.e., about $4 \cdot 10^{-6}\,\mathrm{eV}$ [LR47]. A scheme of their setup is shown in Fig. 2.2. After some improvements of the setup ([LR50], [LR51], [Lam52]), the energy difference, later called Lamb-shift, was undoubtedly confirmed. Lamb was rewarded with the Noble prize in 1955 for this finding. A theoretical explanation was provided by Richard Feynman in the framework of quantum electrodynamics (QED) [Fey48]. The potential for electrons close to the core is reduced by quantum fluctuations and increased by vacuum polarization. Since the effect of quantum fluctuations is larger than the effect of vacuum polarization, and electrons in S-shells ($\ell = 0$) have a higher probability to be close to the core, their binding energy is reduced more than electrons with $\ell > 0$. Today, the theoretical and experimental values of the Lamb-shift are in excellent agreement, and the theoretical value can be calculated with higher precision than it can be measured. In 1956, Feynman, Schwinger, and Tomonaga received a Nobel prize for their work on this matter.
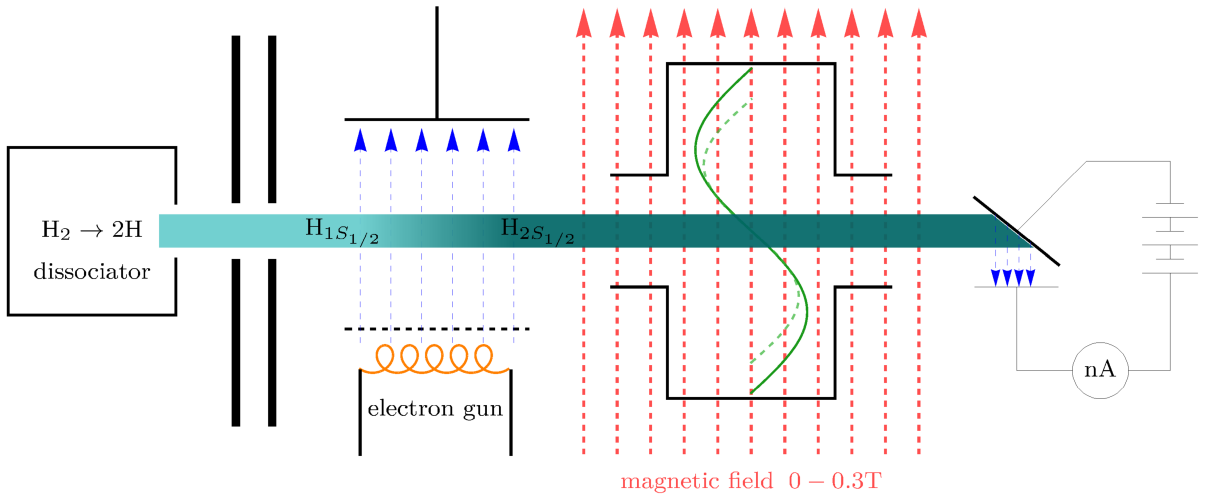
Figure 2.2.: Schematic drawing of the experimental setup of Lamb and Retherford. In an oven hydrogen gas is dissociated to form a beam of hydrogen atoms with thermal energies. By bombardment with electrons atoms are exited to the metastable $2S_{1/2}$ state. After passing through a radio frequency electromagnetic and a static magnetic field, metastable atoms are detected, by collecting electrons, released from a wolfram plate due to impact ionization. While the kinetic energy alone is not sufficient overcome the work function, the excitation energy of the metastable atoms contributes to cause a signal in the detector. If, for a given magnetic field, the frequency of the electromagnetic field matches the energy difference to either the $2P_{1/2}$ or the $2P_{3/2}$ state the amount of metastable atoms in the beam decreases.

2.1.6. Breit-Rabi Diagrams of Hydrogen and Deuterium Atoms

External magnetic fields do not only act on the magnetic moments, produced by electron spin and orbital angular momentum, but also on the magnetic moments created by the nuclear spin, which causes the hyperfine splitting. In a weak magnetic field, the nuclear spin I and the total electron angular momentum J couple to the total spin F. The nuclear spin of hydrogen is $I = \frac{1}{2}$, thus states with $J = \frac{1}{2}$ ($1S_{1/2}$, $2S_{1/2}$, $2P_{1/2}$,...) have a total spin of either $F = 1$ or $F = 0$. In case of $F = 1$, the projections m_F in an external magnetic field can be $m_F = -1, 0, 1$, while for $F = 0$ only $m_F = 0$ is possible. Like the m_j in Eq. (2.10) these projections have different energies in weak external magnetic fields and the state with $F = 0$ is separated from the three other states by the hyperfine energy. The nuclear spin of deuterium is $I = 1$, thus states with $J = \frac{1}{2}$ will have a total spin of either $F = \frac{3}{2}$ or $F = \frac{1}{2}$. Again each projection m_F has a different energy

in weak external fields and the states with $F = \frac{1}{2}$ and $F = \frac{3}{2}$ are separated by the hyperfine energy.

In stronger magnetic fields the coupling between I and J starts to break up, until both spins will align individually in the external field. States are now characterized by m_I and m_J, instead of F and m_F.

For hydrogen atoms with $I = \frac{1}{2}$ the four substates of any state with $J = \frac{1}{2}$ in an external magnetic field are

$$① \quad |F = 1, m_F = +1\rangle \stackrel{\wedge}{=} |m_I = +\tfrac{1}{2}, m_J = +\tfrac{1}{2}\rangle \tag{2.14a}$$

$$② \quad |1, 0\rangle \stackrel{\wedge}{=} \frac{1}{\sqrt{2}} \left(\sqrt{1 + a(B)}\, |-\tfrac{1}{2}, +\tfrac{1}{2}\rangle + \sqrt{1 - a(B)}\, |+\tfrac{1}{2}, -\tfrac{1}{2}\rangle \right) \tag{2.14b}$$

$$③ \quad |1, -1\rangle \stackrel{\wedge}{=} |-\tfrac{1}{2}, -\tfrac{1}{2}\rangle \tag{2.14c}$$

$$④ \quad |0, 0\rangle \stackrel{\wedge}{=} \frac{1}{\sqrt{2}} \left(\sqrt{1 - a(B)}\, |-\tfrac{1}{2}, +\tfrac{1}{2}\rangle - \sqrt{1 + a(B)}\, |+\tfrac{1}{2}, -\tfrac{1}{2}\rangle \right) \tag{2.14d}$$

where

$$a(B) = \frac{\frac{B}{B_\mathrm{c}}}{\sqrt{1 + \left(\frac{B}{B_\mathrm{c}}\right)^2}} \ . \tag{2.15}$$

With $I = 1$ for deuterium atoms, each $J = \frac{1}{2}$ state splits into six substates in an external magnetic field:

$$\text{①} \quad |F = \tfrac{3}{2}, m_F = +\tfrac{3}{2}\rangle \overset{\wedge}{=} |m_I = +1, m_J = +\tfrac{1}{2}\rangle \tag{2.16a}$$

$$\text{②} \quad |\tfrac{3}{2}, +\tfrac{1}{2}\rangle \overset{\wedge}{=} \frac{1}{\sqrt{2}} \left(\sqrt{1 + b(B)}\, |0, +\tfrac{1}{2}\rangle + \sqrt{1 - b(B)}\, |1, -\tfrac{1}{2}\rangle \right) \tag{2.16b}$$

$$\text{③} \quad |\tfrac{3}{2}, -\tfrac{1}{2}\rangle \overset{\wedge}{=} \frac{1}{\sqrt{2}} \left(\sqrt{1 - c(B)}\, |0, -\tfrac{1}{2}\rangle + \sqrt{1 + c(B)}\, |-1, +\tfrac{1}{2}\rangle \right) \tag{2.16c}$$

$$\text{④} \quad |\tfrac{3}{2}, -\tfrac{3}{2}\rangle \overset{\wedge}{=} |-1, -\tfrac{1}{2}\rangle \tag{2.16d}$$

$$\text{⑤} \quad |\tfrac{1}{2}, -\tfrac{1}{2}\rangle \overset{\wedge}{=} \frac{1}{\sqrt{2}} \left(\sqrt{1 + c(B)}\, |0, -\tfrac{1}{2}\rangle - \sqrt{1 - c(B)}\, |-1, +\tfrac{1}{2}\rangle \right) \tag{2.16e}$$

$$\text{⑥} \quad |\tfrac{1}{2}, +\tfrac{1}{2}\rangle \overset{\wedge}{=} \frac{1}{\sqrt{2}} \left(\sqrt{1 + b(B)}\, |1, -\tfrac{1}{2}\rangle - \sqrt{1 - b(B)}\, |0, +\tfrac{1}{2}\rangle \right) \tag{2.16f}$$

where

$$b(B) = \frac{\frac{B}{B_c} + \frac{1}{3}}{\sqrt{1 + \frac{2}{3}\frac{B}{B_c} + \left(\frac{B}{B_c}\right)^2}} \quad \text{and} \quad c(B) = \frac{\frac{B}{B_c} - \frac{1}{3}}{\sqrt{1 - \frac{2}{3}\frac{B}{B_c} + \left(\frac{B}{B_c}\right)^2}} \ . \tag{2.17}$$

The critical magnetic field $B_c \approx \frac{\Delta E_{\text{HFS}}}{2\mu_B}$ is a function of the hyperfine splitting ΔE_{HFS} given in Eq. (2.13). The hyperfine splitting of the ground states of hydrogen and deuterium are among the most precise measured quantities in spectroscopy. The hyperfine splitting of the $2S_{1/2}$ and $2P_{1/2}$ states can be calculated from the ground state splitting, with $\Delta E_{\text{HFS}}(2S_{1/2}) = \frac{1}{8}\Delta E_{\text{HFS}}(1S_{1/2})$ and $\Delta E_{\text{HFS}}(2P_{1/2}) = \frac{1}{24}\Delta E_{\text{HFS}}(1S_{1/2})$. In Tab. 2.1 the hyperfine splittings for $1S_{1/2}$, $2S_{1/2}$, and $2P_{1/2}$ of hydrogen and deuterium, and the critical magnetic fields are listed.

With the Breit-Rabi formula (Eq. (2.18)), named after Gregory Breit and Isidor Rabi, the energy of hyperfine states of hydrogen and deuterium atoms in an external magnetic field can be calculated [BR31]. It combines the Zeeman and the Paschen-Back effects, and is also valid in intermediate fields.

$$E(B) = -\frac{\Delta E_{\text{HFS}}}{2\,(2I + 1)} + m_F g_N \mu_N B \pm \frac{\Delta E_{\text{HFS}}}{2} \sqrt{1 + \frac{4m_F}{(2I + 1)}\frac{B}{B_c} + \left(\frac{B}{B_c}\right)^2} \ , \tag{2.18}$$

Table 2.1.: Hyperfine splittings of $1S_{1/2}$, $2S_{1/2}$, and $2P_{1/2}$ states of hydrogen and deuterium and the critical magnetic fields.

hydrogen atom	
$\Delta E_{\mathrm{HFS}}(1S_{1/2}) = 5.87 \cdot 10^{-6}\,\mathrm{eV}$	$B_{\mathrm{c}}(1S_{1/2}) = 50.7\,\mathrm{mT}$
$\Delta E_{\mathrm{HFS}}(2S_{1/2}) = 7.34 \cdot 10^{-7}\,\mathrm{eV}$	$B_{\mathrm{c}}(2S_{1/2}) = 6.34\,\mathrm{mT}$
$\Delta E_{\mathrm{HFS}}(2P_{1/2}) = 2.45 \cdot 10^{-7}\,\mathrm{eV}$	$B_{\mathrm{c}}(2P_{1/2}) = 2.11\,\mathrm{mT}$
deuterium atom	
$\Delta E_{\mathrm{HFS}}(1S_{1/2}) = 1.35 \cdot 10^{-6}\,\mathrm{eV}$	$B_{\mathrm{c}}(1S_{1/2}) = 11.7\,\mathrm{mT}$
$\Delta E_{\mathrm{HFS}}(2S_{1/2}) = 1.69 \cdot 10^{-7}\,\mathrm{eV}$	$B_{\mathrm{c}}(2S_{1/2}) = 1.46\,\mathrm{mT}$
$\Delta E_{\mathrm{HFS}}(2P_{1/2}) = 5.64 \cdot 10^{-8}\,\mathrm{eV}$	$B_{\mathrm{c}}(2P_{1/2}) = 0.49\,\mathrm{mT}$

where

$$g_N = \begin{cases} 5.586 & \text{g-factor for proton,} \\ 0.857 & \text{g-factor for deuteron,} \end{cases}$$

$$\mu_{\mathrm{N}} = \frac{e\hbar}{2m_{\mathrm{p}}} \approx \frac{1}{1836}\,\mu_{\mathrm{B}} \qquad \text{nuclear magneton, and}$$

$$B_{\mathrm{c}} = \frac{\Delta E_{\mathrm{HFS}}}{\widetilde{\mu}} \qquad \text{with}$$

$$\widetilde{\mu} = (g_{\mathrm{J}}\,\mu_{\mathrm{B}} - g_N\,\mu_{\mathrm{N}}) \approx 2\mu_{\mathrm{B}} \ .$$

Diagrams, in which the energy of different hyperfine states is plotted against the magnetic field, are commonly called Breit-Rabi diagrams. In Figs. 2.3 and 2.4 the Breit-Rabi diagram for $S_{1/2}$ states of hydrogen and deuterium are shown, respectively. The labeling of the Zeeman components correspond to those of Eqs. (2.14a) to (2.14d) and Eqs. (2.16a) to (2.16f).The calculations of Breit and Rabi have been improved by some QED corrections [MS06]. In Sect. 4.3 those QED-corrected Breit-Rabi calculations are used for the analysis of the measurements with the Sona coil setup.

Figure 2.3.: Breit-Rabi-Diagram for S$_{1/2}$ states of hydrogen with the magnetic field given in units of B_{c} and the energy in units of the hyperfine splitting ΔE_{HFS} (see Tab. 2.1).
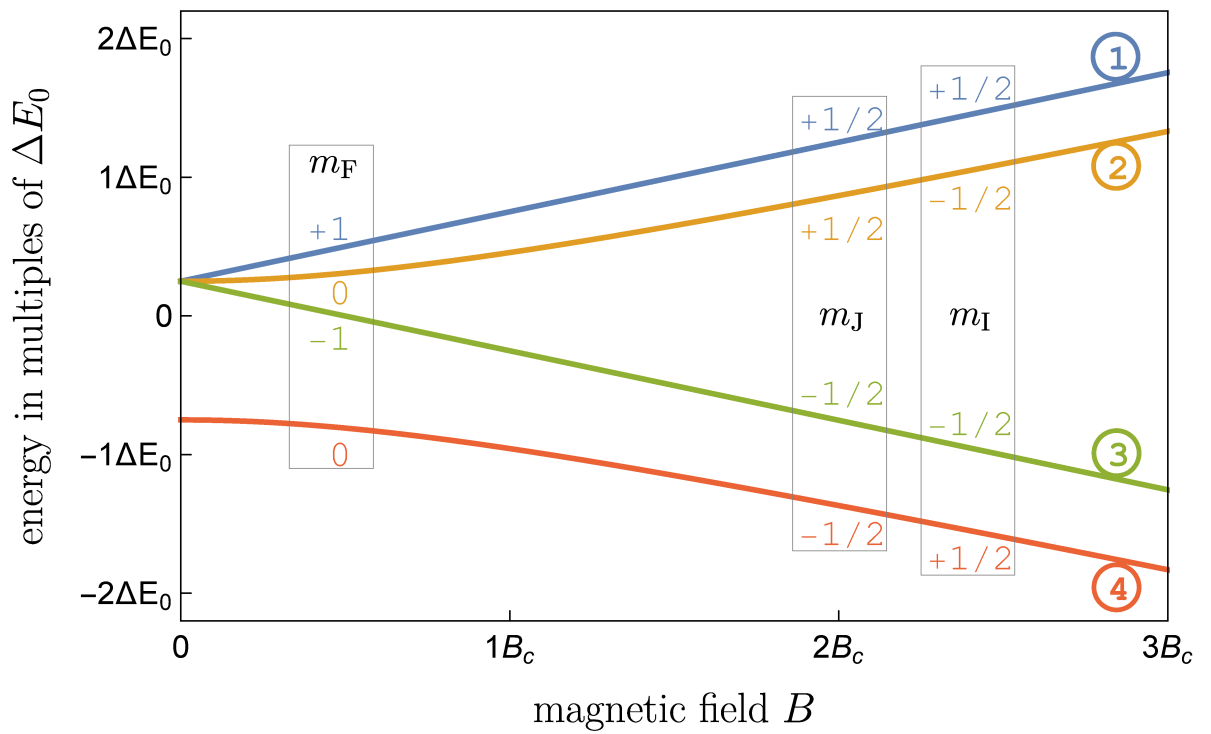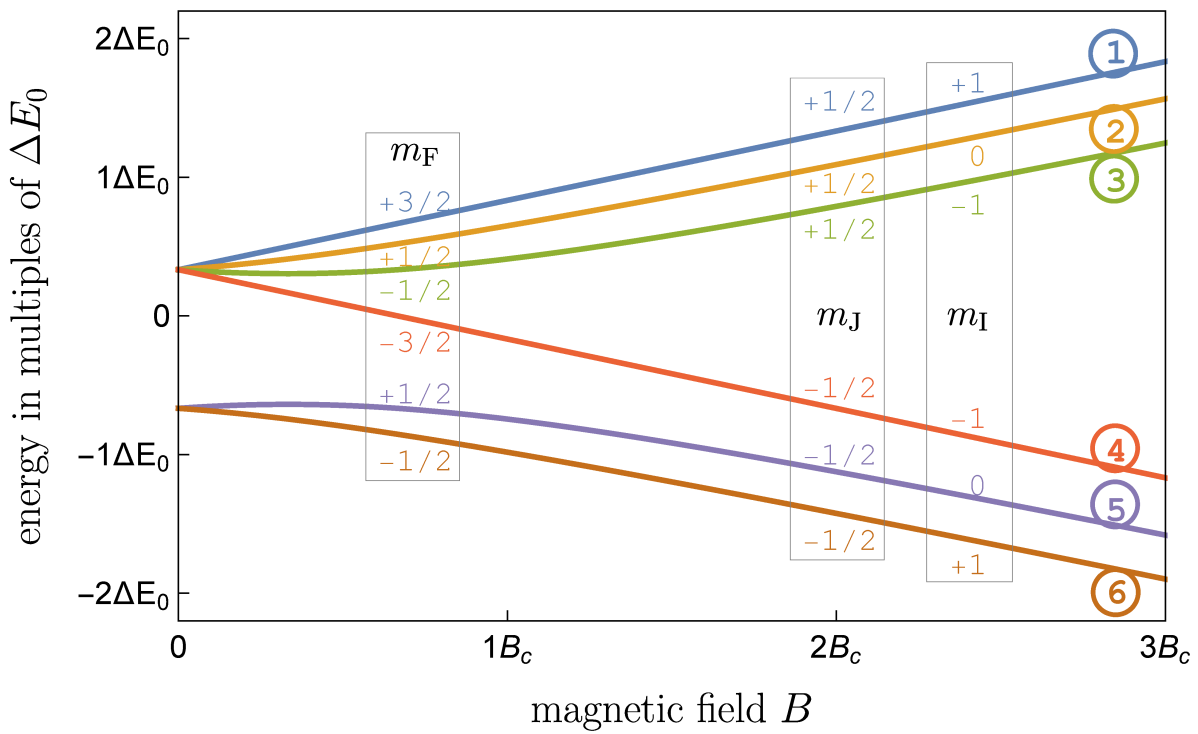
Figure 2.4.: Breit-Rabi-Diagram for $S_{1/2}$ states of deuterium with the magnetic field given in units of B_c and the energy in units of the hyperfine splitting ΔE_{HFS} (see Tab. 2.1).

2.1.7. Polarization

As discussed in Sect. 2.1.1, the angular momentum l of a particle has $2l + 1$ possible orientations in an external magnetic field, and the expectation value of $\hat{L}_z$ is $\langle \hat{L}_z \rangle = \langle l, m | \hat{L}_z | l, m \rangle = \hbar m$. In an ensemble of particles, of angular momentum l, states with different values of m may be occupied by the particles. To find the expectation value of an operator $\hat{A}$ of an ensemble, the density operator $\hat{\rho}$ is used, with

$$\hat{\rho} = \sum_{i=1}^{n} P_i \cdot |\psi_i\rangle \langle \psi_i| \quad , \tag{2.19}$$

with P_i being the probability of a particle to be in the ith state ($|\psi_i\rangle$) in the ensemble with n different possible states, and consequently $\sum_{i=1}^{n} P_i = 1$. The expectation value of the operator $\hat{A}$ then is

$$\langle \hat{A} \rangle = \mathrm{tr}(\hat{\rho} \hat{A}) \; . \tag{2.20}$$

Vector Polarization

The expectation value of $\hat{L}_z$ of an ensemble is the z-component of the polarization vector $\boldsymbol{p}$, with

$$p_z = \frac{1}{l\hbar} \langle \hat{L}_z \rangle = \frac{1}{l\hbar} \mathrm{tr}\left(\hat{\rho} \hat{L}_z\right) = \frac{1}{l\hbar} \mathrm{tr}\left(\sum_{i=1}^{2l+1} P_i \, |l, m_i\rangle \langle l, m_i| \, \hat{L}_z\right) \; . \tag{2.21}$$

The two remaining components p_x and p_y are defined analogously, but since only one component of an angular momentum vector can be measured simultaneously (see Eq. (2.2)), and we chose the z-axis to be the quantization axis, these are not relevant. Commonly p_z is called "vector polarization".

$\underline{l = {}^1\!/2 :}$

In the standard representation

$$
|{}^1\!/2, +{}^1\!/2\rangle_z = |\uparrow\rangle = \begin{pmatrix} 1 \\ 0 \end{pmatrix} \qquad |{}^1\!/2, -{}^1\!/2\rangle_z = |\downarrow\rangle = \begin{pmatrix} 0 \\ 1 \end{pmatrix} \,, \tag{2.22}
$$

the z-component of the angular momentum operator is expressed by $\hat{L}_z = \frac{\hbar}{2}\sigma_z$, with $\sigma_z = \sigma_3 = \begin{pmatrix} 1 & 0 \\ 0 & -1 \end{pmatrix}$ being the third Pauli matrix, and the density operator is

$$
\hat{\rho} = \sum_{i=1}^{2} P_i |l, m_i\rangle \langle l, m_i| = P_\uparrow \begin{pmatrix} 1 & 0 \\ 0 & 0 \end{pmatrix} + P_\downarrow \begin{pmatrix} 0 & 0 \\ 0 & 1 \end{pmatrix} = \begin{pmatrix} P_\uparrow & 0 \\ 0 & P_\downarrow \end{pmatrix} \,, \tag{2.23}
$$

with $P_\uparrow = \frac{N_\uparrow}{N_\uparrow + N_\downarrow}$ and $P_\downarrow = \frac{N_\downarrow}{N_\uparrow + N_\downarrow}$ being the probabilities of a particle to be in state $|\uparrow\rangle$ or $|\downarrow\rangle$, respectively. Thus,

$$
p_z = \frac{2}{\hbar} \operatorname{tr}\left(\hat{\rho}\hat{L}_z\right) = \operatorname{tr}(\hat{\rho}\sigma_z) = \operatorname{tr}\left(\begin{pmatrix} P_\uparrow & 0 \\ 0 & P_\downarrow \end{pmatrix} \cdot \begin{pmatrix} 1 & 0 \\ 0 & -1 \end{pmatrix} \right) = P_\uparrow - P_\downarrow \,. \tag{2.24}
$$

An ensemble of particles with $l = {}^1\!/2$ in an external magnetic field is sufficiently characterized by the vector polarization. The vector polarization can also be expressed by occupation numbers, with $p_z = \dfrac{N_\uparrow - N_\downarrow}{N_\uparrow + N_\downarrow}$.

$\underline{l = 1 :}$

For $l = 1$ the standard representation is

$$
|1, +1\rangle_z = \begin{pmatrix} 1 \\ 0 \\ 0 \end{pmatrix} \qquad |1, 0\rangle_z = \begin{pmatrix} 0 \\ 1 \\ 0 \end{pmatrix} \qquad |1, -1\rangle_z = \begin{pmatrix} 0 \\ 0 \\ 1 \end{pmatrix} \,, \tag{2.25}
$$

and the components of the angular momentum operator are

$$
\hat{L}_x = \frac{\hbar}{\sqrt{2}} \begin{pmatrix} 0 & 1 & 0 \\ 1 & 0 & 1 \\ 0 & 1 & 0 \end{pmatrix} \qquad \hat{L}_y = \frac{\hbar}{\sqrt{2}} \begin{pmatrix} 0 & -i & 0 \\ i & 0 & -i \\ 0 & i & 0 \end{pmatrix}
$$

$$
\hat{L}_z = \hbar \begin{pmatrix} 1 & 0 & 0 \\ 0 & 0 & 0 \\ 0 & 0 & -1 \end{pmatrix} \quad . \tag{2.26}
$$

The density operator, calculates to

$$
\hat{\rho} = \sum_{i=1}^{3} P_i \, |l, m_i\rangle \, \langle l, m_i| = \begin{pmatrix} P_+ & 0 & 0 \\ 0 & P_0 & 0 \\ 0 & 0 & P_- \end{pmatrix} \quad . \tag{2.27}
$$

And, consequently the vector polarization is

$$
p_z = \frac{1}{\hbar} \cdot \hbar \operatorname{tr} \left(\begin{pmatrix} P_+ & 0 & 0 \\ 0 & P_0 & 0 \\ 0 & 0 & P_- \end{pmatrix} \cdot \begin{pmatrix} 1 & 0 & 0 \\ 0 & 0 & 0 \\ 0 & 0 & -1 \end{pmatrix} \right) = P_+ - P_- \ , \tag{2.28}
$$

or in terms of occupation numbers: $p_z = \dfrac{N_+ - N_-}{N_+ + N_0 + N_-}$. Obviously, the vector polarization is not sufficient to fully characterize an arbitrary ensemble of particles with $l = 1$ in a magnetic field, since no statement about the probability P_0 of finding particles in state $|1, 0\rangle$ is made. This information can be completed by the tensor polarization.

Tensor Polarization

The three matrices in Eq. (2.26) and the identity matrix do not build a complete basis for the real vector space of 3×3 hermitian matrices. For this, 8 matrices (for instance the Gell-Mann matrices) plus the identity matrix are needed. However, five more matrices can be constructed from the three angular momentum component matrices to complete the set, with

$$\hat{L}_{ij} = \frac{3}{2\hbar} \left(\hat{L}_i \hat{L}_j + \hat{L}_j \hat{L}_i \right) - 2\hbar \delta_{ij} \cdot \mathbb{1} \; , \tag{2.29}$$

with $i, j = x, y, z$. In principle this would give 9 additional matrices, but since $\hat{L}_{ij} = \hat{L}_{ji}$ three can be discarded immediately. As it can easily be checked, the remaining six matrices are not linearly independent, thus another one can be excluded (e.g. $\hat{L}_{xx} = -\hat{L}_{yy} - \hat{L}_{zz}$). The polarization tensor of second order for $l = 1$ is calculated from the expectation value of these $\hat{L}_{ij}$ operators, with

$$p_{ij} = \frac{1}{\hbar} \langle \hat{L}_{ij} \rangle = \frac{1}{\hbar} \operatorname{tr} \left(\hat{\rho} \hat{L}_{ij} \right) \; . \tag{2.30}$$

With the density operator in the standard representation (see Eq. (2.27)), and

$$\hat{L}_{zz} = \hbar \begin{pmatrix} 1 & 0 & 0 \\ 0 & -2 & 0 \\ 0 & 0 & 1 \end{pmatrix} \; , \tag{2.31}$$

the "tensor polarization" – as p_{zz} is commonly called – is

$$p_{zz} = \frac{1}{\hbar} \cdot \hbar \operatorname{tr} \left(\begin{pmatrix} P_+ & 0 & 0 \\ 0 & P_0 & 0 \\ 0 & 0 & P_- \end{pmatrix} \cdot \begin{pmatrix} 1 & 0 & 0 \\ 0 & -2 & 0 \\ 0 & 0 & 1 \end{pmatrix} \right) = P_+ + P_- - 2P_0 \; , \tag{2.32}$$

or again in terms of occupation numbers: $p_{zz} = \dfrac{N_+ + N_- - 2N_0}{N_+ + N_- + N_0}$. By using both, the vector and the tensor polarization, an ensemble of particles with $l = 1$ can be fully

characterized.

In the following, the term "polarization" refers to the polarization of the nuclear spin I – if not explicitly stated otherwise. For hydrogen, with $I = \frac{1}{2}$, only the vector polarization exists, while for deuterium, with $I = 1$ both vector and tensor polarization can and need to be measured.

2.1.8. Polarization of $S_{1/2}$ Zeeman Components

From Eqs. (2.14a) and (2.14c), it is obvious, that the probabilities $P_\uparrow$ and $P_\downarrow$ for ensembles of hydrogen atoms in one of the $S_{1/2}$ Zeeman components $|F, m_F\rangle = |1, 1\rangle$ and $|1, -1\rangle$ are independent of the strength of the external magnetic field, since both are pure states:

$$\text{①} \; : \; P_\uparrow = 1 \quad P_\downarrow = 0 \; \Rightarrow \; p_z = 1 \tag{2.33}$$

$$\text{③} \; : \; P_\uparrow = 0 \quad P_\downarrow = 1 \; \Rightarrow \; p_z = -1 \; . \tag{2.34}$$

An ensemble of hydrogen atoms in one of the other two $S_{1/2}$ Zeeman components $|1, 0\rangle$ (Eq. (2.14b)) and $|0, 0\rangle$ (Eq. (2.14d)), however, has probabilities $P_\uparrow$ and $P_\downarrow$, which are functions of the magnetic field strength B:

$$\text{②} \; : \; P_\uparrow = \frac{1 - a(B)}{2} \quad P_\downarrow = \frac{1 + a(B)}{2} \; \Rightarrow \; p_z = -a(B) \tag{2.35}$$

$$\text{④} \; : \; P_\uparrow = \frac{1 + a(B)}{2} \quad P_\downarrow = \frac{1 - a(B)}{2} \; \Rightarrow \; p_z = a(B) \; . \tag{2.36}$$

A plot of the polarizations of hydrogen atoms in each of the four Zeeman components is shown in Fig. 2.5.

For deuterium the states $|F, m_F\rangle = |\frac{3}{2}, +\frac{3}{2}\rangle$ (Eq. (2.16a)) and $|\frac{3}{2}, -\frac{3}{2}\rangle$ (Eq. (2.16d)) are pure states, and thus their polarizations are constant:

$$\text{①} \; : \; P_+ = 1 \quad P_0 = 0 \quad P_- = 0 \; \Rightarrow \; p_z = 1 \quad p_{zz} = 0 \tag{2.37}$$

$$\text{④} \; : \; P_+ = 0 \quad P_0 = 0 \quad P_- = 1 \; \Rightarrow \; p_z = -1 \quad p_{zz} = 0 \; . \tag{2.38}$$

Figure 2.5.: Vector polarizations of the four $S_{1/2}$ hyperfine states of hydrogen with the magnetic field given in units of B_c (see Tab. 2.1).

The polarizations of the other four Zeeman components (see Eqs. (2.16b), (2.16c), (2.16e) and (2.16f)) are functions of the magnetic field strength B, with:

$$② \; : \; P_+ = \frac{1-b(B)}{2} \quad P_0 = \frac{1+b(B)}{2} \quad P_- = 0 \tag{2.39}$$

$$\Rightarrow \; p_z = \frac{1-b(B)}{2} \quad p_{zz} = -\frac{1+3b(B)}{2}$$

$$③ \; : \; P_+ = 0 \quad P_0 = \frac{1-c(B)}{2} \quad P_- = \frac{1+c(B)}{2} \tag{2.40}$$

$$\Rightarrow \; p_z = -\frac{1+c(B)}{2} \quad p_{zz} = \frac{3c(B)-1}{2}$$

⑤ : $P_+ = 0 \quad P_0 = \dfrac{1+c(B)}{2} \quad P_- = \dfrac{1-c(B)}{2}$ (2.41)

$$\Rightarrow \quad p_z = \frac{c(B)-1}{2} \quad p_{zz} = -\frac{1+3c(B)}{2}$$

⑥ : $P_+ = \dfrac{1+b(B)}{2} \quad P_0 = \dfrac{1-b(B)}{2} \quad P_- = 0$ (2.42)

$$\Rightarrow \quad p_z = \frac{1+b(B)}{2} \quad p_{zz} = \frac{3b(B)-1}{2}$$

Plots of the vector and tensor polarizations of deuterium atoms in each of the six Zeeman components are shown in Figs. 2.6 and 2.7, respectively.

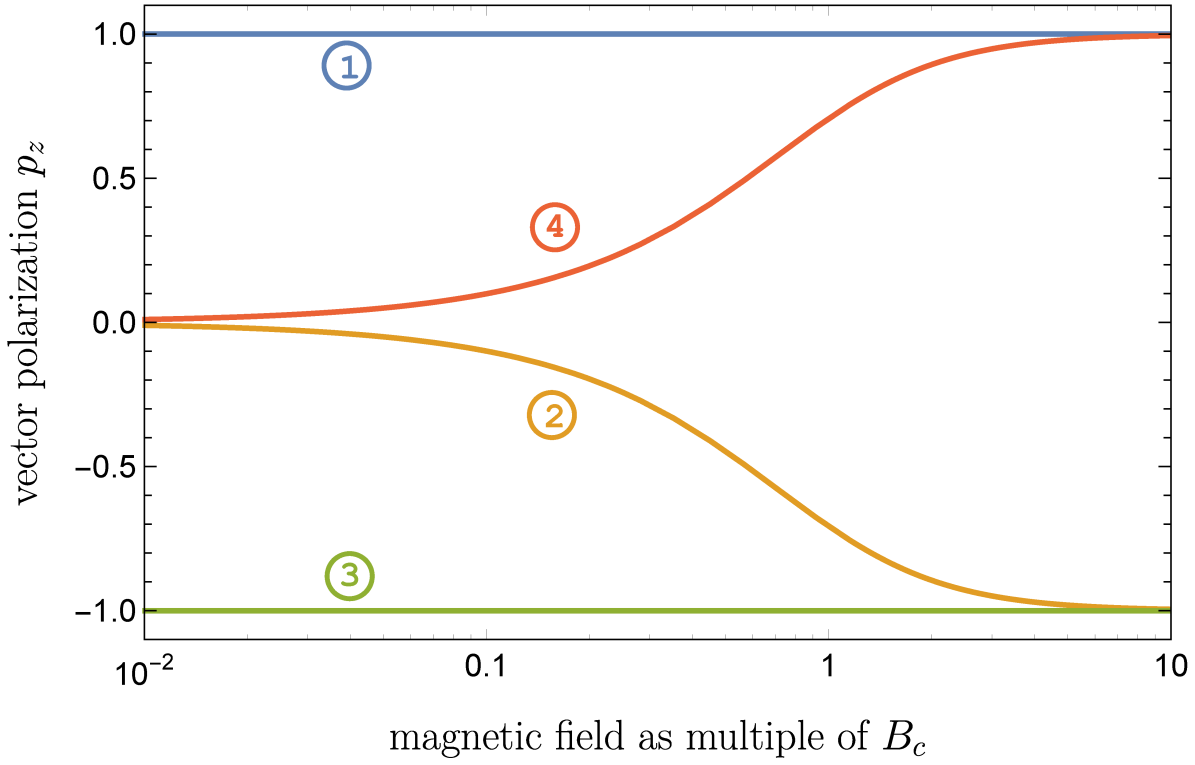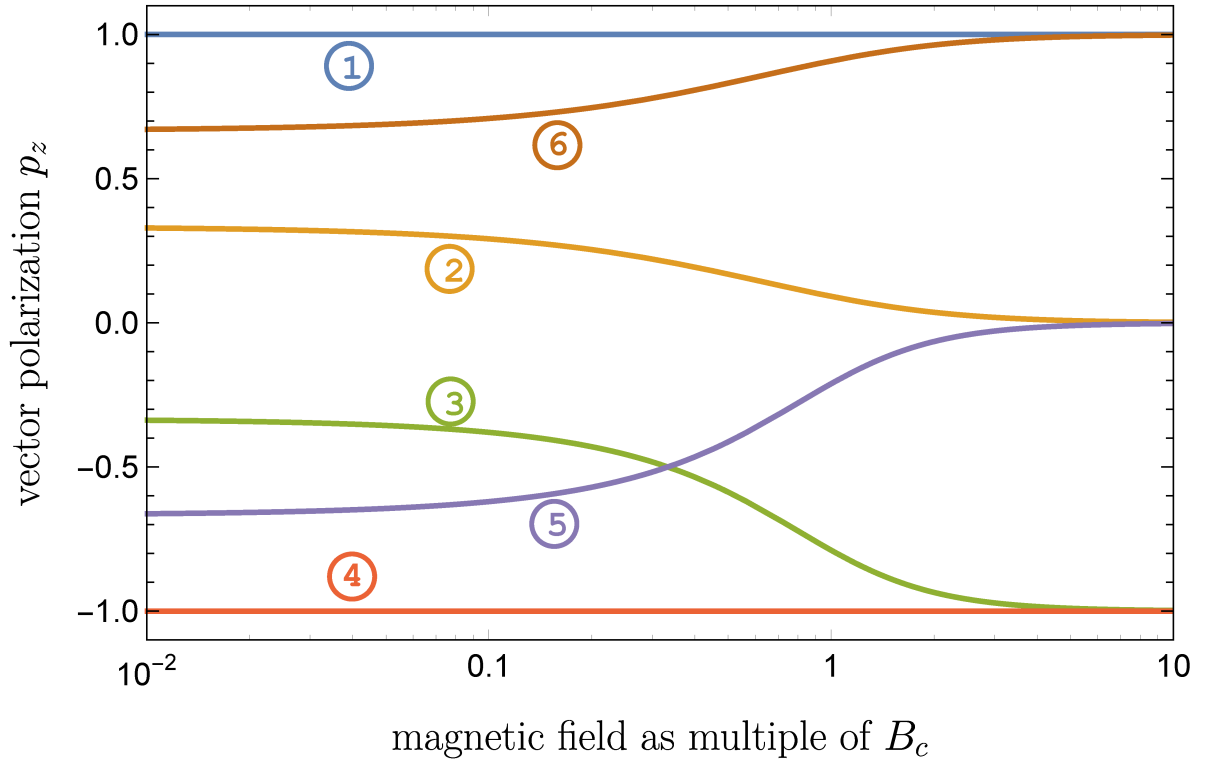

Figure 2.6.: Vector polarizations of the six $S_{1/2}$ hyperfine states of deuterium with the magnetic field given in units of B_c (see Tab. 2.1).
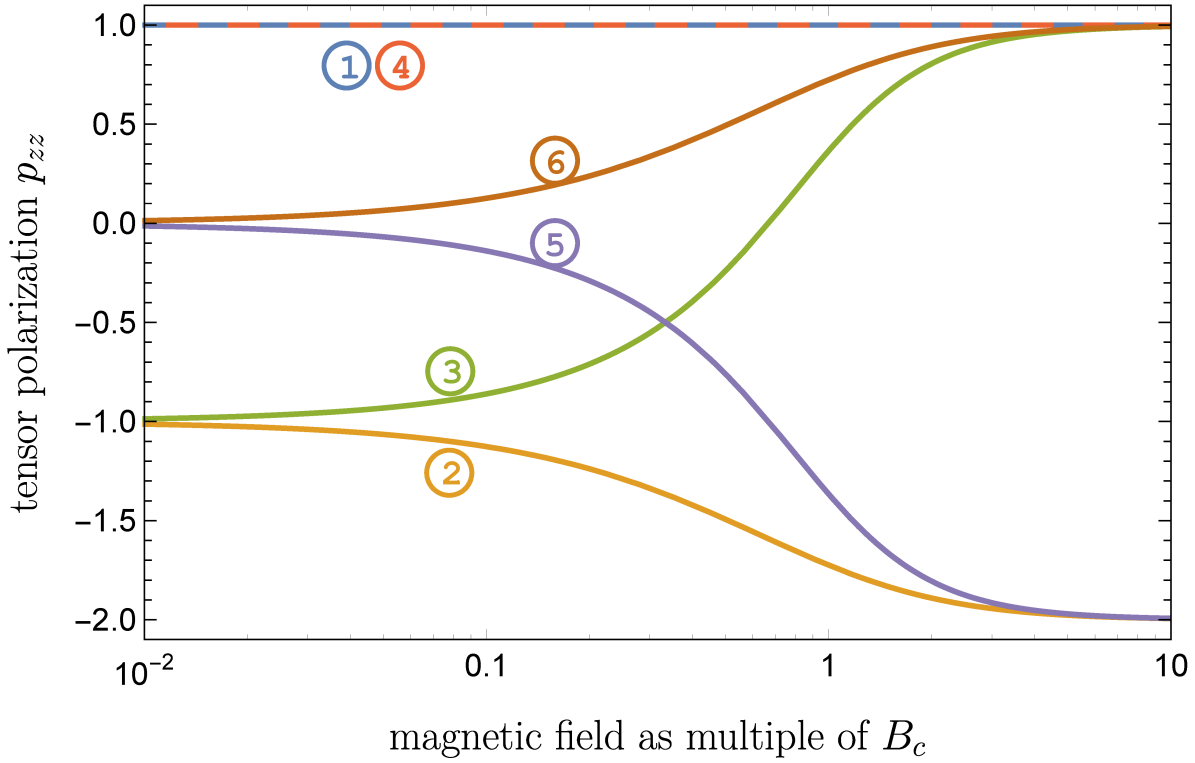
Figure 2.7.: Tensor polarizations of the six $S_{1/2}$ hyperfine states of deuterium with the magnetic field given in units of B_c (see Tab. 2.1).

2.1.9. The Metastable State $2S_{1/2}$ of Hydrogen and Deuterium

Due to the Lamb-shift, the $2S_{1/2}$ and the $2P_{1/2}$ states of hydrogen and deuterium are not degenerate, but separated by $4.375 \cdot 10^{-6}$ eV and $4.381 \cdot 10^{-6}$ eV, respectively [Sch+99]. The $m_J = -1/2$ states of $2S_{1/2}$ (called β states) and the $m_J = +1/2$ states of $2P_{1/2}$ (called e states) cross at a magnetic field of about 57 mT, as it is shown in Fig. 2.8 for hydrogen and in Fig. 2.9 for deuterium. The $m_J = +1/2$ states of $2S_{1/2}$ are called α states and the $m_J = -1/2$ states of $2P_{1/2}$ are called f states. For hydrogen, the β4 state and the e1 state intersect at about 53.8 mT and the intersection of β3 and e2 states is at about 60.5 mT. The intersections for deuterium are at 56.4 mT (β6 with e1), 57.4 mT (β5 with e2), and 58.4 mT (β4 with e3). At these magnetic fields, the energy differences between the states α1 and e1, α2 and e2, and α3 and e3 are all approximately $6.657 \cdot 10^{-6}$ eV or 1.6098 GHz $\cdot h$. This is utilized by the spin filter in the Lamb-shift polarimeter to select a single α state, which will be discussed in Sect. 2.4.4.
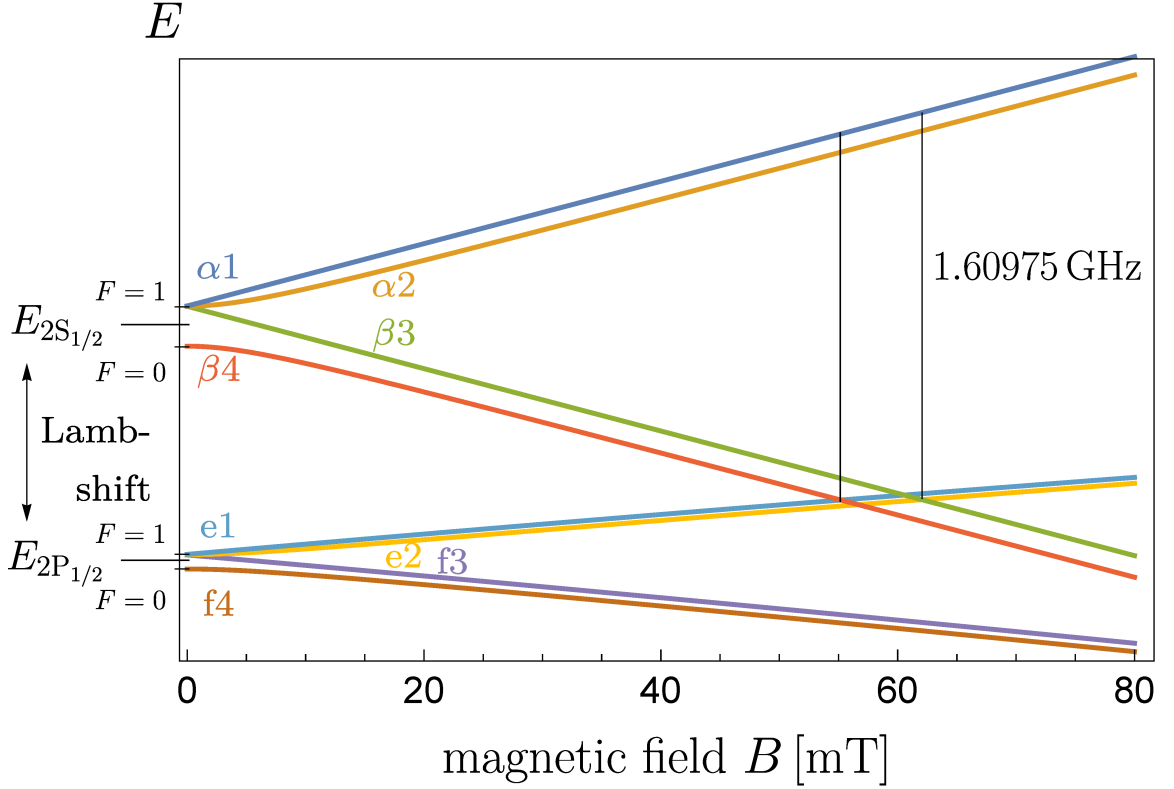
Figure 2.8.: Breit-Rabi diagram of the $2S_{1/2}$ and $2P_{1/2}$ states of hydrogen atoms.

Since electric dipole transitions between the $2P_{1/2}$ states and the ground state are allowed, their lifetime τ is rather short with $\tau_{2P_{1/2}} \approx 1.6 \cdot 10^{-9}\,\mathrm{s}$. The $2S_{1/2}$ states, however, have relatively long lifetimes, since electric dipole and quadrupole transitions to the ground state are forbidden. Without external fields, the lifetime of the $2S_{1/2}$ states is $\tau_{2S_{1/2}} \approx 0.14\,\mathrm{s}$. When an electric field is acting on the atom, Stark mixing with the $2P_{1/2}$ states occurs and the lifetime decreases. According to Lamb and Retherford the $2S_{1/2}$ lifetime in "moderate electric fields"[3] becomes [LR50]:

$$\widetilde{\tau}_{2S_{1/2}} = \tau_{2P_{1/2}} \frac{\hbar^2 \left(\omega^2 + \frac{1}{4}\gamma^2 \right)}{V_E^2} \quad , \tag{2.43}$$

where $\hbar\omega$ is the energy splitting of the $2S_{1/2}$ state and the $2P_{1/2}$ state, $\gamma = \frac{1}{\tau_{2P_{1/2}}}$, and V_E

---

[3]According to [Hae67] this is given as long as the lifetime $\widetilde{\tau}_{2S_{1/2}}$ of the perturbed $2S_{1/2}$ state is considerably shorter than the unperturbed lifetime $\tau_{2S_{1/2}}$ but considerably longer than the $2P_{1/2}$ lifetime.
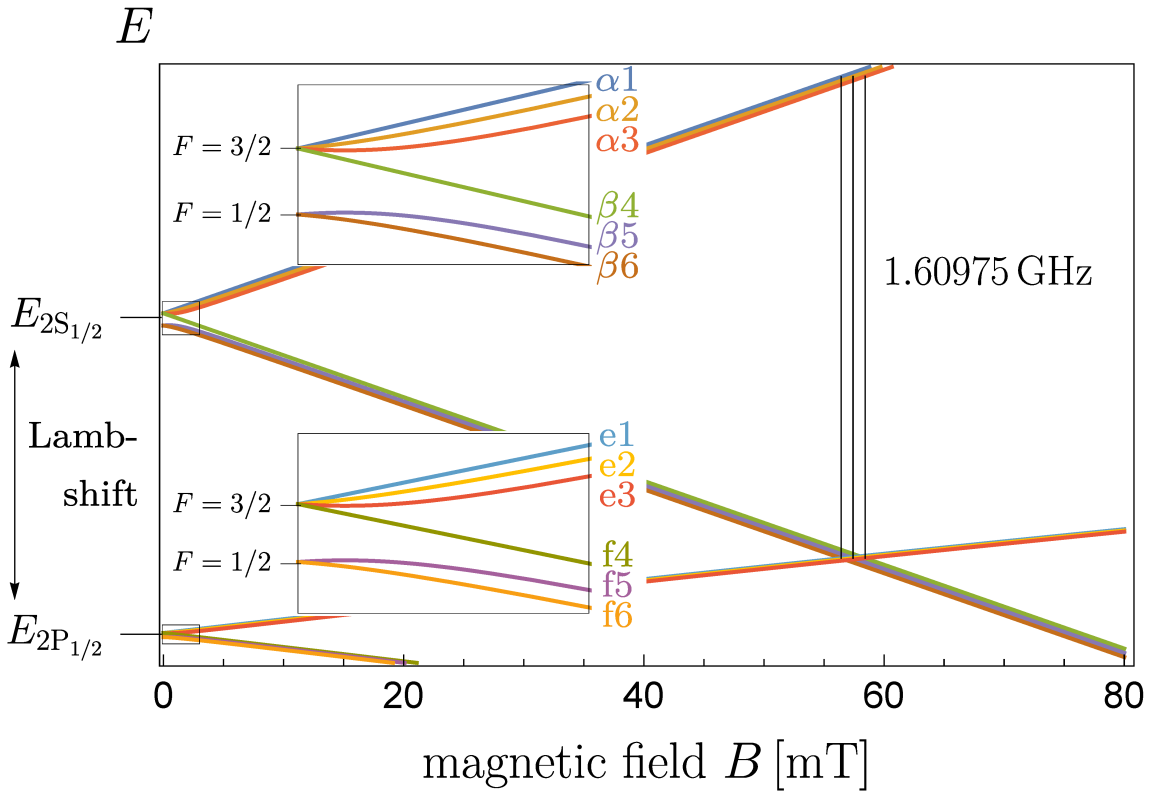
Figure 2.9.: Breit-Rabi diagram of the $2S_{1/2}$ and $2P_{1/2}$ states of deuterium atoms. The inserts show the splitting at low magnetic fields.

is the matrix element of the perturbing field. For electric fields strengths E, as they are applied in experimental setups like the Lamb-shift polarimeter, this can be approximated by [Hae67]:

$$\widetilde{\tau}_{2S_{1/2}} \approx \left(\frac{1.9\,\mathrm{V\,m^{-1}}}{E} \right)^2 \mathrm{s} \ . \tag{2.44}$$

A plot of this approximating function is shown in Fig. 2.10.

Since the Stark coupling of the $2S_{1/2}$ and $2P_{1/2}$ states depends on the energy splitting between the two states (see Eq. (2.43)) this approximation is only valid in absence of external magnetic fields, when the energy splitting is due to the Lamb-shift exclusively. In the presence of external magnetic fields the energy difference is influenced by the Zeeman effect, as discussed in Sect. 2.1.3 and shown in the Breit-Rabi diagrams in Figs. 2.8 and 2.9. Notably, the energy difference between the α and the e hyperfine

Table 2.2.: The magnetic fields, at the intersections of β and e states of hydrogen and deuterium in mT.

		hydrogen atom			deuterium atom		
		$2S_{1/2}$				$2S_{1/2}$	
		β4	β3		β6	β5	β4
	e1	53.8	59.1	e1	56.4	57.2	58.0
$2P_{1/2}$	e2	55.3	60.5	e2	56.7	57.4	58.2
				e3	56.9	57.7	58.4

states is increasing with the magnetic field, while the energy difference between the β and the e hyperfine states is decreasing towards the crossing points around $57\,\mathrm{mT}$ and is increasing again afterwards. According to Haeberli ([Hae67]) the lifetime of the α and β hyperfine states in the presence of an external magnetic field B as well as an external electric field E can be described as

$$\widetilde{\tau}_{2S_{1/2}} \approx \left(\frac{106.3\,\mathrm{V\,m^{-1}}}{E}\right)^2 \cdot \left(\left(574 \pm 10^4\frac{B}{\mathrm{T}}\right)^2 + 716\right)10^{-9}\,\mathrm{s}\ . \tag{2.45}$$

The lifetime of the α hyperfine states results with the plus sign and the lifetime of the β hyperfine states with the minus sign. The lifetime of the $2S_{1/2}$ states in dependence of the magnetic field at an electric field strength of $E = 10\,\mathrm{V\,cm^{-1}}$, a typical value in the spin filter, is shown in Fig. 2.11.

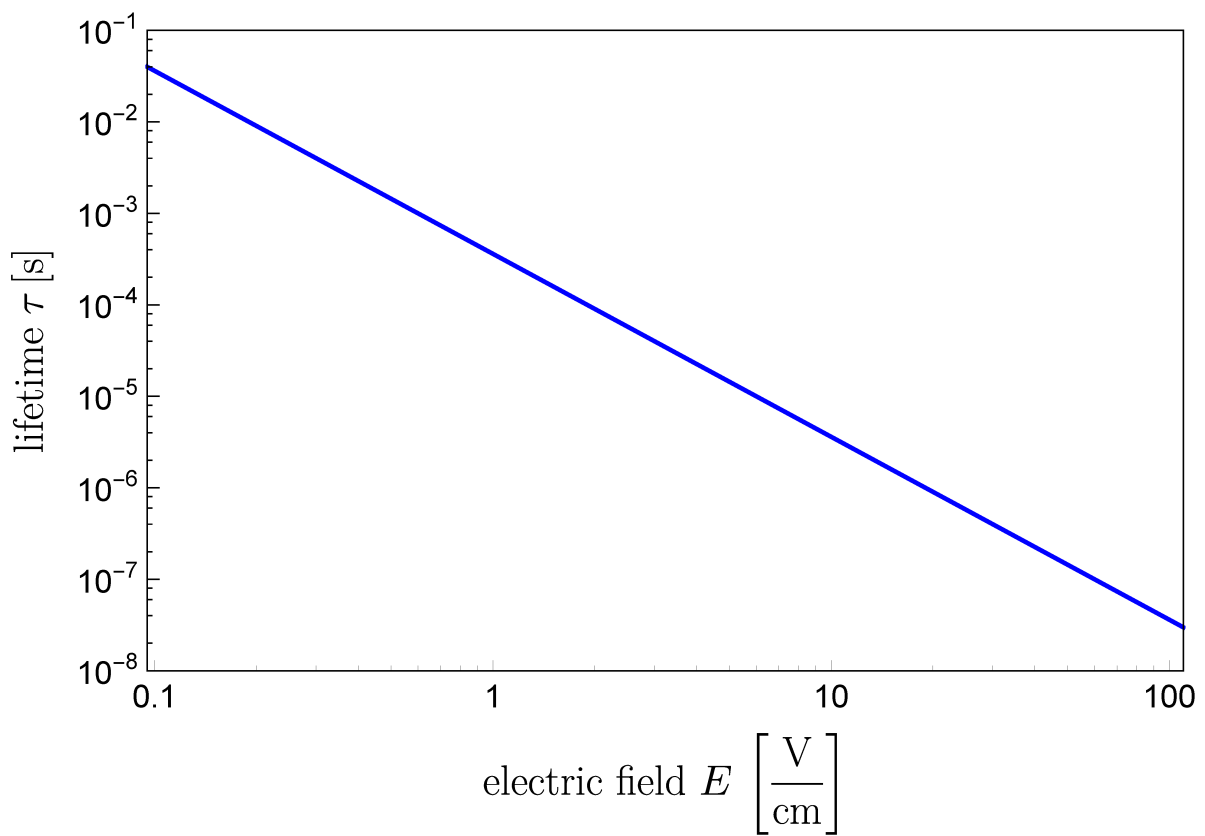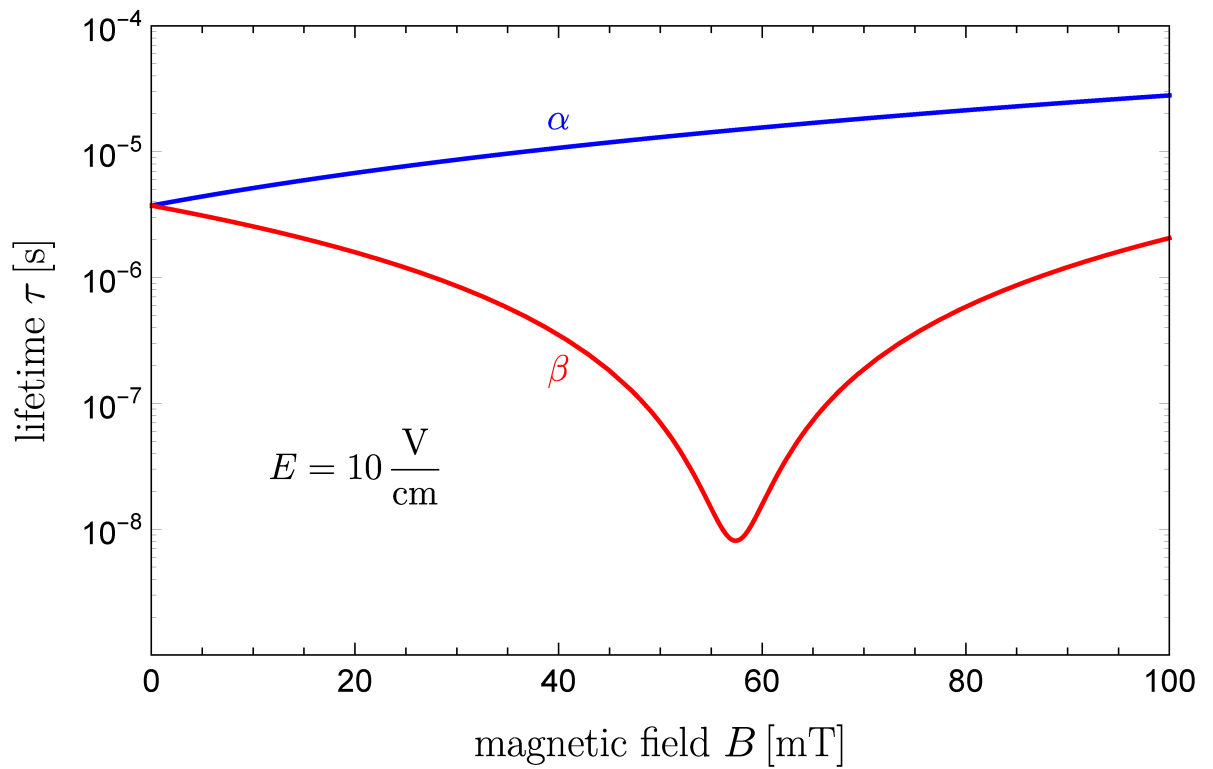Figure 2.10.: The lifetime τ of the $2S_{1/2}$ states as function of the electric field E.

Figure 2.11.: The lifetime τ of the 2S$_{1/2}$ states, plotted against the magnetic field B, in a constant electric field $E = 10\,\mathrm{V\,cm^{-1}}$. The reduction of the lifetime of the β-states by more than two orders of magnitude around $B = 57.5\,\mathrm{mT}$ is utilized in the Lamb-shift polarimeter.

2.2. Hydrogen and Deuterium Molecules

Due to the Pauli principle, hydrogen and deuterium molecules (H_2, D_2, and HD) are only stable, when the spins of the two electrons are anti-parallel. Therefore, the total electron angular momentum of the molecules is zero. Only the nuclear magnetic moments and molecular rotational magnetic moments can interact with external magnetic fields. The nuclear spins of the two atoms (I_1 and I_2, with the projections m_1 and m_2) couple to the total nuclear spin I, with $I = |I_1 - I_2|, ..., |I_1 + I_2 - 1|, |I_1 + I_2|$. As usual, the projection quantum number m_I of the total nuclear spin can take values from $-I$ to $+I$ in steps of one ($m_I = -I, -I + 1, ..., I - 1, I$). The molecular rotational angular momentum quantum number[4] J takes integer values starting with zero.

The dihydrogen molecule H_2 is a system of two identical fermions (protons) with nuclear spins $I_1 = I_2 = \frac{1}{2}$. Thus, the wave-function of the system has to be anti-symmetric under permutation of the particles. It follows that either the part of the wave-function that describes the rotation of the molecule is symmetric and the spin wave-function is anti-symmetric, or vice versa. The symmetry of the rotational wave-function is determined by the molecular rotational angular momentum J. With $J = 0, 2, ...$ the wave-function is symmetric and with $J = 1, 3, ...$ it is anti-symmetric. Dihydrogen molecules with symmetric spin wave-function and, therefore, odd J, are called ortho-hydrogen or o-H_2. Dihydrogen molecules with anti-symmetrical spin wave-function and, therefore, even J, are called para-hydrogen or p-H_2. Ortho-hydrogen is a triplet state with $I = 1$ and para-hydrogen is a singlet with $I = 0$. The different configurations of ortho- and para-hydrogen are shown in Tab. 2.3.

The dideuterium molecule D_2 is a system of two identical bosons (deuterons) with $I_1 = I_2 = 1$. The wave-function of this system has to be symmetric under permutation of the particles. Thus, either the rotational wave-function and the spin wave-function are both symmetric, or both are anti-symmetric. Dideuterium molecules with symmetric spin wave-function and, therefore, even J, are called ortho-deuterium or o-D_2. Dideuterium molecules with anti-symmetric spin wave-function and, therefore, odd J, are called para-deuterium or p-D_2. The ortho-deuterium consists of six states with $I = 0, 2$ and para-deuterium is a triplet with $I = 1$. The different configurations of ortho- and para- deuterium are summarized in Tab. 2.3.

---

[4]Although J is also used for the total electron angular momentum in a different context it is still used here to match the notation commonly used in literature.

Hydrogen-deuteride (HD) is a system of a fermion (proton) and a boson (deuteron). Since these are not identical, they can not be interchanged and, therefore, no symmetry restrictions have to be applied. Consequently, the six possible spin configurations in a weak magnetic field – summarized in Tab. 2.4 – can have any molecular rotational angular momentum quantum number J.

At room temperature H_2 consists of three parts o-H_2 and one part p-H_2 and D_2 is a mixture of two parts o-D_2 and one part p-D_2. Due to the rotational energy, states with $J > 0$ are exited states. E.g., the energy difference between the $J = 0$ and $J = 1$ states of hydrogen is about 15 meV. Therefore, at thermal equilibrium, the para state with $J = 0$ dominates, when the temperature approaches zero. For $J = 0$, as for all para-states, the only allowed spin configuration of the hydrogen molecule is $|0,0\rangle = \frac{1}{\sqrt{2}} \left(|\uparrow,\downarrow\rangle - |\downarrow,\uparrow\rangle \right)$ with a nuclear spin polarization $p_z = 0$. However, conversion rates between different molecular angular momentum states are fairly low at small pressures and low temperatures [Wig97]. Mean lifetimes are in the order of several hours. Therefore, a low temperature hydrogen beam can still contain considerable amounts of ortho-hydrogen, which can be polarized. For the formation of solid hydrogen, however, the molecules will eventually reach thermal equilibrium at very low temperatures (21.15 K at normal pressure), and will be mainly in the $J = 0$ state. Nuclear spin polarized H_2-ice is, therefore, not possible. The lowest molecular rotational state for D_2, however, is a ortho-state and its six substates can have different nuclear spin polarizations (see Tab. 2.3). Therefore, solid D_2 can be polarized. For a molecular beam source it might even be advantageous to increase the ratio of o-D_2, since this will also increase the relative amount of the $m_I = -2$ state which will be more focused than the $m_I = -1$ state. Since for HD the spin configurations and molecular rotational angular momentum are independent of each other, solid HD can contain all six nuclear spin states from Tab. 2.4.

Similar to atomic hydrogen and deuterium, where the magnetic moments of nuclear and electron spin interact with each other and external fields (see Sects. 2.1.3 and 2.1.6), the magnetic moments caused by the molecular rotation and the nuclear spin interact with each other and external magnetic fields. Calculations of these molecular Zeeman and Paschen-Back effects of H_2 and D_2 were performed in 1952 by Norman Ramsey [Ram52]. Breit-Rabi diagrams, for o-H_2 and p-D_2, both with $I = J = 1$, taken from this publication are shown in Figs. 2.12 and 2.13.

Table 2.3.: Nuclear spin configurations of ortho-/para- hydrogen and deuterium. The total nuclear spin I is composed from the nuclear spin of the two atoms: $I = |I_1 - I_2|, ..., |I_1 + I_2 - 1|, |I_1 + I_2|$. With the Clebsch-Gordan coefficients (e.g. [Zyl+20]) the states $|I, m_I\rangle$ can be expressed in the basis of individual spin projections $|m_1, m_2\rangle$. The vector polarization p_z and tensor polarization p_{zz} of an ensemble of molecules in each corresponding state are shown.

H_2: two fermions $\Rightarrow$ anti-symmetric total wave-function

---

<u>ortho-hydrogen</u>

			p_z	
$J = $ odd	$\Leftrightarrow$	triplet: $I = 1$, $m_I = \pm 1, 0$		
		$|1, +1\rangle = |\uparrow, \uparrow\rangle$	1	
		$|1, -1\rangle = |\downarrow, \downarrow\rangle$	-1	
		$|1, 0\rangle = \frac{1}{\sqrt{2}} \left(|\uparrow, \downarrow\rangle + |\downarrow, \uparrow\rangle \right)$	0	

<u>para-hydrogen</u>

			p_z	
$J = $ even	$\Leftrightarrow$	singlet: $I = 0$, $m_I = 0$		
		$|0, 0\rangle = \frac{1}{\sqrt{2}} \left(|\uparrow, \downarrow\rangle - |\downarrow, \uparrow\rangle \right)$	0	

D_2: two bosons $\Rightarrow$ symmetric total wave-function

<u>ortho-deuterium</u>

			p_z	p_{zz}
$J = $ even	$\Leftrightarrow$	sextet: $I = 0, 2$, $m_I = \pm 2, \pm 1, 0$		
		$|2, +2\rangle = |\uparrow, \uparrow\rangle$	1	1
		$|2, +1\rangle = \frac{1}{\sqrt{2}} \left(|\uparrow, \rightarrow\rangle + |\rightarrow, \uparrow\rangle \right)$	$1/2$	$-1/2$
		$|2, 0\rangle = \frac{1}{\sqrt{6}} \left(|\uparrow, \downarrow\rangle + 2 |\rightarrow, \rightarrow\rangle + |\downarrow, \uparrow\rangle \right)$	0	-1
		$|2, -1\rangle = \frac{1}{\sqrt{2}} \left(|\rightarrow, \downarrow\rangle + |\downarrow, \rightarrow\rangle \right)$	$-1/2$	$-1/2$
		$|2, -2\rangle = |\downarrow, \downarrow\rangle$	-1	1
		$|0, 0\rangle = \frac{1}{\sqrt{3}} \left(|\uparrow, \downarrow\rangle - |\rightarrow, \rightarrow\rangle + |\downarrow, \uparrow\rangle \right)$	0	0

<u>para-deuterium</u>

			p_z	p_{zz}
$J = $ odd	$\Leftrightarrow$	triplet: $I = 1$, $m_I = \pm 1, 0$		
		$|1, +1\rangle = \frac{1}{\sqrt{2}} \left(|\uparrow, \rightarrow\rangle - |\rightarrow, \uparrow\rangle \right)$	$1/2$	$-1/2$
		$|1, 0\rangle = \frac{1}{\sqrt{2}} \left(|\uparrow, \downarrow\rangle - |\downarrow, \uparrow\rangle \right)$	0	1
		$|1, -1\rangle = \frac{1}{\sqrt{2}} \left(|\rightarrow, \downarrow\rangle - |\downarrow, \rightarrow\rangle \right)$	$-1/2$	$-1/2$

Table 2.4.: Nuclear spin configurations of HD molecules. The vector polarization p_z^{p} of the protons, vector polarization p_z^{d} and tensor polarization p_{zz}^{d} of the deuterons of an ensemble of HD molecules in each corresponding state are shown.

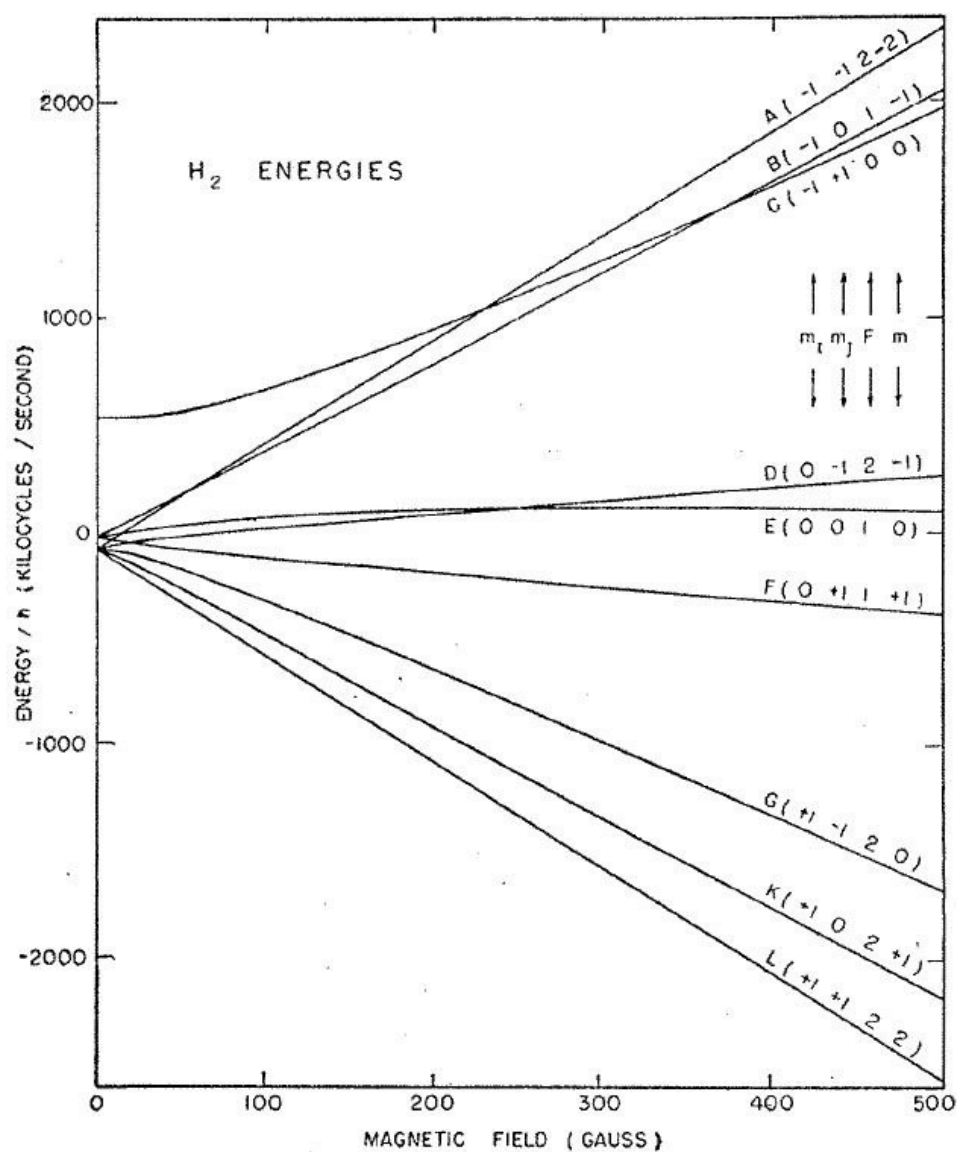| HD molecule			
$\lvert I, m_I \rangle = \lvert m_{\mathrm{p}}, m_{\mathrm{d}} \rangle$	p_z^{p}	p_z^{d}	p_{zz}^{d}
$\lvert 3/2, +3/2 \rangle = \lvert 1/2, 1 \rangle$	1	1	1
$\lvert 3/2, +1/2 \rangle = \lvert 1/2, 0 \rangle$	1	0	-2
$\lvert 3/2, -1/2 \rangle = \lvert -1/2, 0 \rangle$	-1	0	-2
$\lvert 3/2, -3/2 \rangle = \lvert -1/2, -1 \rangle$	-1	-1	1
$\lvert 1/2, +1/2 \rangle = \lvert -1/2, 1 \rangle$	-1	1	1
$\lvert 1/2, -1/2 \rangle = \lvert 1/2, -1 \rangle$	1	-1	1

Figure 2.12.: Breit-Rabi diagram of o-H_2 with $J = 1$ from [Ram52]. The nine states are characterized by $|m_I, m_J, F, m\rangle$, with the projection of the total nuclear spin m_I, the projection of the molecular rotational angular momentum m_J, the total spin F and its projection m ($= m_F$). For states with $m_I = -1$ (A, B, C) the energy increases, for states with $m_I = 1$ (G, K, L) the energy decreases, and for states with $m_I = 0$ (D, E, F) the energy stays almost constant with increasing magnetic fields.
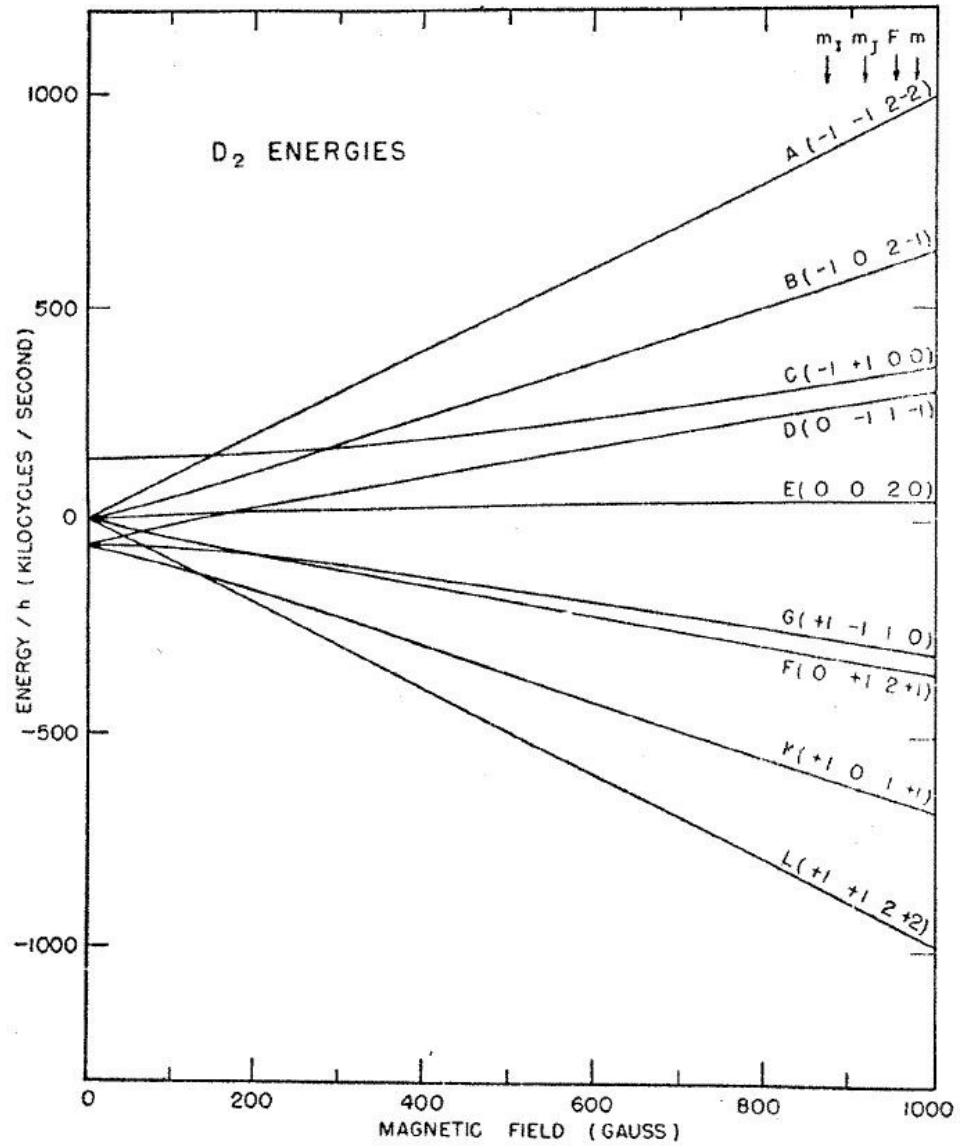
Figure 2.13.: Breit-Rabi diagram of p-D_2 with $J = 1$ from [Ram52]. For states with $m_I = -1$ (A, B, C) the energy increases, with increasing magnetic fields, however, much less compared with those of o-H_2 (see Fig. 2.12).

2.3. Atomic and Molecular Beam Sources

The principle of using an inhomogeneous magnetic field to separate a beam of silver atoms by the projection of the spin to the quantization axis, as in the Stern-Gerlach experiment (see Sect. 2.1.2), can also be applied to hydrogen atoms. A separation of an atomic hydrogen beam into two components with $m_J = \pm 1/2$ was first achieved by Phipps and Taylor [PT27]. When cylindrical multi-pole magnets are used instead of the dipole magnet in the original Stern Gerlach experiment, atoms are either focused onto the beam axis or defocused, depending on the orientation of their magnetic moment. By using quadropole magnets with relatively small magnetic fields, but high gradients at the beam axis, Clausnitzer et al. were able to focus (ground state) hydrogen atoms with $|m_I, m_J\rangle = |+1/2, +1/2\rangle$ and defocus $|-1/2, -1/2\rangle$, while the mixed substates of $1S_{1/2}$ (see Eqs. (2.14b) and (2.14d)) were almost undisturbed [CFS56]. By selecting the focused part of the beam they were able to produce a beam of nuclear spin polarized hydrogen atoms.

Typical modern atomic beam sources use a combination of two (sets of) sextupole magnets and transition units to produce beams of hydrogen and deuterium atoms in single Zeeman components or in combinations of two. The magnets eliminate states with $m_J = -1/2$ and the transition units in between and after both magnets can exchange the occupation numbers of different Zeeman components. Beam intensities of up to 10^{17} atoms/s are possible [Zel+05].

An atomic beam source, with superconducting sextupole magnets, is located in the BINP in Novosibirsk. The magnetic field gradient of this superconducting magnet is steeper than those of the usual permanent magnets in other atomic beam sources [Isa+98]. However, compared to sources with permanent sextupole magnets, the beam intensity is not increased, since the intensity is limited by intra-beam scattering. The intra-beam scattering is mainly caused by the focusing of atoms with two different velocities (within the Maxwell distribution), which occurs regardless of whether permanent or superconducting magnets are used.

A Stern-Gerlach experiment with hydrogen molecules was first performed by Robert Frisch and Otto Stern in 1933 [FS33]. To archive a separation of hydrogen and deuterium molecules (H_2, D_2, and HD) directly by their nuclear magnetic moments, which are three orders of magnitude smaller than the magnetic moments caused by the elec-

trons in hydrogen and deuterium atoms, these three orders of magnitude have to be compensated by a steeper gradient and/or a longer interaction time of the molecules with the magnetic field for which the length of the magnets can be increased and the velocity of the molecules be decreased. The dipole magnet they used had a length of 10 cm and provided a gradient $\frac{\partial B}{\partial z} = 22\,\mathrm{T\,cm^{-1}}$. The hydrogen was cooled to about 90 K and, thus, the most probable velocity for the hydrogen molecules was about $860\,\mathrm{m\,s^{-1}}$ (Maxwell-Boltzmann distribution). With this setup they were able to estimate the proton magneton μ_p between two and three nuclear magnetons μ_N (literature value today $\mu_\mathrm{p} = 2.79284734463(82)\,\mu_\mathrm{N}$ [NIS94]). However, the beam intensities presumably were rather low (absolute intensity and polarization measurements are not published in the paper). For an intense molecular beam source with high polarization this setup is not suited.

A molecular beam source intended to provide polarized protons for accelerators was proposed in 1958 by Garwin [Gar58]. The proposal was based on a conventional Stern-Gerlach separation with a dipole magnet. The design aimed for $2 \cdot 10^{13}$ polarized molecules per second, or $2 \cdot 10^{12}$ polarized protons after an ionizer. The proposal was never turned into reality.

With the unique feature of superconducting magnets the cryogenic atomic beam source at the BINP offers the opportunity to investigate a molecular beam source based on multi-pole magnets [She+98]. In Fig. 2.14 a scheme of the prototype molecular beam source in Novosibirsk is shown. It is based on a modification of the cryogenic atomic
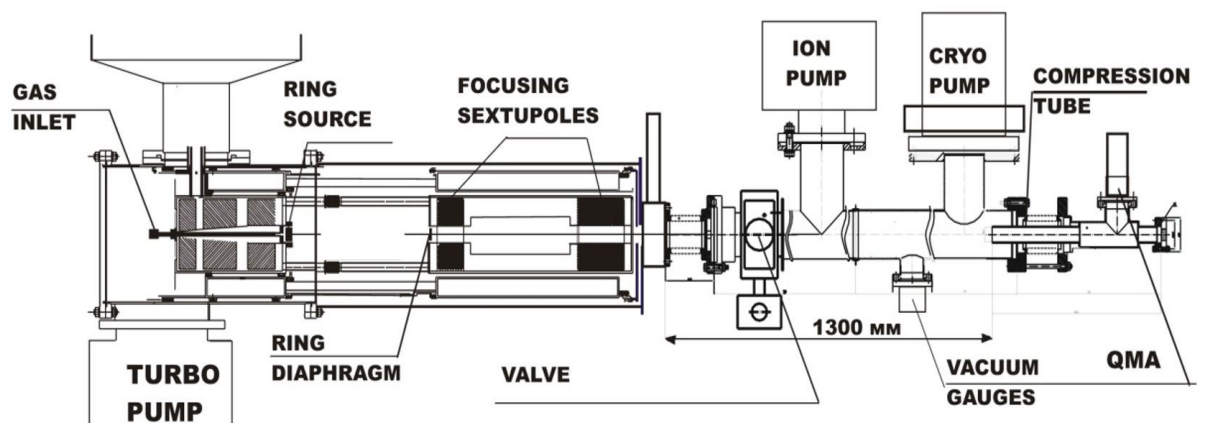

Figure 2.14.: Schematic drawing of the prototype molecular beam source in Novosibirsk [She+19].

beam source. The first set of superconducting magnets of the atomic beam source are cooled, but not operated. With them, the unpolarized hydrogen/deuterium gas is cooled, before it passes through a ring shaped nozzle (outer diameter of 41.9 mm and inner diameter of 41.7 mm), which is cooled to adjustable temperatures ($\geqslant 6.5$ K). The resulting ring shaped beam of hydrogen molecules is collimated by a ring shaped aperture (outer diameter of 42 mm and inner diameter of 40 mm) just before the second set of sextupoles of the atomic beam source. This way, the hydrogen molecules are directed to pass close to the poles of the superconducting magnets, where the fields have their maximum gradients. This causes a separation of the beam by the projection of the nuclear spin (m_I) as discussed before. The magnets are cooled with liquid helium which – under reduced pressure – reaches temperatures as low as 2.5 K in the setup. With surfaces this cold scattered or defocused hydrogen molecules are condensed and removed from the beam. In a first step the focusing ability of the molecular beam source was verified with a compression tube. It is positioned at an ideal distance – determined by Monte Carlo simulations ([She+19]) – of 135 cm behind the end of the magnets. With a diameter of 30 mm it is smaller than those of nozzle and aperture. Therefore, molecules, which are not deflected ($m_I = 0$) or defocused ($m_I = 1$) by the gradient field, will miss the compression tube, while molecules with $m_I = -1$ will be directed into the compression tube. In Fig. 2.15 – taken from [She+19] – the pressure in the compression tube and the current through the superconducting magnets are shown. The increase of the pressure in the compression tube whenever the magnets are switched on is evidence for a deflection of parts of the beam due to the magnetic field gradient. With this prototype molecular beam source beam intensities of $3 \cdot 10^{12}$ (presumably) polarized molecules per second have been achieved [Top+17]. To measure the polarization of this beam a Lamb-shift polarimeter was build within the framework of this thesis.

Based on the experiences with this prototype molecular beam source a completely new source exclusively for polarized molecules can be developed. A design of a tapered 60-pole superconducting magnet with an inner diameter of 400 mm at the entrance and 370 mm at the exit and a length of 2 m has been proposed in [Yur+17]. The tapered design aims for a more efficient removal of the hydrogen molecules in states with $m_I = 0, +1$ (deuterium molecules in states with $m_I = 0, +1, +2$). From Monte Carlo simulations an increase in beam intensity by four orders of magnitude compared to the prototype molecular beam source discussed above is expected for hydrogen, and an in-
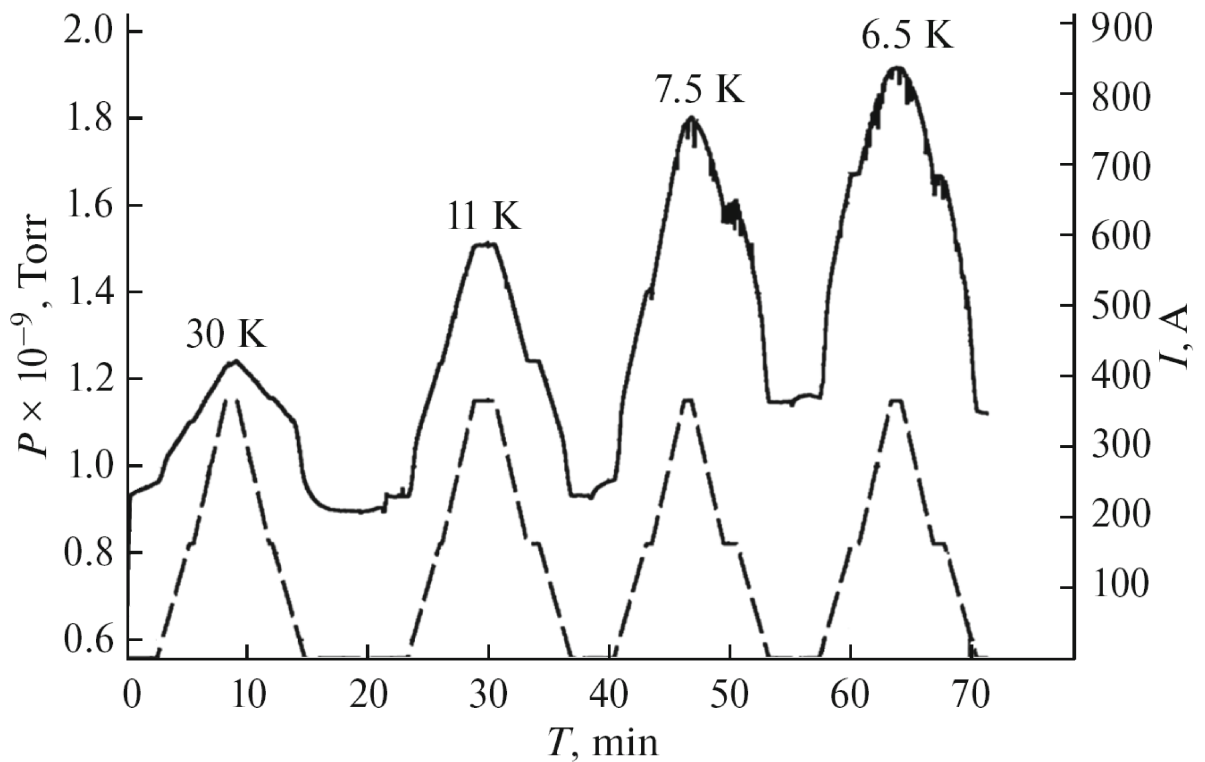
Figure 2.15.: The pressure in the compression tube (solid line) and the current through the superconducting magnets (dashed line) over time. A clear increase in pressure when the magnets are operated and a clear decrease in pressure when the magnets are turned off again visible. The temperature of the nozzle is indicated above the peaks. [She+19]

crease of three order of magnitude for deuterium. With these flow rates which are close to the rates of highly optimized atomic beam sources it could be an alternative source of protons/deuterons for accelerators or for internal targets. But more importantly, the molecular beam allow for different applications, like fuel for polarized fusion or polarized D_2-ice for solid targets.

2.4. Lamb-Shift Polarimeter

As discussed in Chap. 1 the Lamb-shift polarimeter is a device to measure the nuclear spin polarization of beams of atomic hydrogen isotopes (mostly H and D), their molecules (H_2, HD, and D_2), and their ions (H^+, H^-, H_2^+, H_3^+, ...). In the following the functional
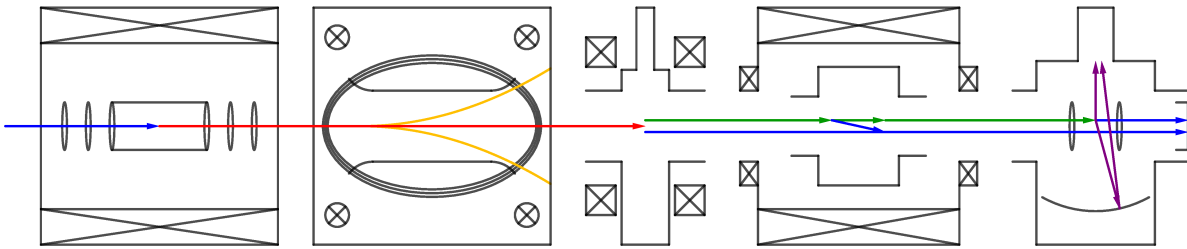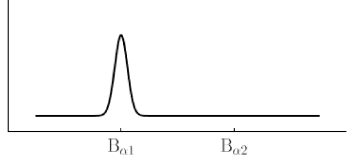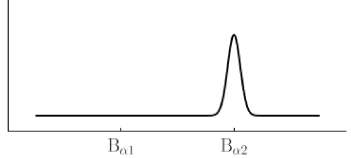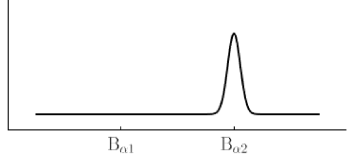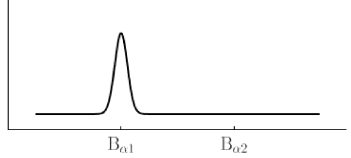
Figure 2.16.: Schematic of the Lamb-shift polarimeter with a beam direction from left to right. Blue arrows indicate beams of neutral particles in the ground state. The red arrows indicates the ion beam formed in the ionizer consisting of ions of different masses. Ions of undesired masses (marked in gold) are deflected in the Wienfilter. Metastable atoms are denoted in green. In the spin filter they are brought to the ground state and only at certain conditions a single α state may pass. In the quenching chamber, all remaining metastable atoms are quenched to the ground state, whereas Lyman-α photons (marked in purple) are emitted, which can be detected by a photomultiplier.

principle of the Lamb-shift polarimeter will be described. A scheme of the Lamb-shift polarimeter and its components is shown in Fig. 2.16.

Generally, the Lamb-shift polarimeter consists of five main components, which, in beam direction, are: an ionizer, a Wienfilter, a cesium cell, a spin filter, and a quenching chamber. As the name implies the ionizer is used to ionize the neutral particles of the incoming beam. The ions are then accelerated towards the Wienfilter, in which the ions are separated by their mass and a single mass is selected from the beam. In the cesium cell metastable atoms are formed by a charge transfer. The spin filter is able to selectively transmit one of the α states (see Sect. 2.1.9), while the β states and the other one α state (hydrogen atom) or two α states (deuterium atom) is/are brought to the ground state. Remaining metastable atoms are quenched to the ground state in the quenching chamber. Lyman-α photons emitted in this process are detected in a photomultiplier. With a Faraday cup at the end of the Lamb-shift polarimeter the current of the ion beam can be measured if it is not deflected by the electrical fields of the spin filter. Longitudinal magnetic fields in the ionizer, the cesium cell, and the spin filter and a perpendicular magnetic field in the Wienfilter ensure a well defined quantization axes along the whole Lamb-shift polarimeter.

Table 2.5.: Polarization conservation for hydrogen atoms in the Lamb-shift polarimeter. The nuclear spin is indicated by the smaller and the electron spin by the larger arrows.

ABS $\vec{\text{H}}$	ionizer $\vec{\text{H}}^+$	cesium cell $\vec{\text{H}}_{2S_{1/2}}$	spin filter $\vec{\text{H}}_{2S_{1/2}}$	spectrum $\vec{\text{H}}_{1S_{1/2}}$ + Ly-α
↑↑ ① ↑↑	↑	↑↑ α1 ↑↓ β4	↑↑ α1	
↓↑ ② ↓↑+↑↓	↓	↓↑ α2 ↓↓ β3	↓↑ α2	
↓↓ ③ ↓↓	↓	↓↑ α2 ↓↓ β3	↓↑ α2	
↑↓ ④ ↑↓−↓↑	↑	↑↑ α1 ↑↓ β4	↑↑ α1	
$B \to \infty$ $B \to 0$	$B \to \infty$	$B \to \infty$	$B = B(t)$	$E = 100\,\text{V cm}^{-1}$

2.4.1. Ionizer

Various types of ionizers can be used in a Lamb-shift polarimeter. A quantization axis, given by a magnetic field is mandatory to preserve the polarization of the beam. For most applications an electron impact ionizer, as for instance the Glavish-type ionizer [Gla68] is best suited. Since they generally operate at lower pressures than plasma ionizers, like an ECR ionizer, there is no need for a buffer gas and, therefore, no need for a differential pumping between ionizer and the atomic or molecular beam source, where ultrahigh vacuum is needed. Furthermore, Glavish-type ionizers can be operated at different

magnetic fields, which enables the distinction between pure and mixed hyperfine states in the beam. For example, at strong magnetic fields in the ionizer the polarization is approximately 1 for hyperfine states ① and ④, but at weak fields the polarization of ① remains at 1 while that of ④ tends to zero.

A Glavish-type ionizer consists of a solenoid, capable to produce a strong longitudinal magnetic field, a filament, and several ring shaped electrodes – five in the ionizers used in this work. An electron beam, parallel and coaxial to the entering atomic or molecular beam, is formed by the hot filament and the first electrode. The electrons, after traveling through the second and the long, cylindrical third electrode, which are both on positive potentials, are reflected by the negative potential of the fourth and fifth electrodes. Due to the space charge they create, they would like to diverge, but are forced onto spiral like trajectories by the strong longitudinal magnetic field. This way a high density of electrons is realized inside the third electrode, which forms the actual ionization volume. Ideally, all ions are produced in this volume and, thus, the beam energy would be precisely equal to the difference of the third electrode's potential and earth potential. The second electrode is used to stop ions from moving towards the entrance of the ionizer and into the atomic or molecular beam source by creating a potential wall. As mentioned before the forth and fifth electrode are used to form a potential trap for the electrons, but at the same time they serve as electrostatic lens for the extraction of the ions.
If the beam, of which the polarization should be measured, is already composed of ions instead of neutral atoms or molecules the ionizer will be removed.

2.4.2. Wienfilter

The Wienfilter is a velocity filter for charged particles named after Wilhelm Wien, who developed the device in 1898 [Wie98]. Its underlying principle is the Lorentz- or electromagnetic force acting on a particle with electric charge q, which is traveling through an electrical field $\boldsymbol{E}$ and a magnetic field $\boldsymbol{B}$ with the velocity $\boldsymbol{v}$

$$\boldsymbol{F} = q \cdot \boldsymbol{E} + q \cdot \boldsymbol{v} \times \boldsymbol{B} \ . \tag{2.46}$$

In an ideal Wienfilter the magnetic field, the electric field and the beam axis (z) are pairwise perpendicular to each other in every point ($z \perp \boldsymbol{E} \perp \boldsymbol{B} \perp z$). A particle does

not experience a net force if

$$|v| = \frac{E}{B} \ ,$$
(2.47)

where $E = \|\boldsymbol{E}\|$, and $B = \|\boldsymbol{B}\|$. If the velocity of a particle does not satisfy this relation the particle is deflected. These particles are then stopped by an aperture at the end of the Wienfilter. For mono-energetic ion beams, like they are produced in an electron-impact ionizer, a velocity filter is equivalent to a mass filter, since

$$v = \sqrt{\frac{2E_{\text{kin}}}{m}} \ , \quad \text{or} \quad m = \frac{2E_{\text{kin}}}{v^2} \ .$$
(2.48)

Therefore, the mass accepted by the Wienfilter can be selected by the ratio of magnetic and electric field strengths:

$$m = 2E_{\text{kin}} \frac{B^2}{E^2} \ .$$
(2.49)

An important feature of the Wienfilter reveals, when the magnetic moments of the beam particles are taken into account. Before entering the Wienfilter the quantization axis for the magnetic moments is defined by the strong longitudinal field of the ionizer. Therefore, these magnetic moments will start to precess around the perpendicular magnetic field of the Wienfilter with the Larmor frequency

$$\omega_{\text{L}} = -\gamma \cdot B \ ,$$
(2.50)

with γ being the gyromagnetic ratio of the particle. Some gyromagnetic ratios are given in Tab. 2.6. The angle α by which the magnetic moments will rotate by passing through

Table 2.6.: Some gyromagnetic ratios [NIS94].

$\gamma_p =$	$267.5 \, \text{MHz} \, \text{T}^{-1}$	for a proton
$\gamma_n =$	$183.2 \, \text{MHz} \, \text{T}^{-1}$	for a neutron
$\gamma_d =$	$41.1 \, \text{MHz} \, \text{T}^{-1}$	for a deuteron
$\gamma_e =$	$176.1 \, \text{GHz} \, \text{T}^{-1}$	for a free electron

the Wienfilter is determined by the Larmor frequency and the duration of the interaction,

ergo the time of flight through the magnetic field of the Wienfilter. Further, their time of flight Δt can be expressed by the effective length $\hat{l}$ of the magnetic field $\hat{B}$ and the beam velocity or kinetic energy, respectively:

$$\alpha = \omega_{\mathrm{L}} \cdot \Delta t = -\gamma \cdot \sqrt{\frac{m}{2E_{\mathrm{kin}}}} \cdot \hat{B} \cdot \hat{l} \ . \tag{2.51}$$

Since, in the spin filter, the projection of the polarization vector to the beam axis is determined, rotation angles have to be chosen carefully and correction factors have to be applied, whenever the polarization of a proton or deuteron beam is measured.

This is different for molecular ions. The magnetic moment of the (unpaired) electron, which is present in the molecular ions, is about three orders of magnitude larger than those of proton or deuteron. Therefore, the electron spin will realign with the magnetic field of the Wienfilter adiabatically. The magnetic field, with which the nuclear magnetic moments of the molecular ions are coupled to, is in the order of $10\,\mathrm{T}$, which causes the nuclear magnetic moments to follow the electron spin. Since these adiabatic realignments do not only happen between the ionizer and Wienfilter fields, but also between the Wienfilter and cesium cell fields, the polarization vector of the molecular ions are independent of the magnetic field in the Wienfilter.

For typical Wienfilter setups for Lamb-shift polarimeter $\hat{l}$ is less than $30\,\mathrm{cm}$ and magnetic fields commonly do not exceed $30\,\mathrm{mT}$. With beam energies varying between $500\,\mathrm{eV}$ and $5\,\mathrm{keV}$ the rotation angle for protons can occasionally be adjusted to up to $360°$. However, rotations of $180°$ are usually more feasible, in which case the a correction factor of -1 has to be applied to the measured polarization. Since the deuteron mass is roughly twice the proton mass, but the gyromagnetic ratio is less than $1/6$ of the gyromagnetic ratio of the proton, typical Wienfilter setups are not sufficient to rotate the polarization vector of deuterons by $180°$.

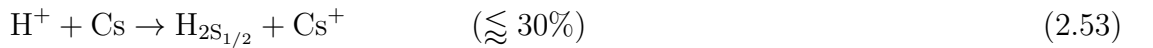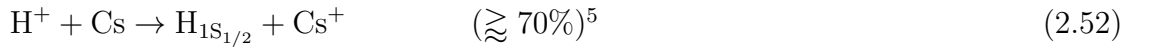## 2.4.3. Cesium Cell

The cesium cell is used to produce metastable atoms ($H_{2S_{1/2}}$ or $D_{2S_{1/2}}$) from the incoming ions by a charge exchange reaction with cesium vapor. Today, charge exchange reactions with alkali metal vapor are the method of choice for the production of metastable hydrogen atoms. When Lamb and Retherford performed their experiments, which led to

the discovery of the Lamb-shift (see Sect. 2.1.5), they had to rely on collisions of ground state atoms and electrons from an electron beam, crossing the atomic beam [LR47]. The efficiency was of the order of 10^{-8}. With charge exchange reactions of proton beams with hydrogen gas, the efficiency was increased to about 10^{-3} [MO59]. Another increase in efficiency to 10^{-1} was achieved by using low energy proton beams and cesium vapor instead of hydrogen gas, as proposed by Donnally et al. [Don+64]. A schematic drawing of a cesium cell is shown in Fig. 2.17.

In case of atomic ions (H^+, D^+), a cesium atom provides an electron, which is captured by the ion. The reaction is described as a "nearly resonant process" by Pradel at al. [Pra+74]. For protons with a kinetic energy of about $550 \, \text{eV}$ and deuterons with a kinetic energy of about $1100 \, \text{eV}$ a maximum efficiency of about 30% can be reached.

$$H^+ + Cs \rightarrow H_{1S_{1/2}} + Cs^+ \qquad (\gtrsim 70\%)^5 \tag{2.52}$$

$$H^+ + Cs \rightarrow H_{2S_{1/2}} + Cs^+ \qquad (\lesssim 30\%) \tag{2.53}$$

From Fig. 2.18 a maximum cross section for the production of metastable atoms can be read off as $6 \cdot 10^{-15} \, \text{cm}^2$ at a proton energy of $550 \, \text{eV}$. The optimum areal number density of the cesium target was found to be about $10^{14} \, \text{atoms/cm}^2$. For higher proton-energies the density needs to be slightly higher to be optimal.

The production of metastable atoms from molecular ions (H_2^+, HD^+, D_2^+) is also possible as several measurements show (see [Eng+14], and [Eng+20b]). However, if the metastable atoms are created in a two-step process, of which the first step is a stripping reaction, by which H^+ is produced and the second step is identical to Eqs. (2.52) and (2.53), or in a single-step process is not resolved until now. The reactions might either look like:

$$H_2^+ + Cs \rightarrow 2H^+ + Cs^+ + 2e^- \qquad \text{and then}$$
$$\tag{2.54}$$
$$H^+ + Cs \rightarrow H_{2S_{1/2}} + Cs^+ \ ,$$

---
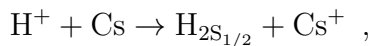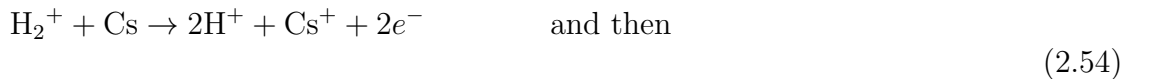
[5]Reactions resulting in radiative states like $2P_{1/2}$ are included here, since these atoms will end up in the $1S_{1/2}$ state shortly after the reaction.
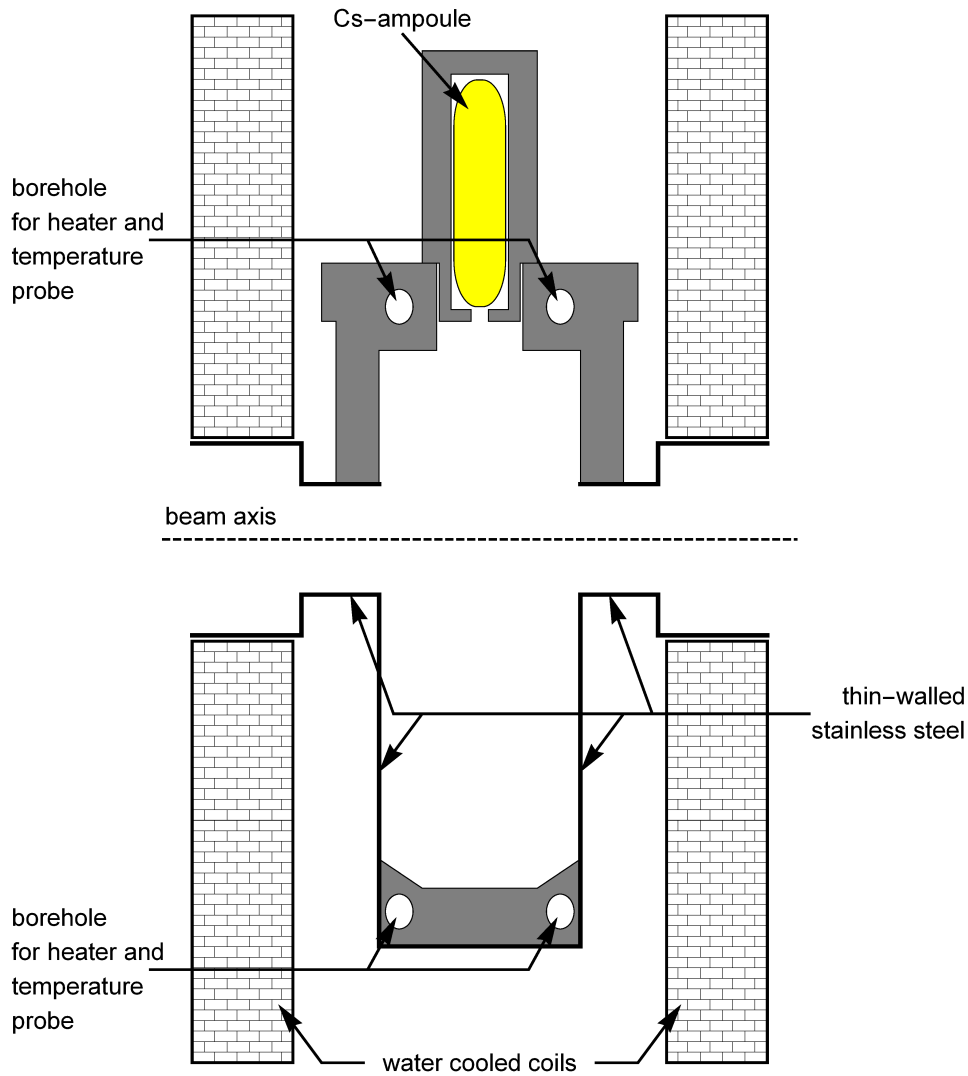
Figure 2.17.: Schematic drawing of a cesium cell. After cracking of the ampule, the liquid cesium will fall to the bottom. There it can be heated to produce a vapor of desired density. Cesium condensing on the cooler top parts of the cell will drop back to the bottom. The two coils provide a strong longitudinal magnetic field inside the cell.

which is one possible two-step process, or:

$$H_2{}^+ + Cs \rightarrow H_{1S_{1/2}} + H_{2S_{1/2}} + Cs^+ \quad, \tag{2.55}$$

which would be a single-step process. For a two step process the optimal areal number density is expected to be higher as compared to the atomic ion case, since the molecular ions travel some distance in the target column before breaking up and the resulting atomic ions start their travel through the cesium vapor. In case of the single-step process, the optimal areal number density might be smaller, since the molecular ions are much larger than the proton or deuteron. Other than for atomic ions the optimal beam energies and areal number densities are not known. An attempt to identify these parameters is discussed in Sect. 4.1.

In first order, the areal number density n is equal to the product of the number density n' and the length of the vapor column l. While the length of the column is fixed by the geometry of the cell, the number density can be adjusted by temperature and pressure:

$$n\left(p, T\right) = n'\left(p, T\right) \cdot l = n_n' \frac{p}{T} \frac{T_n}{p_n} \cdot l \quad, \tag{2.56}$$

with $T_n = 273\,\mathrm{K}$, $p_n = 1013\,\mathrm{mbar}$, and $n_n' = 2.69 \cdot 10^{19}\,\mathrm{atoms/cm^3}$ being temperature, pressure, and number density of cesium at standard conditions, respectively, and assuming, that the vapor contains atomic cesium only and can be regarded as an ideal gas. The vapor pressure over liquid cesium as function of the temperature is described by Taylor and Langmuir as [TL37]:

$$\log_{10}\left(\frac{p}{\mathrm{Torr}}\right) = 11.0531 - 1.35\log_{10}\left(\frac{T}{\mathrm{K}}\right) - \frac{4041\,\mathrm{K}}{T} \quad. \tag{2.57}$$

To preserve the nuclear spin polarization of the beam a longitudinal magnetic field is needed in the interaction region of the cesium cell, as it will be discussed in the following paragraph. Even with strong magnetic fields of $1\,\mathrm{T}$ the polarization of electrons – exchanged between the cesium atoms and the beam ions – would only be around $0.3\,\%$ ($P_e = 1 - e^{\frac{2\mu_\mathrm{B} \cdot B}{k_\mathrm{B} \cdot T}}$). Thus, the probability of the exchanged electron being either spin up

or spin down is effectively $^{1}/_{2}$. Metastable atoms created from protons[6] with spin up, therefore, will be in states $|m_I = +^{1}/_{2}, m_J = +^{1}/_{2}\rangle$ and $|m_I = +^{1}/_{2}, m_J = -^{1}/_{2}\rangle$ in equal amounts, while metastable atoms created from protons with spin down will be in states $|-^{1}/_{2}, +^{1}/_{2}\rangle$ and $|-^{1}/_{2}, -^{1}/_{2}\rangle$. As discussed in Sect. 2.1.6, $|+^{1}/_{2}, +^{1}/_{2}\rangle$ and $|-^{1}/_{2}, -^{1}/_{2}\rangle$ are pure states and can be assigned to α1 and β3, respectively, independent of the magnetic field strength. However, states $|+^{1}/_{2}, -^{1}/_{2}\rangle$ and $|-^{1}/_{2}, +^{1}/_{2}\rangle$ can only be assigned to β4 and α2, respectively, in the limit $B \to \infty$. For finite magnetic field strength the probabilities of finding $|m_I = +^{1}/_{2}, m_J = -^{1}/_{2}\rangle$ in the state $\alpha 2 = |F = 1, m_F = 0\rangle$ and finding $|m_I = -^{1}/_{2}, m_J = +^{1}/_{2}\rangle$ in the state $\beta 4 = |F = 0, m_F = 0\rangle$ are both equal to $\dfrac{1 - a(B)}{2}$, with $a(B) = \dfrac{B/B_c}{\sqrt{1 + (B/B_c)^2}}$ (see Eqs. (2.14b) and (2.14d)).

Obviously, the probabilities of finding a proton with spin up $P_\uparrow$, and one with spin down $P_\downarrow$ in a beam of protons with polarization p_z are:

$$
\begin{aligned}
P_\uparrow &= \frac{1 + p_z}{2} \\[2mm]
P_\downarrow &= \frac{1 - p_z}{2} \quad .
\end{aligned}
\tag{2.58}
$$

Thus, the probabilities of creating certain $2S_{1/2}$ substates P_i, with $i = \alpha 1, \alpha 2, \beta 3, \beta 4$ are:

$$
P_{\alpha 1} = \epsilon \cdot \left(P_\uparrow \cdot \frac{1}{2} \right) = \epsilon \cdot \left(\frac{1 + p_z}{4} \right) \quad ,
\tag{2.59}
$$

$$
\begin{aligned}
P_{\alpha 2}(B) &= \epsilon \cdot \left(\left(P_\uparrow \cdot \frac{1}{2} \cdot \frac{1 - a(B)}{2} \right) + \left(P_\downarrow \cdot \frac{1}{2} \cdot \frac{1 + a(B)}{2} \right) \right) \\[2mm]
&= \epsilon \cdot \left(\frac{(1 + p_z)(1 - a(B))}{8} + \frac{(1 - p_z)(1 + a(B))}{8} \right) \\[2mm]
&= \epsilon \cdot \left(\frac{1 - p_z \cdot a(B)}{4} \right) \quad ,
\end{aligned}
\tag{2.60}
$$

---

[6]The protons may originate from split up molecular ions or directly from a proton beam.

$$P_{\beta 3} \quad = \epsilon \cdot \left(P_{\downarrow} \cdot \frac{1}{2} \right) = \epsilon \cdot \left(\frac{1 - p_z}{4} \right) \quad , \tag{2.61}$$

$$
\begin{aligned}
P_{\beta 4}(B) &= \epsilon \cdot \left(\left(P_{\uparrow} \cdot \frac{1}{2} \cdot \frac{1 + a(B)}{2} \right) + \left(P_{\downarrow} \cdot \frac{1}{2} \cdot \frac{1 - a(B)}{2} \right) \right) \\
&= \epsilon \cdot \left(\frac{\left(1 + p_z \right) \left(1 + a(B) \right)}{8} + \frac{\left(1 - p_z \right) \left(1 - a(B) \right)}{8} \right) \\
&= \epsilon \cdot \left(\frac{1 + p_z \cdot a(B)}{4} \right) \quad ,
\end{aligned}
\tag{2.62}
$$

with ϵ being the efficiency of metastable creation. Since a spin filter can only transmit the two α states, the measured polarization p_{m} is also a function of the magnetic field in the cesium cell:

$$
\begin{aligned}
p_{\mathrm{m}}(B) &= \frac{P_{\alpha 1} - P_{\alpha 2}}{P_{\alpha 1} + P_{\alpha 2}} \\
&= \frac{\left(1 + p_z \right) - \left(1 - p_z \cdot a(B) \right)}{\left(1 + p_z \right) + \left(1 - p_z \cdot a(B) \right)} \\
&= \frac{p_z \cdot \left(1 + a(B) \right)}{2 + p_z \cdot \left(1 - a(B) \right)} \quad .
\end{aligned}
\tag{2.63}
$$

Thus, the measured polarization is equal to the polarization of the incident beam only[7] in the limit $B \to \infty \Rightarrow a(B) \to 1$. Since an infinitely strong magnetic field is obviously not achievable a correction factor $C_{\mathrm{Cs}}(B_{\mathrm{Cs}}, p_{\mathrm{m}})$ has to be applied to the measured polarization. Rearranging Eq. (2.63) gives:

$$p_z = \frac{2}{1 + a(B) - \left(1 - a(B) \right) p_{\mathrm{m}}} \cdot p_{\mathrm{m}} = C_{\mathrm{Cs}}(B_{\mathrm{Cs}}, p_{\mathrm{m}}) \cdot p_{\mathrm{m}} \quad . \tag{2.64}$$

Notably the correction factor is not only a function of the magnetic field in the cesium cell

---

[7]Apart from the two trivial cases: $p_z = 0$ and $p_z = -1$

(B_{Cs}) but also a function of the measured polarization. However, with increasing magnetic field the influence of the measured polarization to the correction factor decreases and the correction factor will approach 1. The critical magnetic field for metastable hydrogen $B_c = 6.34\,\mathrm{mT}$ is smaller than the magnetic field usually applied to the cesium cell (see Sect. 3.3) by a factor of 7 or more. Thus the correction factor is restricted to $C_{\mathrm{Cs}}(B_{\mathrm{Cs}} > 7B_c, p_{\mathrm{m}}) \in [1; 1.01011]$.

The probabilities of finding a deuteron in a certain m_I-state can be expressed by the vector- p_z and the tensor- polarization p_{zz}:

$$
P_+ = \frac{2 + 3p_z + p_{zz}}{6}
$$

$$
P_- = \frac{2 - 3p_z + p_{zz}}{6} \tag{2.65}
$$

$$
P_0 = \frac{1 - p_{zz}}{3} \quad .
$$

Again, the probability of observing an electron with spin up is equal to the probability of finding one with spin down ($P(m_J = 1/2) = P(m_J = -1/2) = 1/2$). Using Eqs. (2.16b), (2.16c), (2.16e) and (2.16f) , the probabilities of creating a metastable deuterium atom in each of the six $2\mathrm{S}_{1/2}$ substates P_i, with $i = \alpha 1, \alpha 2, \alpha 3, \beta 4, \beta 5, \beta 6$ calculate to:

$$
P_{\alpha 1} = \epsilon \cdot \left(P_+ \cdot \frac{1}{2} \right) = \epsilon \cdot \left(\frac{2 + 3p_z + p_{zz}}{12} \right) \quad , \tag{2.66}
$$

$$
\begin{aligned}
P_{\alpha 2}(B) &= \epsilon \cdot \left(\left(P_+ \cdot \frac{1}{2} \cdot \frac{1 - b(B)}{2} \right) + \left(P_0 \cdot \frac{1}{2} \cdot \frac{1 + b(B)}{2} \right) \right) \\
&= \epsilon \cdot \left(\frac{(2 + 3p_z + p_{zz})\left(1 - b(B)\right)}{24} + \frac{(2 - 2p_{zz})\left(1 + b(B)\right)}{24} \right) \tag{2.67} \\
&= \epsilon \cdot \frac{1}{24} \left(4 + 3\left(1 - b(B)\right) p_z - \left(1 + 3b(B)\right) p_{zz} \right) \quad ,
\end{aligned}
$$

$$P_{\alpha 3}(B) = \epsilon \cdot \left(\left(P_- \cdot \frac{1}{2} \cdot \frac{1 + c(B)}{2} \right) + \left(P_0 \cdot \frac{1}{2} \cdot \frac{1 - c(B)}{2} \right) \right)$$

$$= \epsilon \cdot \left(\frac{(2 - 3p_z + p_{zz})\left(1 + c(B)\right)}{24} + \frac{(2 - 2p_{zz})\left(1 - c(B)\right)}{24} \right) \tag{2.68}$$

$$= \epsilon \cdot \frac{1}{24} \left(4 - 3\left(1 + c(B)\right) p_z + \left(3c(B) - 1\right) p_{zz} \right) \ ,$$

$$P_{\beta 4} = \epsilon \cdot \left(P_- \cdot \frac{1}{2} \right) = \epsilon \cdot \left(\frac{2 - 3p_z + p_{zz}}{12} \right) \ , \tag{2.69}$$

$$P_{\beta 5}(B) = \epsilon \cdot \left(\left(P_- \cdot \frac{1}{2} \cdot \frac{1 - c(B)}{2} \right) + \left(P_0 \cdot \frac{1}{2} \cdot \frac{1 + c(B)}{2} \right) \right)$$

$$= \epsilon \cdot \left(\frac{(2 - 3p_z + p_{zz})\left(1 - c(B)\right)}{24} + \frac{(2 - 2p_{zz})\left(1 + c(B)\right)}{24} \right) \tag{2.70}$$

$$= \epsilon \cdot \frac{1}{24} \left(4 + 3\left(c(B) - 1\right) p_z - \left(1 + 3c(B)\right) p_{zz} \right) \ ,$$

$$P_{\beta 6}(B) = \epsilon \cdot \left(\left(P_+ \cdot \frac{1}{2} \cdot \frac{1 + b(B)}{2} \right) + \left(P_0 \cdot \frac{1}{2} \cdot \frac{1 - b(B)}{2} \right) \right)$$

$$= \epsilon \cdot \left(\frac{(2 + 3p_z + p_{zz})\left(1 + b(B)\right)}{24} + \frac{(2 - 2p_{zz})\left(1 - b(B)\right)}{24} \right) \tag{2.71}$$

$$= \epsilon \cdot \frac{1}{24} \left(4 + 3\left(1 + b(B)\right) p_z + \left(3b(B) - 1\right) p_{zz} \right) \ ,$$

$$\text{with} \quad b(B) = \frac{\frac{B}{B_c} + \frac{1}{3}}{\sqrt{1 + \frac{2}{3}\frac{B}{B_c} + \left(\frac{B}{B_c}\right)^2}} \quad \text{and} \quad c(B) = \frac{\frac{B}{B_c} - \frac{1}{3}}{\sqrt{1 - \frac{2}{3}\frac{B}{B_c} + \left(\frac{B}{B_c}\right)^2}} \quad .$$

Since, again, the polarization is measured using the α states only, both the measured vector polarization p_{m} and measured tensor polarization p_{mm} are functions of the magnetic field during the production of the metastable atoms:

$$
\begin{aligned}
p_{\mathrm{m}}(B) &= \frac{P_{\alpha 1} - P_{\alpha 3}}{P_{\alpha 1} + P_{\alpha 2} + P_{\alpha 3}} \\[2mm]
&= \frac{\big(3 + c(B)\big) \cdot p_z + \big(1 - c(B)\big) \cdot p_{zz}}{4 + \big(2 - b(B) - c(B)\big) \cdot p_z + \big(c(B) - b(B)\big) \cdot p_{zz}} \quad,
\end{aligned}
\tag{2.72}
$$

$$
\begin{aligned}
p_{\mathrm{mm}}(B) &= \frac{P_{\alpha 1} + P_{\alpha 3} - 2P_{\alpha 2}}{P_{\alpha 1} + P_{\alpha 2} + P_{\alpha 3}} \quad, \\[2mm]
&= \frac{\big(2b(B) - c(B) - 1\big) \cdot p_z + \big(2b(B) + c(B) + 1\big) \cdot p_{zz}}{4 + \big(2 - b(B) - c(B)\big) \cdot p_z + \big(c(B) - b(B)\big) \cdot p_{zz}} \quad.
\end{aligned}
\tag{2.73}
$$

Solving for p_z and p_{zz}, the corrected vector- and tensor- polarization as function of the magnetic field and the measured polarizations[8] is:

$$
p_z = \frac{(2b + c + 1) \cdot p_m + (c - 1) \cdot p_{mm}}{(bc + b + c + 1) + \frac{1}{2}(3bc - b - c - 1)\, p_m + \frac{1}{2}(bc + b - 3c + 1)\, p_{mm}} \quad,
\tag{2.74}
$$

$$
p_{zz} = \frac{(c - 2b + 1) \cdot p_m + (c + 3) \cdot p_{mm}}{(bc + b + c + 1) + \frac{1}{2}(3bc - b - c - 1)\, p_m + \frac{1}{2}(bc + b - 3c + 1)\, p_{mm}} \quad.
\tag{2.75}
$$

Fortunately, the critical magnetic field for metastable deuterium atoms $B_{\mathrm{c}} = 1.5\,\mathrm{mT}$ is considerably smaller than the magnetic field provided by the coils of the cesium cell, so that the uncorrected measured polarizations deviate from the actual ones insignificantly (e.g. for $B_{\mathrm{Cs}} = 20 \cdot B_{\mathrm{c}} = 30\,\mathrm{mT}$: $|p_{zz} - p_{mm}| < 0.0017$, $|p_z - p_m| < 0.0006$).

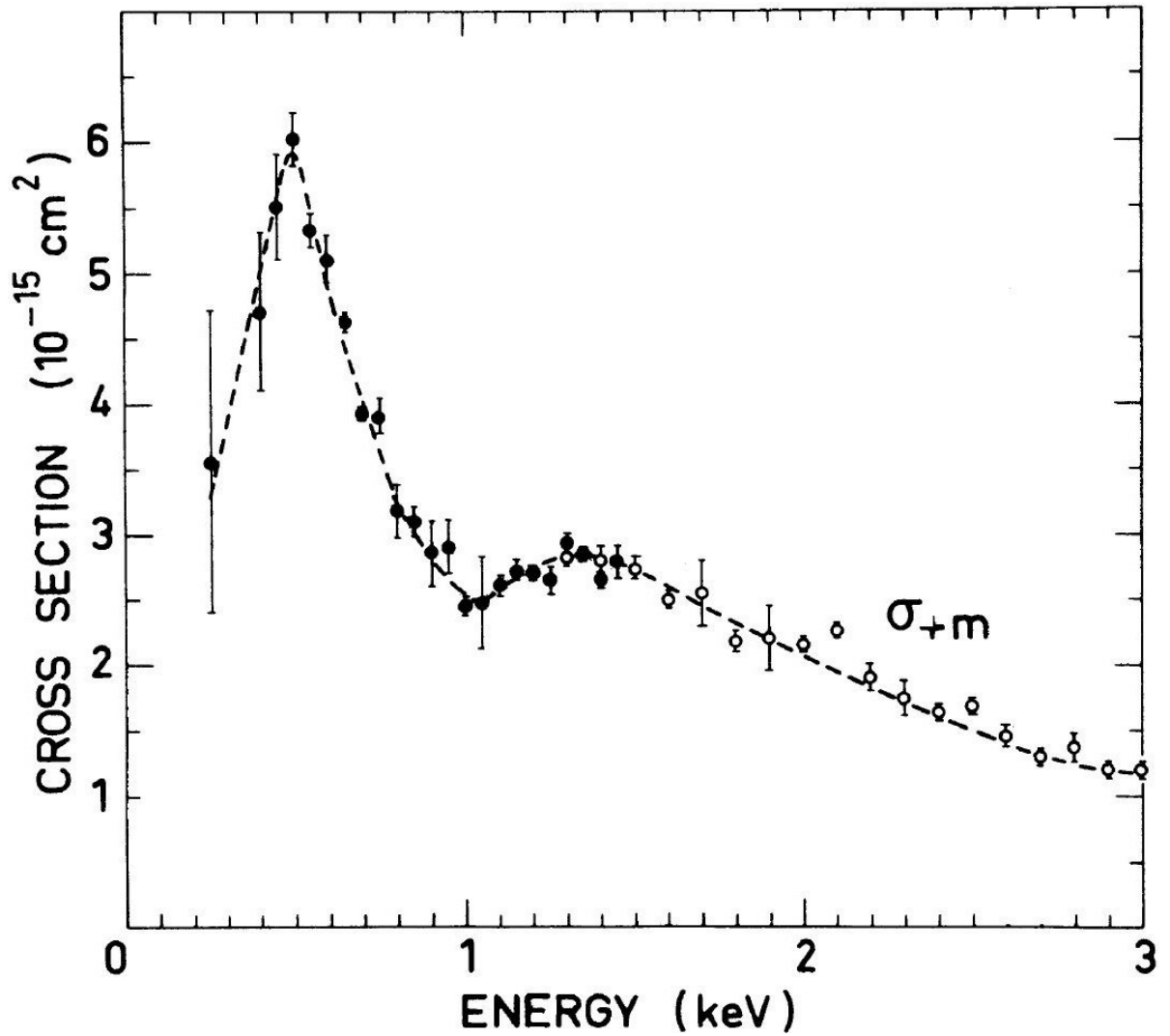[8]To shorten the expressions $b = b(B)$ and $c = c(B)$ are used.

Figure 2.18.: Cross section of charge transfer reactions: ($\bullet$) $Cs + D^+ \rightarrow Cs^+ + D_{2S_{1/2}}$, ($\circ$) $Cs + H^+ \rightarrow Cs^+ + H_{2S_{1/2}}$ as function of the energy of the proton (e.g. D^+ with $E_{kin} = 2\,keV$ is approximately equivalent to H^+ with $E_{kin} = 1\,keV$). [Pra+74]

2.4.4. Spin Filter

The spin filter is the most important part of the Lamb-shift polarimeter. It was first introduced by McKibben, Lawrence, and Ohlsen in context of the Los Alamos Lamb-shift polarized ion source [MLO68].

In a spin filter a combination of static electric, static magnetic, and radio frequency electromagnetic fields are used to initially quench all four (for hydrogen atoms) or six (for deuterium atoms) Zeeman components of the metastable $2S_{1/2}$-state – produced in the cesium cell – into the ground state. Only at certain resonances, which occur at different magnetic fields, atoms in a single α state are trapped in an oscillation between this α state and a corresponding e state, so that after the spin filter this particular α state is still populated. States that are already quenched into the ground state inside the spin filter can no longer contribute to the signal of the photomultiplier produced from the Lyman-α photons emitted by the (unspecific) quenching in the quenching chamber. In other words, only the α state, which the spin filter allows to be partially populated, can be detected by the photomultiplier.

The working principle of the spin filter for hydrogen is illustrated in the diagrams in Fig. 2.19. Without external fields the $2S_{1/2}$ states can only decay via a rare two photon transition indicated by the thin arrows. With typical kinetic energies of metastable atoms in Lamb-shift polarimeters only an insignificant amount would decay between the cesium cell and quenching chamber. As discussed in Sect. 2.1.9, the lifetime of the β states can be reduced by coupling them to the short lived $2P_{1/2}$ states with a combination of static electric and static magnetic fields. The coupling of the β and $2P_{1/2}$ states is indicated by the green arrows in Fig. 2.19. The fast decay from the $2P_{1/2}$ states to the ground state via a dipole transition is illustrated by the thick black arrows. With an electric field of about $10\,\mathrm{V\,cm^{-1}}$ and a magnetic field between $50\,\mathrm{mT}$ and $65\,\mathrm{mT}$ the lifetime of the β states is well below $10^{-7}\,\mathrm{s}$. With this lifetime and typical velocities in a Lamb-shift polarimeter almost no β states will be left in the beam after passing the spin filter. The α states are coupled to the e states via radio frequency electromagnetic fields. Depending on the strength of the coupling, three cases are possible: If the coupling is "weak", not all atoms in an initial α-state will move into an e-state during there flight through the spin filter, and consequently stay in this metastable state. With a "moderate" coupling strength, all atoms in an α-state are brought into the corresponding e-state, from were they decay into the ground state, before the electromagnetic field is

(a) At $B \approx 53.5 \, \mathrm{mT}$ the α1 state is partially transmitted.

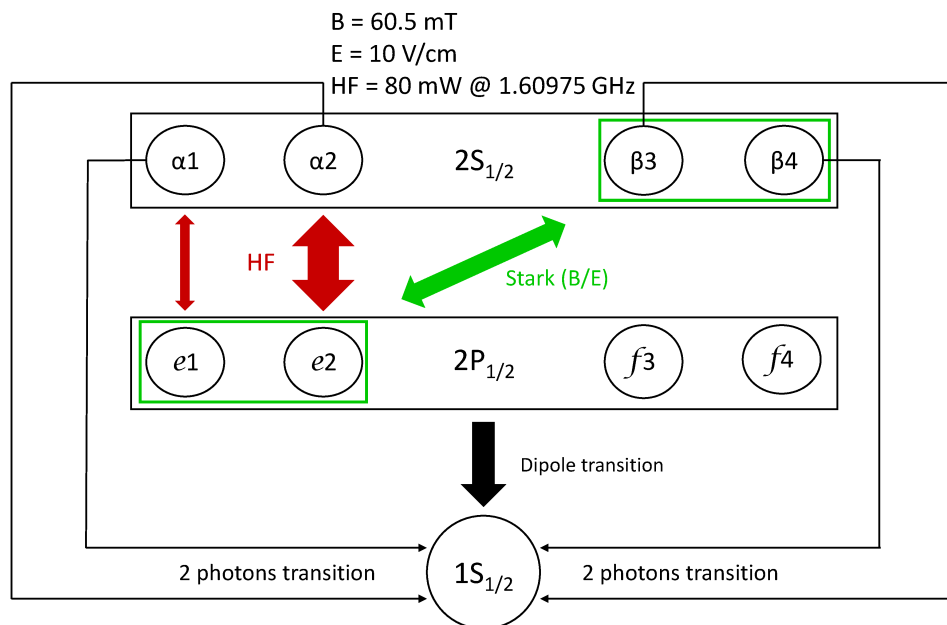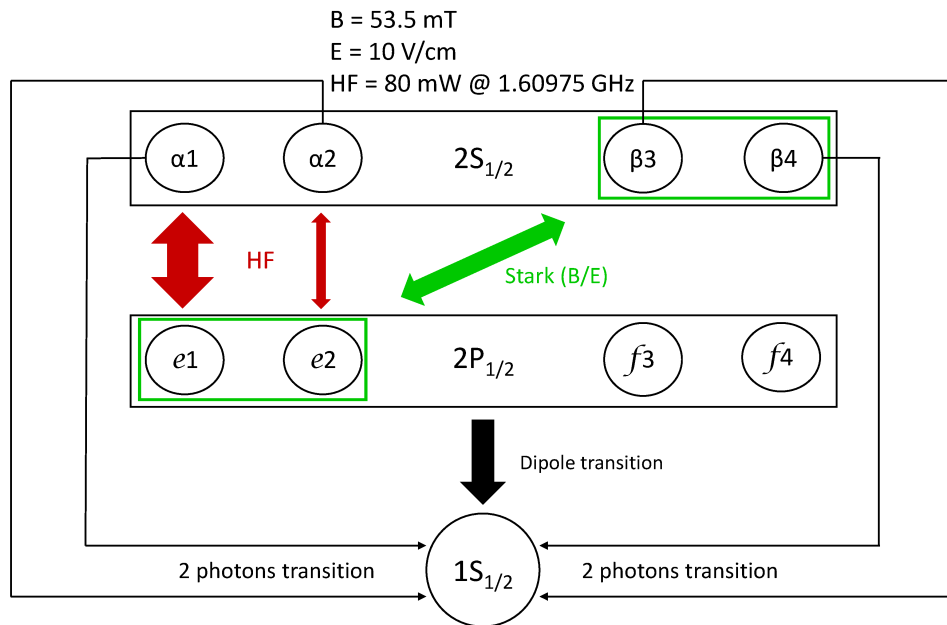(b) At $B \approx 60.5 \, \mathrm{mT}$ the α2 state is partially transmitted.

Figure 2.19.: Coupling scheme for metastable hydrogen atoms in a spin filter.

able to bring them back to their original α-state. This case is illustrated by the thinner of both red arrows in Fig. 2.19a and Fig. 2.19b. Only if the coupling is much "stronger" there is a chance that atoms – after a transition to a e state – are re-exited to their original α state before they could decay to the ground state. The last case is expressed by the thick arrows in the diagrams. With a spin filter the coupling strength changes with the magnetic field in such a way, that for a broad range the coupling is "moderate" for every α state simultaneously, but becomes "strong" for each α state at a separate, smaller interval within this range. How this is achieved will be discussed in the following paragraph using the example of hydrogen.

The energy difference between the α1 and the e1 state, as well as the energy difference between the α2 and the e2 state is a function of the magnetic field (see Fig. 2.8). To allow transitions between these states, this energy difference has to match the photon energy of the radio frequency electromagnetic field ($\Delta E = E_{\mathrm{ph}} = h\nu \Leftrightarrow \nu = \frac{\Delta E}{h}$). For a given frequency ν, there will be a corresponding magnetic field at which the energy difference between α1 and e1 is equal to the photon energy and a second (stronger) magnetic field at which the energy difference of α2 and e2 matches. This is illustrated in Fig. 2.20. If the photon energy is equal to the energy difference between two states, a photon can either be absorbed or cause a stimulated emission. Since the $2\mathrm{P}_{1/2}$ states have a short lifetime there are no atoms in this state before entering the spin filter. Thus, initially, the photons can only be used to induce transitions from the more energetic α states to the lower energetic $2\mathrm{P}_{1/2}$ states. Only if the transition rate induced by the photons exceed the decay rate of the $2\mathrm{P}_{1/2}$ state, photons are able to re-excite atoms in a $2\mathrm{P}_{1/2}$ state back to their original $2\mathrm{S}_{1/2}$ state. To induce the necessary photon density, the radio frequency electromagnetic field is stored in a cavity, which, as every practical cavity, does not provide a single, discrete frequency, but a continuous spectrum given by the resonance curve. This resonance curve is usually described by a Lorentz distribution. The cavities for Lamb-shift polarimeters are designed specifically to have a quality factor $Q = \frac{\nu_0}{\Delta\nu}$ of $Q \in [1000; 3000]$, with the resonance frequency ν_0 and the FWHM of the resonance curve $\Delta\nu$. A logarithmic plot of a Lorentz curve with $Q = 2000$ and $\nu_0 = 1.609\,75\,\mathrm{GHz}$ is provided in Fig. 2.21. With adequate overall power, the electromagnetic field is coupled into the cavity, there is a broad interval (see green area in Fig. 2.21) of frequencies, in which the intensity is sufficient to bring all atoms in α states to their corresponding e state and a narrow interval (see red area in Fig. 2.21), in which the intensity is even high enough to bring them back into their initial α state, if
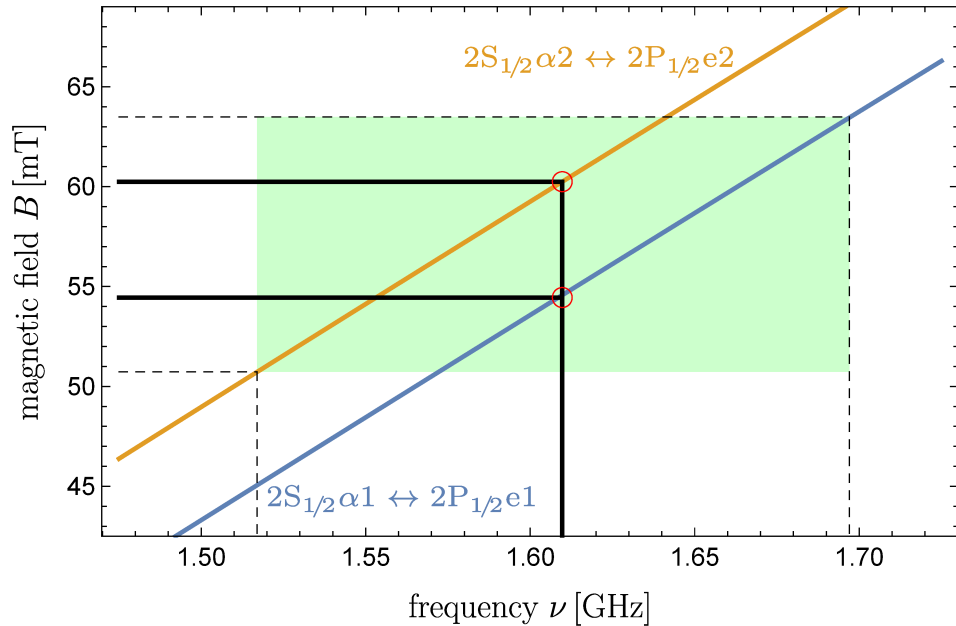
Figure 2.20.: The magnetic fields matching to the transition frequencies between α1 and e1 (blue) and between α2 and e2 (orange). With typical settings for the cavity the "moderate" coupling spans roughly over the interval indicated by the green area. The solid lines indicate the typical resonance frequency ($\nu_0 = 1.609\,75\,\text{GHz}$) and the corresponding magnetic fields for both transitions of the α states of hydrogen. The "strong" coupling occurs in a small interval around the resonance frequency.

the frequency matches the energy difference. Since the energy difference, and therefore also the fitting frequency, are functions of the magnetic field, these frequency intervals correspond to magnetic field strength intervals (see green area in Fig. 2.20). At this point it is worth noting that the resonance frequency of the cavity does not need to match the energy differences of α states with the corresponding e states at the crossing points of the e states and the β states (see Sect. 2.1.9), which would be $\nu_0 = 1.609\,75\,\text{GHz}$, but may also take other values. However, for this type of Lamb-shift polarimeter the magnetic fields, at which the resonance frequency matches should roughly be between $50\,\text{mT}$ and $65\,\text{mT}$, to ensure, that all β states are quenched to the ground state (see Fig. 2.11). A different approach will be discussed in Chap. 5.

In conclusion: which α-state, if any, is able to partially pass the spin filter, is determined by the magnetic field strength. Thus, a typical measurement is done by detecting the amount of metastable atoms behind the spin filter while the magnetic field is changed in
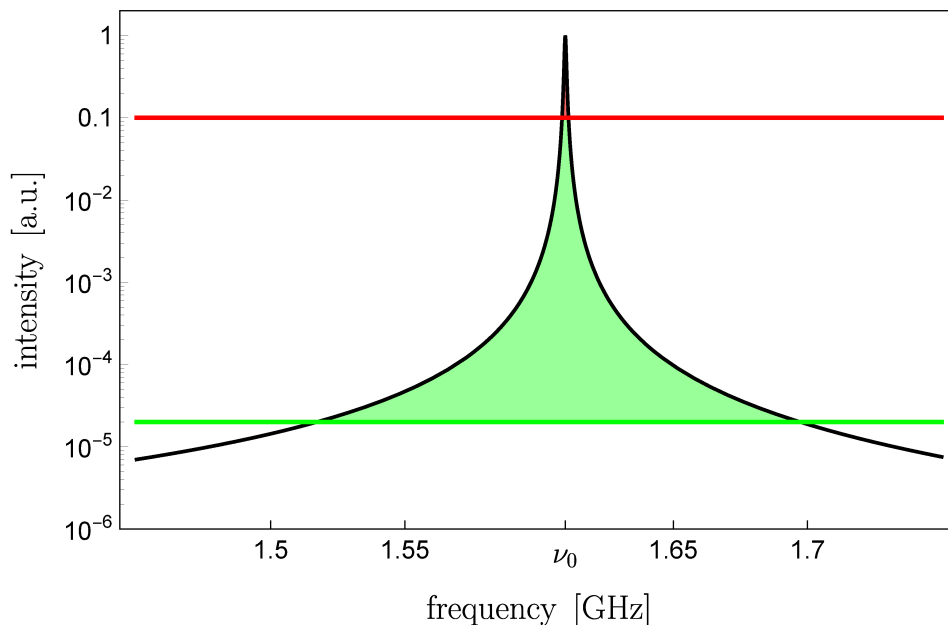
Figure 2.21.: Resonance curve of a cavity with resonance frequency $\nu_0 = 1.609\,75\,\text{GHz}$ and quality factor $Q = 2000$. Above the lower threshold – marked by the green line – the intensity is sufficient to bring all atoms in α states to e states. Above the higher threshold – marked by the red line – the intensity is sufficient to bring atoms in e states to α states, before they can decay to the ground state.

a saw-tooth pattern. This way a spectrum is created, which consists of one peak for every α-state present in the beam – two in chase of a pure H or H_2-beam, three in chase of pure D or D_2, and five in chase of a beam consisting of both isotopes. Depending of the beam intensity, averaging over a few of those measurements is necessary. Schematic spectra for both, hydrogen and deuterium, are shown in Fig. 2.22. At low magnetic fields the signal intensity is high, since there is not enough electromagnetic field intensity of the fitting frequencies to bring atoms in any α state to the corresponding e state. With increasing magnetic field the frequencies needed for the transitions also increases and the cavity can provide sufficient intensity to completely depopulate the α states – this creates a valley in the spectrum. In small intervals around the five magnetic fields, at which the resonance frequency of the cavity is exactly equal to the energy difference of one of the two α states of hydrogen or three α states of deuterium and the corresponding e states, the photon density is so large that the atoms oscillate between the corresponding $2S_{1/2}$ and $2P_{1/2}$ substates and only a few will decay from the $2P_{1/2}$ substates into the ground state.

Thus, about 50% of the atoms in this single oscillation will stay in the correponding $2S_{1/2}$ substate and will be detected in the quenching chamber. Accordingly, one peak for each α state present in the beam appears in the spectrum. At stronger magnetic fields the frequencies needed for transitions between α and e states are insufficiently provided by the cavity and, therefore, atoms in α states can pass the spin filter. The amount of metastable atoms detected increases and, thus, the valley in the spectrum ends.

The area of each peak in the spectrum is a measure of the amount of atoms in the corresponding α states in the beam. Since the shape of the peaks is identical[9], the integral and the height of a peak are correlated, so that the the peak height can also be used to calculate the polarization. At high intensities it is sufficient to measure the peak heights, while at low intensities it is advisable to use the integral to minimize the statistical uncertainties.

If the nuclear spin polarization of the beam is conserved until it reaches the spin filter the polarization can be measured by the occupation numbers of the α states only (see Tab. 2.5). Therefore, the polarization can be calculated from the peaks' areas or heights. However, since the measurement relies on the ability of the spin filter to allow the α states to partially pass at different magnetic fields, the probability of atoms passing the spin filter should ideally be the same for each α state. These transmission probabilities are primarily influenced by the homogeneity of every single magnetic resonance field the solenoid provides at the volume of the beam in the cavity. Thus, a careful tuning of the solenoid, aiming for high homogeneity, is advisable, and will be further discussed in Sect. 3.4.1. Still, differences in transition probabilities can occur, but measurements with unpolarized beams can help to correct for this effect. If p_z is the polarization of hydrogen atoms in the α states before the spin filter, the measured polarization p_m is:

$$p_m = \frac{t_{\alpha 1} P_{\alpha 1} - t_{\alpha 2} P_{\alpha 2}}{t_{\alpha 1} P_{\alpha 1} + t_{\alpha 2} P_{\alpha 2}} \tag{2.76}$$

$$= \frac{t_{\alpha 1} (1 + p_z) - t_{\alpha 2} (1 - p_z)}{t_{\alpha 1} (1 + p_z) + t_{\alpha 2} (1 - p_z)} \quad , \tag{2.77}$$

with $t_{\alpha 1}$ and $t_{\alpha 2}$ being the transition probabilities for atoms in states α1 and α2, respectively, and $P_{\alpha 1}$ and $P_{\alpha 2}$ the probability of atoms being in these states. Therefore, the

---

[9]Assuming identical homogeneities of the magnetic field around each peak, the shape is determined by the resonance curve of the cavity, the beam energy, and the static electric fields.

polarization of atoms in the α states results from the measured polarization and the transition probabilities as:

$$p_z = \frac{(t_{\alpha 1} + t_{\alpha 2}) - \frac{1}{p_m}(t_{\alpha 1} - t_{\alpha 2})}{(t_{\alpha 1} + t_{\alpha 2}) - p_m(t_{\alpha 1} - t_{\alpha 2})} \cdot p_m = C_{\mathrm{Sp,H}}(t_{\alpha 1}, t_{\alpha 2}, p_m) \cdot p_m \ , \tag{2.78}$$

which defines the correction factor of the spin filter for hydrogen $C_{\mathrm{Sp,H}}$. To avoid measuring the transition probabilities directly, the polarization of an unpolarized beam $p_{m,0}$ can be measured. With $p_z = 0$, Eq. (2.77) calculates to

$$p_{m,0} = \frac{t_{\alpha 1} - t_{\alpha 2}}{t_{\alpha 1} + t_{\alpha 2}} \ , \tag{2.79}$$

and the correction factor can be simplified:

$$C_{\mathrm{Sp,H}}(p_m, p_{m,0}) = \frac{1 - \frac{p_{m,0}}{p_m}}{1 - p_m \cdot p_{m,0}} \ . \tag{2.80}$$

Notably, this correction factor again is a function of the measured polarization. In the limits $p_m \to \pm 1$, however, it approaches 1, which is reasonable, since in these cases one of the two α states is not populated and therefore, the corresponding transition probability is irrelevant.

In case of deuterium, the measured vector polarization p_m and tensor polarization p_{mm} results from the probabilities of atoms being in the three α states ($P_{\alpha 1}$, $P_{\alpha 2}$, $P_{\alpha 3}$), with:

$$p_m = \frac{t_{\alpha 1} P_{\alpha 1} - t_{\alpha 3} P_{\alpha 3}}{t_{\alpha 1} P_{\alpha 1} + t_{\alpha 2} P_{\alpha 2} + t_{\alpha 3} P_{\alpha 3}} \tag{2.81}$$

$$= \frac{t_{\alpha 1}(2 + 3p_z + p_{zz}) - t_{\alpha 3}(2 - 3p_z + p_{zz})}{t_{\alpha 1}(2 + 3p_z + p_{zz}) + t_{\alpha 2}(2 - 2p_{zz}) + t_{\alpha 3}(2 - 3p_z + p_{zz})} \ , \tag{2.82}$$

and:

$$p_{mm} = \frac{t_{\alpha 1} P_{\alpha 1} - 2t_{\alpha 2} P_{\alpha 2} + t_{\alpha 3} P_{\alpha 3}}{t_{\alpha 1} P_{\alpha 1} + t_{\alpha 2} P_{\alpha 2} + t_{\alpha 3} P_{\alpha 3}} \tag{2.83}$$

$$= \frac{t_{\alpha 1}(2 + 3p_z + p_{zz}) - 2t_{\alpha 2}(2 - 2p_{zz}) + t_{\alpha 3}(2 - 3p_z + p_{zz})}{t_{\alpha 1}(2 + 3p_z + p_{zz}) + t_{\alpha 2}(2 - 2p_{zz}) + t_{\alpha 3}(2 - 3p_z + p_{zz})} \ , \tag{2.84}$$

with p_z and p_{zz} being the vector- and tensor-polarization of atoms in the α states before the spin filter. By using the measured vector- and tensor-polarization of an unpolarized $(p_z = p_{zz} = 0)$ beam

$$p_{m,0} = \frac{t_{\alpha 1} - t_{\alpha 3}}{t_{\alpha 1} + t_{\alpha 2} + t_{\alpha 3}} \tag{2.85}$$

$$p_{mm,0} = \frac{t_{\alpha 1} - 2t_{\alpha 2} + t_{\alpha 3}}{t_{\alpha 1} + t_{\alpha 2} + t_{\alpha 3}} \quad , \tag{2.86}$$

the vector- and tensor-polarization before the spin filter can be calculated from these "zero-measurements" and the measured polarizations by:

$$p_z = \frac{1}{D} \left(2p_m \left(2 - p_{mm,0} \left(1 + p_{mm,0} \right) \right) + 2p_{mm}p_{m,0} \left(p_{mm,0} - 1 \right) \right.$$

$$\left. + 4p_{m,0} \left(p_{mm,0} - 1 \right) \right) \quad , \tag{2.87}$$

and,

$$p_{zz} = \frac{1}{D} \left(6p_m p_{m,0} \left(p_{mm,0} - 1 \right) + 2p_{mm} \left(2 + p_{mm,0} - 3p_{m,0}^2 \right) \right.$$

$$\left. - 2p_{mm,0} \left(2 + p_{mm,0} \right) + p_{m,0}^2 \right) \quad , \tag{2.88}$$

with the denominator D in both expression:

$$D = \left(4 + 6p_m p_{m,0} \left(p_{mm,0} - 1 \right) + p_{mm} \left(3p_{m,0}^2 - p_{mm,0} \left(p_{mm,0} + 2 \right) \right) \right.$$

$$\left. - 3p_{m,0}^2 - p_{mm,0}^2 \right) \quad . \tag{2.89}$$

Since the homogeneity of the magnetic field, and, therefore, also the transition probabilities, usually changes less between field strengths that are close to each other than for fields that are further apart, the correction is much more important for hydrogen, than for deuterium.
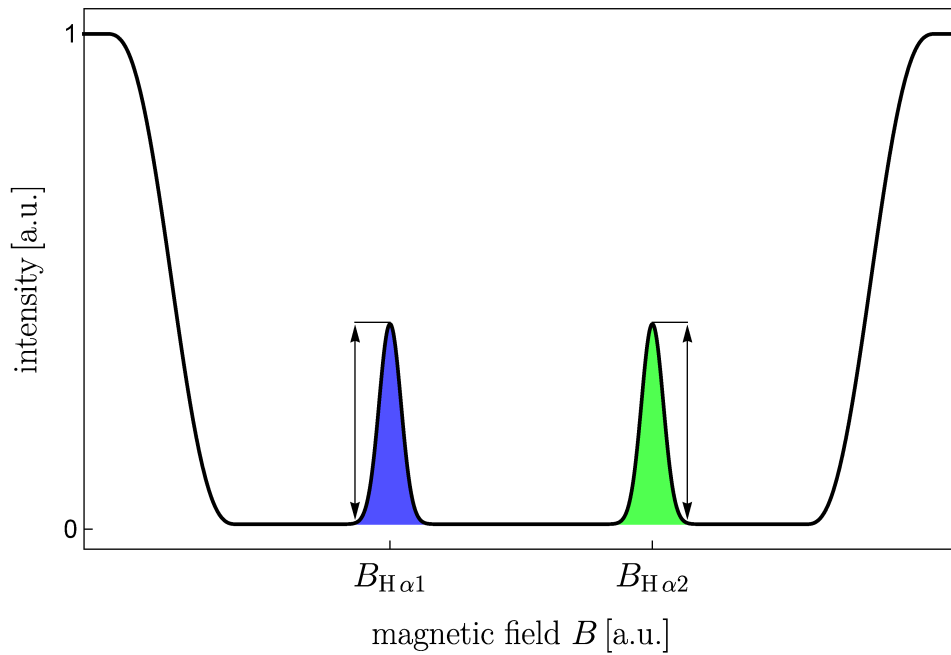
(a) A schematic spectrum for Hydrogen. At the magnetic field $B_{\text{H}\alpha1}$ atoms in the $\alpha1$ state can pass the spin filter, while at $B_{\text{H}\alpha2}$ the $\alpha2$ state will still be populated.
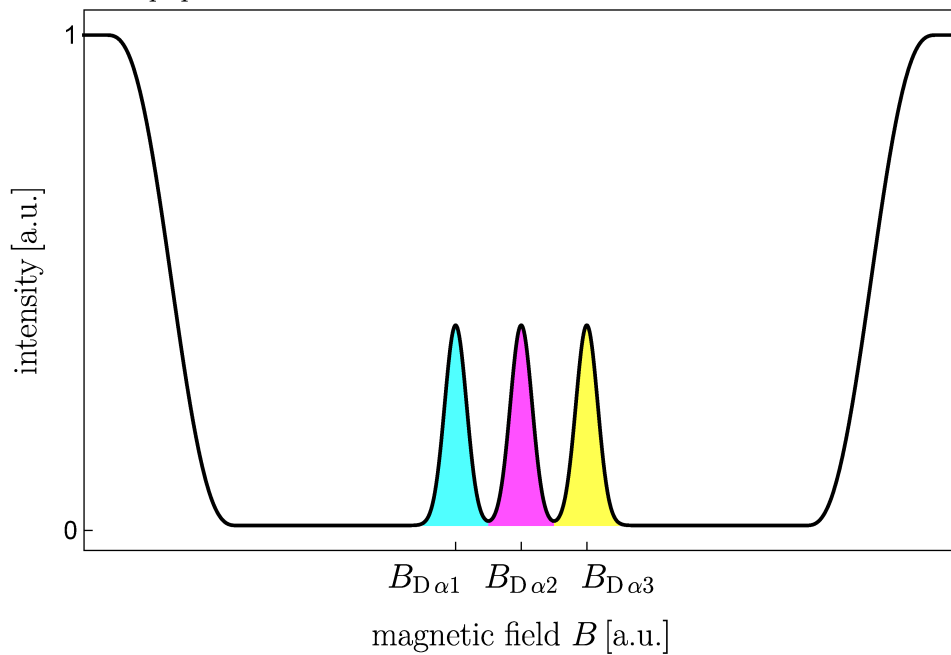
(b) A schematic spectrum for Deuterium. The peaks associated with the three α-states of Deuterium lie in between the two peaks of Hydrogen.

Figure 2.22.: Schematic spectra for pure Hydrogen (a) and pure Deuterium (b) beams. If the resonance frequency of the cavity is $\nu_0 = 1.609\,75\,\text{GHz}$ the peaks occur at: $B_{\text{H}\alpha1} = 53.8\,\text{mT}$, $B_{\text{D}\alpha1} = 56.4\,\text{mT}$, $B_{\text{D}\alpha2} = 57.4\,\text{mT}$, $B_{\text{D}\alpha3} = 58.4\,\text{mT}$, and $B_{\text{H}\alpha2} = 60.5\,\text{mT}$

2.4.5. Quenching Chamber

Directly after passing the spin filter the beam enters the quenching chamber. The essential purpose of the chamber is to measure the amount of remaining metastable atoms in the beam.

One option for the detection of metastable atoms is the method used in the original Lamb-shift experiment, where the beam is terminated by a sheet of tungsten metal, from which electrons are released by exited atoms [LR50]. While an ionization of the tungsten atoms by impact of ground state atoms would violate the four-momentum conservation, the excitation energy of an incoming atom can be transferred to an electron with less binding energy, which consequently will be released. This process is called "collision of second kind" [LR50]. These free electrons are collected by a second electrode, which is connected to the tungsten sheet via a voltage source. The resulting current is proportional to the rate of excited atoms hitting the tungsten sheet. At high metastable intensities, this method is viable, but for lower intensities other methods proved to be better.

The two set-ups which are subject to this thesis utilize a different detection method. As discussed in Sect. 2.1.9 the lifetime of the metastable $2S_{1/2}$ state can be reduced drastically by electrical fields via the Stark effect. By applying a significantly stronger field to the atoms than in the spin filter, the lifetime becomes short enough that most of the remaining metastable atoms are quenched to the ground state within a small volume. Each atom, which is quenched to the ground state, emits a Lyman-α photon ($E_\nu \approx 10.2\,\text{eV}$ or $\lambda \approx 121\,\text{nm}$). The photons are converted to an electrical signal by a photomultiplier, which is specifically designed to detect photons in a small wavelength interval around the Lyman-α wavelength. For example 110 nm to 230 nm with a CsI-photocathod or 110 nm to 165 nm with a KBr-photocathod and MgF-windows. Since the photons are emitted evenly distributed in all directions only about 1 % reach the window of the photomultiplier. With a quantum efficiency of about 10 % this results in a detection efficiency of 10^{-3}. Efforts, to specify a preferred radiation direction via a magnetic field, failed, since the magnetic field disturbed the photomultiplier. In principle, with an ellipsoidal mirror made from glass with a coating of pure aluminum – the only known material which is highly reflective for Lyman-α radiation – the effective coverage of the photomultiplier can be increased. One of the two focal points is

located in the quenching region and the other one at the photomultiplier window. Since pure aluminum will build an oxide layer when exposed to air thin coatings of Lyman-α transparent MgF are needed. Experiments with such a mirror have been done in Jülich [Eng].

Another detector is currently tested by the BoB group at the TU Munich [Sch+19]. The detection principle can be seen as a combination of both methods discussed above. Instead of the tungsten sheet the beam is directed onto a Microchannel-Plate (MCP). Like the photomultiplier the MCP is based on multiplication of secondary electrons. The voltage between the front- and the back-side of the MCP, which is needed for the multiplication, can either be applied such, that the front side is on earth potential and the back side is on a positive potential, or the back side is grounded and the front side on a negative potential. In the first case the primary electrons are produced by collisions of second kind, as in the original Lamb-shift experiment. In the second case the metastable atoms see an electric field, before they hit the MCP and are quenched via the Stark effect. Now, the Lyman-α photons are able to produce free electrons via the photo-effect. Since this happens close to the surface of the MCP, a solid angle of almost 2π is covered by the detector. Unlike the original Lamb-shift experiment, in which the kinetic energy of the beam atoms was around $\frac{1}{40}$ eV and, thus, much lower than typical work functions (2 to 6 eV), the beam energy is significantly higher in typical applications of the Lamb-shift polarimeter (e.g. 325.7 eV in the BoB experiment). Although ionization by collision of neutral atoms in the ground state is less likely than by collisions with charged particles or exited atoms, a background signal from ground state hydrogen atoms cannot be ruled out. The detection efficiency and background characteristics of both operation modes are currently tested.

Another detection method which is discussed in context of the BoB experiment utilizes the charge exchange reaction $H + Ar \rightarrow H^- + Ar^+$. With an initial kinetic energy of the hydrogen atoms of 325.7 eV, the H^- ions created from ground state hydrogen atoms have a kinetic energy of 309.9 eV, while the H$^-$ ions created from hydrogen atoms in the $2S_{1/2}$ state have a kinetic energy of 320.1 eV [Sch+19]. The ions can be separated by their energy (e.g. by means of an electric counter field) and detected (e.g. with a scintillator crystal after re-acceleration and deflection from the beam).

2.5. Bound Beta Decay Experiment

Lamb-shift polarimeters can be used for a number of experiments in different fields. On example is the bound-beta decay experiment that is under preparation in a collaboration with the Technical University of Munich. As well known, a free neutron n decays into a proton p, an electron e^-, and an electron-antineutrino $\overline{\nu}_e$:

$$n \to p + e + \overline{\nu}_e \ . \tag{2.90}$$

With a branching ratio $BR \approx 4 \cdot 10^{-6}$ [Nem80], the proton and electron can be found in a bound state, which is nothing else than the hydrogen atom:

$$n \to H + \overline{\nu}_e \ . \tag{2.91}$$

About $10\,\%$ of these hydrogen atoms are expected to be in the metastable $2S_{1/2}$ state. Since this is a two body decay, the kinetic energy of the hydrogen atom is fixed with $E_{\text{kin}} \approx 325.7\,\text{eV}$, and the atom and the $\overline{\nu}_e$ move in opposing directions. If only the conservation of angular momentum is assumed, there are six possible spin configurations for the neutron decay in an external magnetic field, which are shown in Tab. 2.7. If the

Table 2.7.: Spin configurations of the neutron decay in a magnetic field [Sch+06]. With the hydrogen atoms moving in the direction of the magnetic field, the probabilities P_i for each configuration, assuming a purely left-handed V-A interaction, is derived in [NO80].

	n	→ p	+ e	+ $\overline{\nu}_e$	$B \gg B_c$	$P_i\,[\%]$
1)	↑	↑	↑	↓	$\alpha 1$	0.622(11)
2)	↑	↑	↓	↑	$\beta 4$	0
3)	↑	↓	↑	↑	$\alpha 2$	0
4)	↓	↑	↓	↓	$\beta 4$	44.14(5)
5)	↓	↓	↑	↓	$\alpha 2$	55.24(4)
6)	↓	↓	↓	↑	$\beta 3$	0

atoms which are moving in the direction of the magnetic field are detected, configurations 2), 3) and 6) would result in left-handed electron antineutrinos. Thus, these configurations are forbidden, when a purely left-handed V-A interaction is assumed. With this

assumption, the probabilities P_i of the configurations can be calculated [NO80]. Other than the states α2 and β4, the state β3 can only be formed by emission of a left-handed electron antineutrino. The detection of hydrogen atoms in the β3 state would, therefore, be proof for the existence of left-handed antineutrinos. In principle, at a kinetic energy of 325 eV of metastable hydrogen atoms a Lamb-shift polarimeter is able to measure the (relative) occupation numbers of the α states. Unfortunately, the spin filter, which is discussed in Sect. 2.4.4 cannot be used to detect the β states. One option to detect the β3 state, nevertheless, is to exchange the occupation numbers of the states α1 and β3, which is discussed in the following section. Another option, involving a new type of spin filter, is discussed in Chap. 5.

2.6. Sona Transition

The Lamb-shift polarimeter, as it is discussed in the previous sections, can be used to measure the nuclear spin polarization of ions and atoms in the ground state, which are then brought in the metastable $2S_{1/2}$ state, by determining the ratio of occupation numbers of the α states. However, in the configuration discussed before, it is not able to detect β states, since they are all forced into the ground state inside the spin filter. If, for instance for the BoB experiment [Sch+06], the β3 state of hydrogen needs to be detected, in principle a Sona transition can be used to exchange the occupation numbers of α1 and β3 [Son67]. However, as it will be discussed in the following, in practice it is rather complicated to achieve a reliable β3 measurement.

A Sona transition consists of two solenoids, which are coaxial with the beam, but with opposing magnetic fields. With this configuration a controlled zero crossing of the longitudinal magnetic field can be achieved. A schematic drawing of such a setup between two spin filters is shown in Fig. 2.23. For a hydrogen atom in state α1 both, the electron and the nuclear spin, are parallel to the magnetic field (see Eq. (2.14a)), whereas in the β3 state both spins are anti parallel to the magnetic field (see Eq. (2.14c)). If the direction of the magnetic field is reversed in the Sona transition, the spins of the atoms, which had been in state β3 are now parallel with the magnetic field, and, therefore, are then in the state α1, and vice versa. This can also be understood, by extending the Breit-Rabi diagram to negative magnetic fields, as it is shown in Fig. 2.24. This process, however,
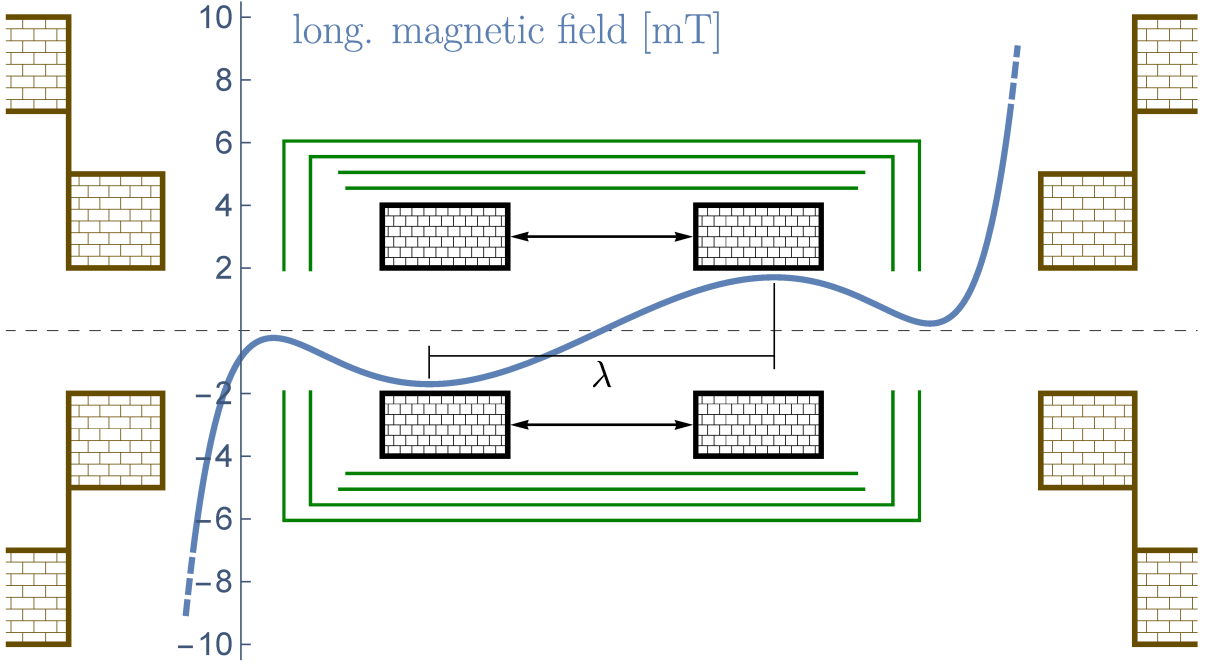
Figure 2.23.: Schematic setup of the Sona transition. The two opposing coils are shielded by four layers of μ-metal (green) against the strong stray field of the two spin filters (brown). The distance between the Sona coils is adjustable. A typical longitudinal magnetic field curve is overlayed in blue.

can only work, if the Larmor frequency of the total spin F in the radial magnetic field is lower than the reversal of the longitudinal magnetic field, which is ensured if [Son67]:

$$\frac{\partial B_\mathrm{z}}{\partial z} < \frac{8\,v_\mathrm{H}\,m_\mathrm{e}}{e\,r^2} \quad , \tag{2.92}$$

with $v_\mathrm{H} = \sqrt{2E_\mathrm{kin}/m}$ being the velocity of the hydrogen atoms, $m_\mathrm{e} = 511\,\mathrm{keV/c^2}$ the electron mass, $e = 1.602 \cdot 10^{-19}\,\mathrm{C}$ the electron charge, and r the radius of the beam. Otherwise, the spins would be able to reverse their direction within a half Larmor precession too, and, thus, stay in their initial state. From Gauss law for magnetism ($\nabla \cdot \boldsymbol{B} = 0$) and the symmetries of a solenoid follows for the radial component of the magnetic field:

$$B_\mathrm{rad}(z, \rho) = -\frac{\rho}{2} \cdot \frac{\partial B_\mathrm{z}}{\partial z} \quad , \tag{2.93}$$
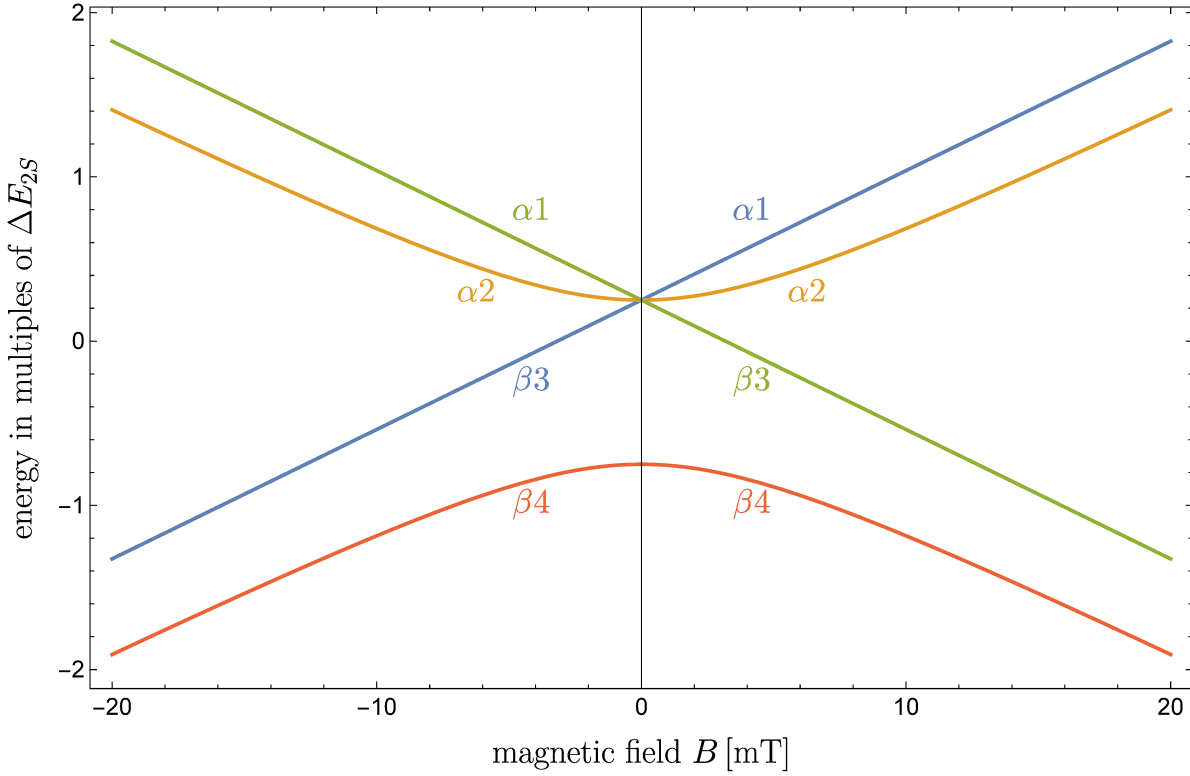
Figure 2.24.: Breit-Rabi diagram for $2S_{1/2}$ of hydrogen around $B = 0$. By crossing $B = 0$ α1 becomes β3 and β3 becomes α1. The states α2 and β4 do not change.

where ρ is the distance from the z-axis. Because the atoms are traveling through the magnetic field with a constant velocity the z-dependence of the magnetic field can as well be expressed as a time dependence. Thus, the atoms will experience a changing magnetic field in time. With a Fourier analysis of the radial magnetic field the harmonic frequencies of the electromagnetic field seen by the atoms during their flight can be obtained. Noteworthy, these frequencies are fully determined by the velocity v_{H} of the atoms and the geometry of the Sona transition (expressed in the wavelength λ), but are independent of the magnetic field strength in the Sona coils and the radial distance of the atom from the beam axis. The important[10] second harmonic frequency is:

$$\nu = \frac{v_{\mathrm{H}}}{\lambda} \quad . \tag{2.94}$$

---

[10]The first harmonic corresponds to a half wave only, while the second harmonic, a full wave, represents a photon in the particle picture.

Typical orders of magnitude are: $v_{\mathrm{H}} \sim 10^5\,\mathrm{m\,s^{-1}}$, $\lambda \sim 10^{-1}\,\mathrm{m}$ and, thus, $\nu \sim 1\,\mathrm{MHz}$. The oscillating radial magnetic field can induce σ-transitions in the atom, if the energy difference between the initial state and a suitable ($\Delta m_F = \pm 1$) final state is equal to $E_{\mathrm{ph}} = h\nu$ or an integer multiple of it. Thus, at different magnetic fields in the Sona coils (multi-) photon transitions occur between $\beta 3$ and $\alpha 2$ and between $\alpha 2$ and $\alpha 1$. The dominating magnetic field B that defines the energy difference between the substates corresponds directly to the maximal longitudinal field inside the Sona coils. In Fig. 2.25 the (multi-) photon transitions for $\nu = 5\,\mathrm{MHz}$ (e.g. $v_{\mathrm{H}} = 5 \cdot 10^5\,\mathrm{m\,s^{-1}}$, $\lambda = 10^{-1}\,\mathrm{m}$) are drawn into the Breit-Rabi diagram. Consequently, atoms starting in the $\beta 3$ state
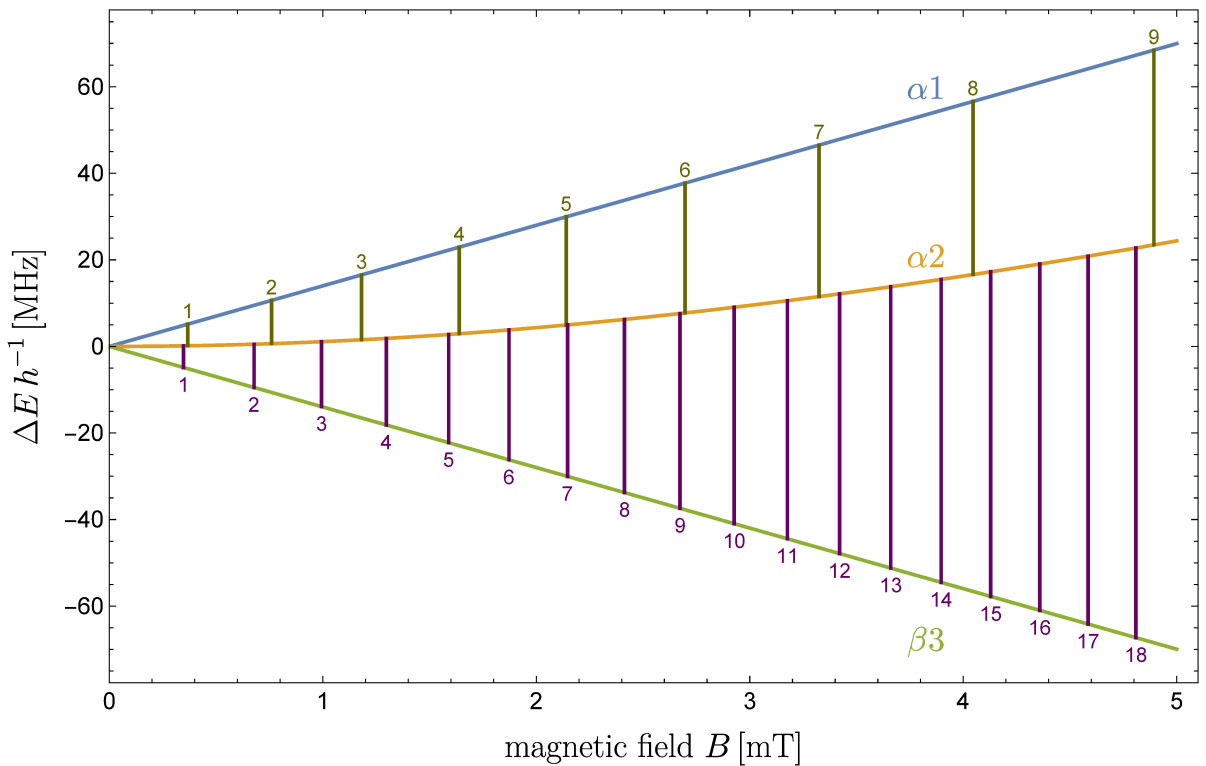
Figure 2.25.: Transitions in $2\mathrm{S}_{1/2}$ of hydrogen induced by $B_{\mathrm{rad}}(t)$ in a Sona set up with $\nu = 5\,\mathrm{MHz}$. The counting labels also indicate the number of photons needed for the transition. Noteworthy, the difference in magnetic fields between two $\alpha 2 \leftrightarrow \alpha 1$ transitions increases with the magnetic field, while the difference between two $\alpha 2 \leftrightarrow \beta 3$ transitions decreases.

before the Sona transition, are initially in state $\alpha 1$ after the zero crossing, but from there they may change to the $\alpha 2$ state and in a second step even back to $\beta 3$. Thus, not all atoms in $\beta 3$ will end up in $\alpha 1$. Moreover, atoms starting in state $\alpha 1$ before the

Sona transition, are initially in β3, but can change to the α2 state in a first step and back to α1 in a second one. Atoms starting in state α2 are not affected by the field reversal directly, but, nevertheless, experience an electromagnetic field which can induce transitions to α1 or β3. Thus, not all atoms ending up in α1 had been in state β3 before the Sona transition. However, with known and fixed beam velocity and geometry of the Sona setup, the magnetic field in the Sona coils can be adjusted such, that it is positioned right between possible transitions in the Breit-Rabi diagram. In conclusion, an exchange of the occupation numbers of β3 and α1, and, therefore, a measurement of the β3 occupation number is not trivial, but needs precise knowledge and control of the beam velocity, the geometry and the magnetic field strength in the Sona transition. Moreover, the fact, that the wavelength λ and frequency ν of the electromagnetic field, the atoms interact with, are not linked to each other via the speed of light, but the velocity of the atoms, opens up the opportunity for a new kind of spectroscopy. I.e., if one wants to perform a spectroscopy measurement with a standing electromagnetic field in a cavity with a frequency $\nu = 1\,\mathrm{MHz}$, the cavity will need to have a size of about $300\,\mathrm{m}$, which is rather unpractical, while the Sona setup allows for the same frequencies in a space of less than a meter. Therefore, a well-tuned Sona transition unit can be a helpful tool to increase the options of a Lamb-shift polarimeter.

3. Preparatory Measurements

As mentioned in Chap. 1 the measurements presented in this thesis were performed with two different Lamb-shift polarimeter setups. One is located in the Institute of Nuclear Physics (IKP) at the research center Jülich, the other in the Budker Institute of Nuclear Physics (BINP) in Novosibirsk. The setup at the BINP is part of a research cooperation supported by Deutsche Forschungsgemeinschaft (grant no. BU 2227/1-1) and the Russian Science Foundation (grant no. RSF 16-42-01009). Apart from the ionizer, which was manufactured at the BINP to the same blueprint the ionizer in Jülich was made from, the parts for the Lamb-shift polarimeter were build and pre-assembled at the IKP and then shipped to Novosibirsk. Measurements of the magnetic field homogeneity inside the spin filter at different currents (see Sect. 3.4.1), the magnetic field in the cesium cell at different currents (see Sect. 3.3) and the resonance curve of the cavity (see Sect. 3.4.2), were performed prior to the shipment. A re-measurement of the resonance curve showed, that the cavity was not affected by any impacts or vibrations during transport. It is assumed, that the homogeneity of the magnetic field of the spin filter is not compromised either, since it is much more robust than the cavity. For the shipment the bench with the mounted Lamb-shift polarimeter parts and the rack with all power supplies were packed together in a box, while the photomultipier, cables, the pre-pump and other auxiliaries were packed in a second box. Apart form a broken water supply connection on one of the cesium cell coils no damages were found. The damaged water supply connection is a minor problem, since the coil can still be cooled by a second water cycle and the temperature of the water supply usually is fairly low. A vacuum leak, between a teflon connection piece and the photomultiplier, was found and fixed by enlarging the inner diameter of the teflon piece, so that the photomultiplier is able to slide into the opening more easily. Another problem occurred, when the first cesium ampule was cracked in the cesium cell. Due to its slightly different shape compared to those which are used in Jülich, it did not break at the bottom as intended, but at the

top. Consequently the liquid cesium initially was not able to drop down to the bottom of the cesium cell. By carefully rotating the cell back and forth by more than 90° without braking the vacuum a sufficent amount of cesium was transferred to the main chamber of the cell. This rotation was only possible, because the special "Karlsruher Norm" vacuum connection. Unfortunately, during this procedure, a piece of glass probably got stuck in such a way that part of the beam was blocked and the intensity was reduced. A higher intensity was only achieved again after the cesium was renewed. The ionizer was mounted to the bench of the Lamb-shift polarimeter and connected to the Wienfilter with a valve in between. Since all parts of the Lamb-shift polarimeter are mounted on the same bench, an alignment is easily achievable, whereas the alignment between the beam source and the Lamb-shift polarimeter is rather difficult, since there is no fixture or bench, on which the beam source is mounted to. Therefore, the bench of the Lamb-shift polarimeter has to be aligned with the beam tube of the source manually. A picture of the setup at BINP is shown in Figure 3.1. In the following primarily the components of the Lamb-shift polarimeter at the BINP are described. The components of the Lamb-shift polarimeter in the IKP are very similar.
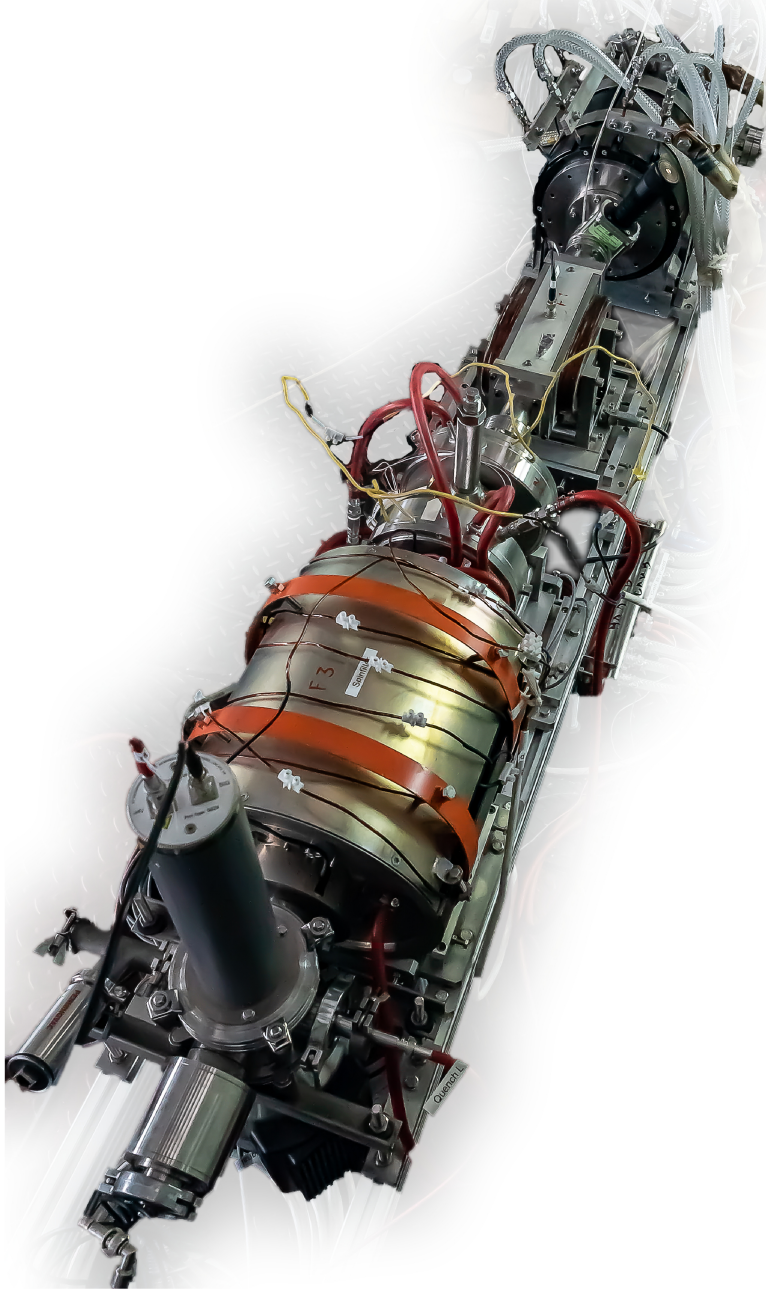
Figure 3.1.: The Lamb-shift polarimeter at BINP. From top right to bottom left the components are: Ionizer, Wienfilter, cesium cell, spin filter, and quenching chamber.

3.1. Ionizer

The ionizer for the BINP Lamb-shift polarimeter is of the Glavish type. A short description of the working principle of such an ionizer can be found in Sect. 2.4.1.

To provide strong magnetic fields, the solenoidal coil is made from copper pipes with a quadratic outer cross-section ($0.5\,\mathrm{cm} \times 0.5\,\mathrm{cm}$), and a circular inner cross-section (diameter $= 0.3\,\mathrm{cm}$), though which cold water is forced. This way currents of up to $600\,\mathrm{A}$ can be send through the coils without overheating, resulting in magnetic fields of about $0.5\,\mathrm{T}$. A thick iron jacked reduces stray fields. Inside four ring-shaped and one cylindrical electrode and a wolfram filament are mounted on three threaded rods. Each electrode is connected to a high voltage vacuum feed-through. Thus, they can be set on different electrical potentials. The filament is connected to a higher current feed-through, to allow currents of up to $8\,\mathrm{A}$ to heat the tungsten wire to more than $2500\,\mathrm{K}$. The third electrode, which is the cylindrical one, is perforated to allow for better pumping. Around the inner electrode structure a getter pump, consisting of several cartridges and heating elements, is mounted. When activated, it is able to absorb about $2000\,\mathrm{l\,s^{-1}}$ of H_2 or D_2, and to collect other gases, except noble gases, due to chemical binding on the surface. Thus, residual unpolarized gas is removed and, consequently, the background signal is reduced [Eng+05].

In the ideal case, the kinetic energy is determined by the third electrode exclusively. Unfortunately, during very recent measurements with the Sona transition unit in Jülich, it was realized, that this is only the case if the ionizer is working in the electron collision mode and not in the – much more efficient – plasma mode. In the plasma mode the beam energy is influenced by the potential of the second electrode, since the plasma is build up due to the electrical gradient field between these electrodes. Therefore, the beam energy gets smaller than the corresponding potential at the third electrode. An example of the beam energy as function of the potential at the third electrode is shown in Fig. 3.2. Since the beam energy in the plasma mode is most likely also a function of the vacuum pressure and the potentials of the second electrode, the data shown in Fig. 3.2 can not be regarded as a calibration curve, but instead the beam energy has to be determined differently, if the ionizer is operated in the plasma mode. As discussed in Sect. 2.4.2 the magnetic field in the Wienfilter has to be adjusted to the beam energy, when the polarization of protons and deuterons is measured. Therefore, an energy
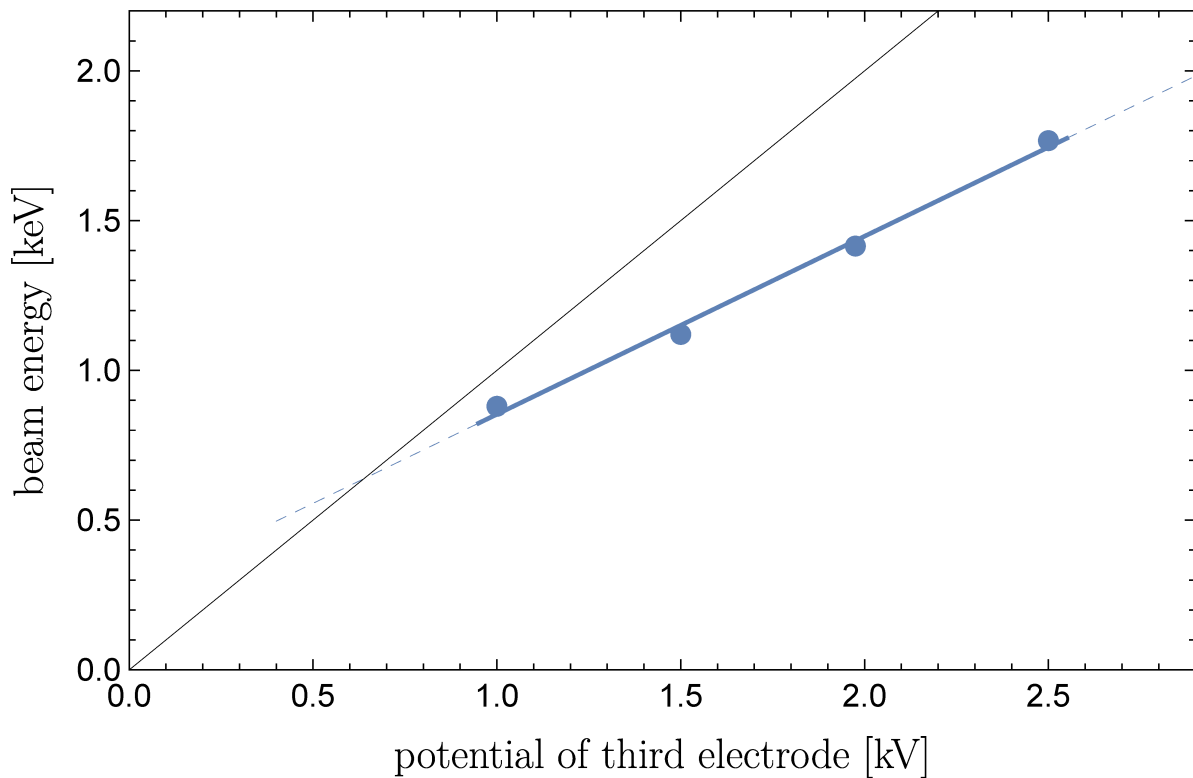
Figure 3.2.: The beam energy determined by the analysis of the Sona measurements as function of the potential of the third electrode of the ionizer (blue). Ideally, the data points would lie on the black line.

calibration of the Wienfilter would be desirable. With low pressure, in the ionizer, the ionizer operates in the electron collision mode. Hence, the beam energy is determined by E3. By varying the magnetic field in the Wienfilter and detecting, at which electric field the protons are able to pass with a Faraday-cup, such a calibration curve can be acquired. For measurements with molecular ions, however, it is not necessary to know the beam energy precisely, for the Lamb-shift polarimeter to work properly, since the measured polarization is not influenced by the Wienfilter.
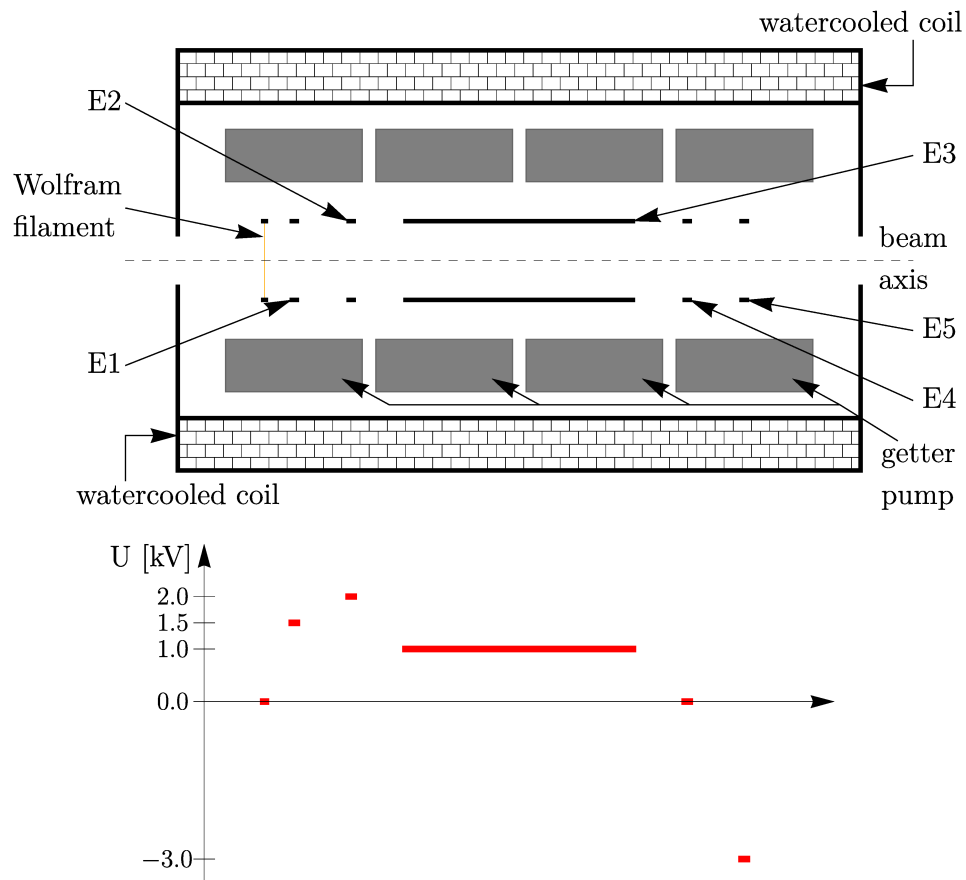
Figure 3.3.: A schematic drawing of the ionizer and typical potentials of the electrodes. Atoms and molecules enter the ionizer from the left. Electrons are emitted by the hot wolfram filament. Inside the cylindrical electrode E3 they, preferably, collide and ions are produced. The ions are then accelerated towards the right.

3.2. Wienfilter

As discussed in Sect. 2.4.2 a Wienfilter utilizes perpendicular magnetic and electric fields to filter the ion beam by the velocity of the particles, and, thus, by their mass. Hence, it is possible to measure the polarization of each ion type (H^+, H_2^+, D^+, HD^+, and D_2^+) separately. The only exceptions are the two ions H_2^+ and D^+, since the difference of their masses can not be resolved by the Wienfilter. However, since the spectra of metastable hydrogen and deuterium measured by the spin filter are easily distinguishable, this is not a problem. The Wienfilter send to BINP is a relatively simple, but nevertheless

effective and reliable device, which had been used in an older Lamb-shift polarimeter in Cologne. It consists of a cuboid vacuum chamber made from aluminum, with two isolated, parallel stainless steel plates – one on the top and one on the bottom of the chamber. Outside of the chamber, a thick plate of magnetic steel is mounted on each side. Coils around a yoke, connecting both plates, are glued to them. The yoke also serves as holding structure. A picture of it is shown in Fig. 3.4. The coils are only
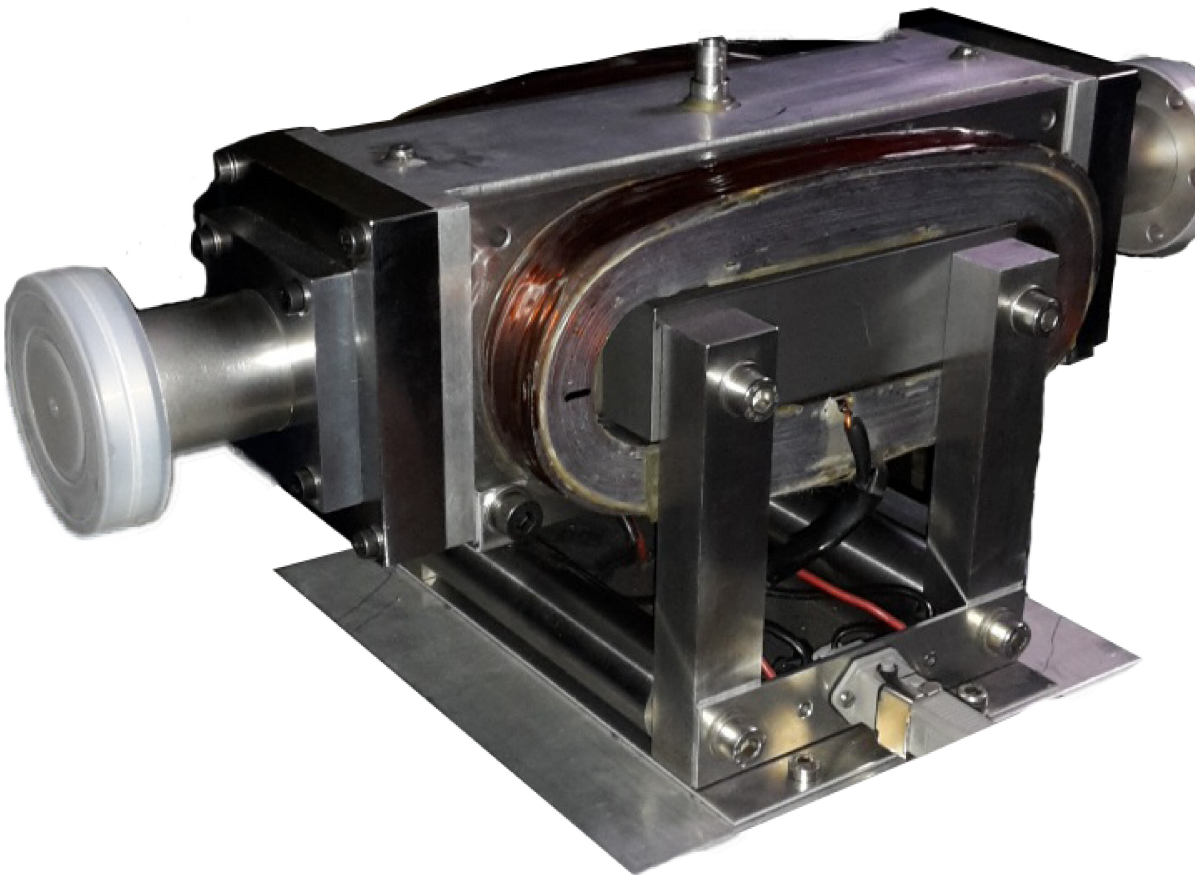
Figure 3.4.: The Wienfilter for the Lamb-shift polarimeter at BINP.

cooled by convection, but can still be operated safely with currents up to 8 A, resulting in a magnetic field of about 33 mT in the center of the Wienfilter. A calibration curve is shown in Fig. 3.5. As discussed before, the nuclear spin of protons and deuterons will precess in the Wienfilter due to the Larmor precession, and, thus, the measured polarization is a function of the magnetic field in the Wienfilter (see Eq. (2.51)). With a known rotation angle the measured polarization can be corrected. Therefore it is reasonable to measure a "Wienfilter curve" for each beam energy, at which the Lamb-
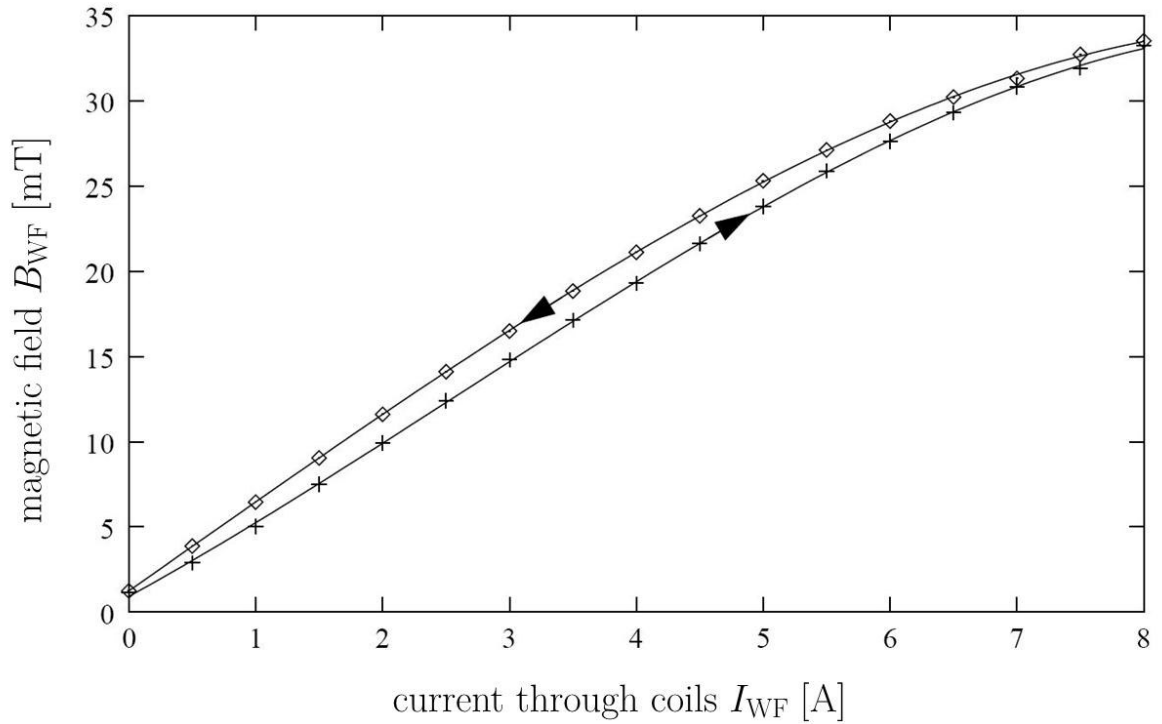
Figure 3.5.: The calibration curve of the Wienfilter at BINP. Measured at its former place of use in Cologne [Eng+02]. The magnetic field was measured at the center of the Wienfilter. Up to about 5 A saturation effects are small and the curve is almost linear. The magnetic steel causes a hysteresis, therefore, the "direction" from which the current is set is important to obtain consistent magnetic fields. Without any current a small magnetic field is still present due to the magnetization of the steel.

shift polarimeter is operated. In Fig. 3.6 the measured polarization as a function of the current through the coils is shown for a beam energy of 2000 eV. In this case the polarization vector is rotated by 180° at a current of about 2.70 A. Measurements with protons at this energy should therefore be done, with a current through the Wienfilter coils of 2.70 A. The measured polarization then needs to be corrected by the factor $C_{WF} = -1$.

$$p_{\mathrm{m}}(I) = 0.007 - 0.569 \cdot \\ \cdot \cos(1.103\frac{I}{\mathrm{A}} + 0.163)$$
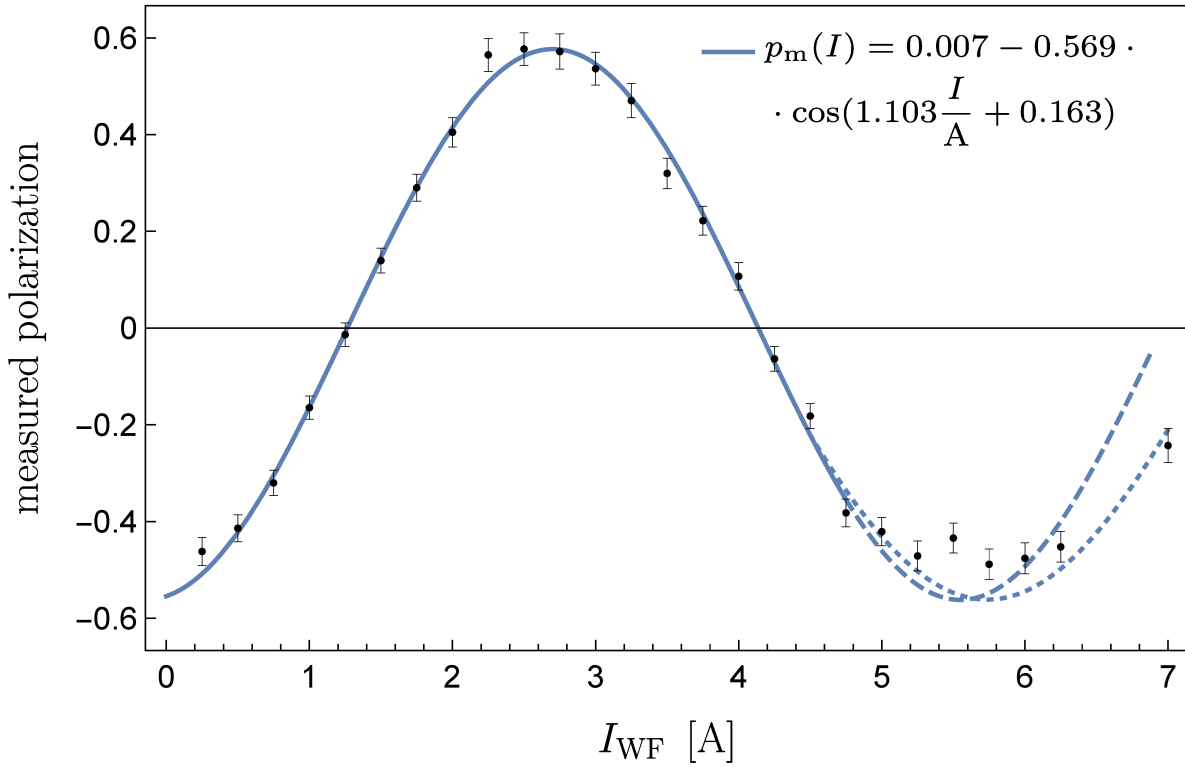
Figure 3.6.: Wienfilter curve for a proton beam. The measured polarization is a function of the magnetic field in the Wienfilter. At $I = 2.70\,\mathrm{A}$ the polarization vector is rotated by $\alpha = \pi$ and the maximum measured polarization is 0.576. With the correction factor for $\alpha = \pi \Rightarrow C_{\mathrm{WF}} = -1$ the polarization of the proton beam was determined to be -0.576. At currents above $5\,\mathrm{A}$ the magnetic field saturates (see Fig. 3.5), thus the "frequency" of the cosine curve decreases.

3.3. Cesium Cell

The cesium cell essentially consists of a vacuum chamber, with heatable bottom and top parts, a mechanism to hold and crack glass ampules filled with cesium, and two water-cooled coils outside of the chamber. The chamber is made from stainless steel. Both, the bottom and the top piece incorporate two boreholes each, which are equipped with a heating cartridge and a Pt-100 thermal sensor. A picture of the cesium cell send to Novosibirsk is shown in Fig. 3.7. In combination with two PID controller the heating cartridges and the Pt-100 sensors ensure stable temperature settings of the bottom and the top ($\Delta T \leq 0.1\,°C$). With the temperature of the bottom the vapor pressure over the liquid cesium (melting point: $28\,°C$ at $1013\,mbar$) is controlled (see Eq. (2.57)). The vapor will rise in the cell and cross the beam before it will hit the top. Since the top is set to a lower temperature (usually around $60\,°C$) the vapor condenses and the liquid cesium will drop back to the bottom of the cell, closing the cycle. Noteworthy, the vapor will cool down while rising due to collisions with the cooler walls, which cause the vapor pressure, and therefore, the number density of cesium atoms in the beam-vapor interaction region to be lower than one would expected by considering the bottom temperature only. Earlier measurements indicate, that the number density in the interaction region can be approximated by multiplying the number density, calculated from the bottom temperature, by a factor of 0.44 [Eng+14].

The two coils – one on each side of the cesium cell – are concentric with the beam axis, and thus create a longitudinal magnetic field. As discussed in Sect. 2.4.3, a strong magnetic field in the beam-vapor interaction region is necessary to preserve the polarization during the production of the metastable atoms. The magnetic field profile along the beam axis was measured at different currents (see Fig. 3.8). Averaged over the interaction region, the magnetic field as function of the current through the coils is plotted in Figure 3.9. When cooled with water, the coils can safely be operated with currents of $20\,A$. The critical magnetic field for $H_{2S_{1/2}}$ ($B_c = 6.34\,mT$) is reached at approximately $2.55\,A$, while the critical magnetic field for $D_{2S_{1/2}}$ ($B_c = 1.5\,mT$) is already surpassed with currents grater than $0.58\,A$.

Apart from the important polarization preservation the magnetic field has a second effect: Due to the Lorentz force all ions, which are not perfectly parallel to the magnetic field, are forced on corkscrew-like trajectories. This increases their average path-length
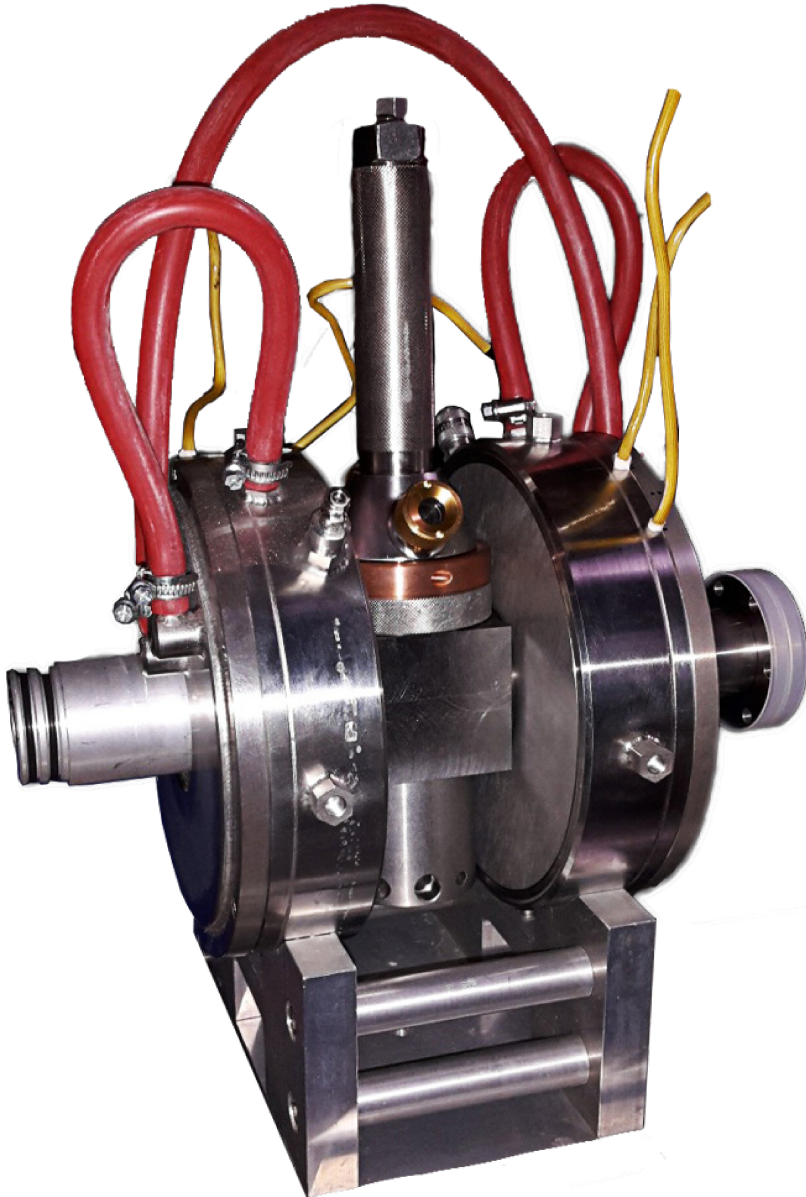
Figure 3.7.: The cesium cell at the BINP. The interaction region is in the central cubic
part. Underneath the liquid cesium is stored and heated. Above one of
two windows is visible. A stamp inside the long cylinder is used to crush
the cesium ampule. The coils are electrically connected in series. On the
left the "Karlsruher norm" connects to the spin filter, while on the right a
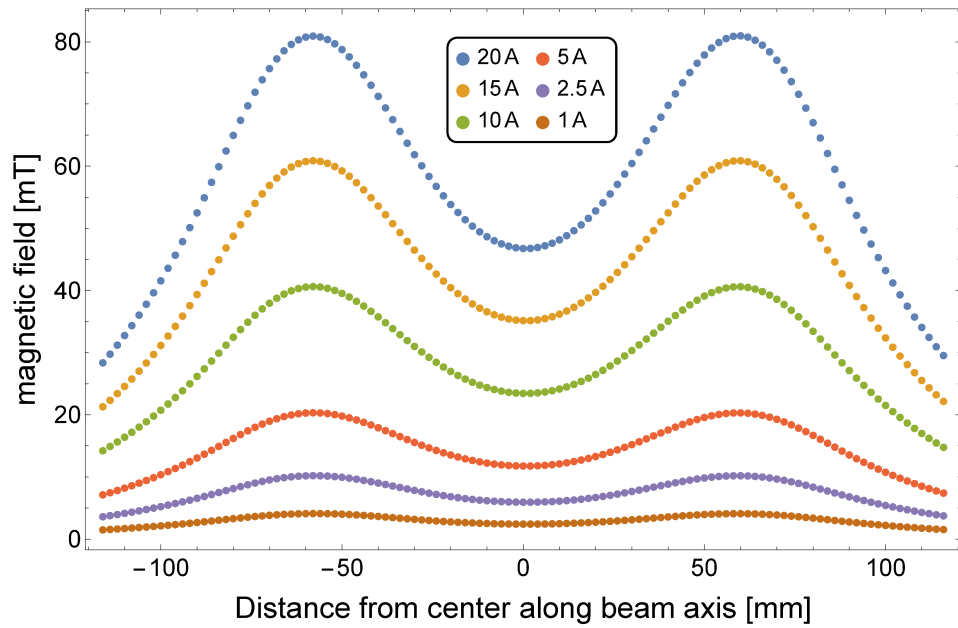CF-flange connects to the Wienfilter.

Figure 3.8.: Magnetic field in the cesium cell along the beam axis for different currents. The production of metastable atoms takes place in an interval of about ±15 mm around the center.
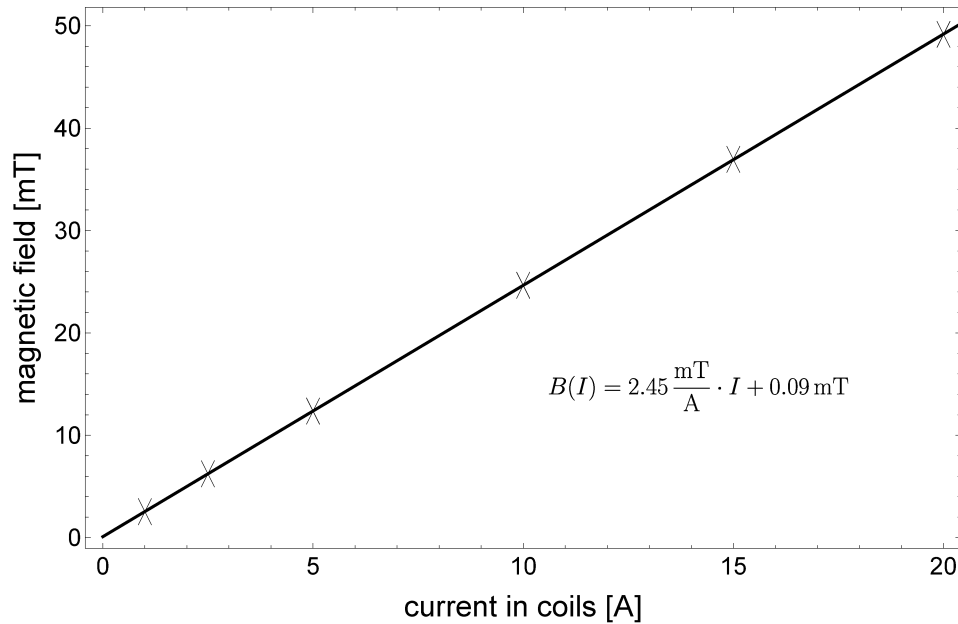
Figure 3.9.: Mean magnetic field strength in the interaction region as function of the current through the coils. The linear fit can be used as calibration curve. The small offset of 0.09 mT is due to a small remanence of the cesium cell.

in the cesium vapor. Accordingly the vapor pressure can and should be decreased to achieve maximum efficiency for the production of metastable atoms, which has the benefit, that the rate the cesium dissipation is reduced. With $B_{\text{rad}}(z, r) = {}^{-dB_z}/_{dz} \cdot {}^{r}/_{2}$ the radial component of the magnetic field for a radial distance r from the axis at a distance z from the center of the cell can be calculated. Even at $r = 8\,\text{mm}$ the radial magnetic field stays below $2\,\text{mT}$, so that misrepresentation of the polarization due to tilting of the polarization vector is lower than $0.06\,\%$, and therefore, negligible.

3.4. Spin Filter

As discussed in Sect. 2.4.4 the spin filter is the most essential part of a Lamb-shift polarimeter, as it allows for a selective transmission of atoms in a single α state, while atoms in all other metastable $2S_{1/2}$ states are forced into the ground state. To achieve this, a finely tuned combination of static magnetic, static electric and radio frequency electromagnetic fields are needed. The static magnetic field is provided by a solenoid, coaxial with the beam. In the center of the solenoid a special cavity is located, which supplies both, the static electric field and the radio frequency electromagnetic field. The cavity is primarily designed to have a resonance frequency ν_0 of $1.609\,75\,\text{GHz}$ and a quality factor $Q \in [1000; 3000]$. A schematic drawing of a spin filter is given in Fig. 3.10.

3.4.1. Solenoid

The solenoid is designed to create magnetic fields with a high homogeneity at every field strength between $50\,\text{mT}$ and $65\,\text{mT}$ in the region of the cavity. It consists of five coils, which are electrically connected in series. The windings of the central three coils – one main and two secondary coils – are easy to access, so windings can be added or removed to meet the required homogeneity of $\frac{\Delta B}{B} \leqslant 10^{-3}$. The two end coils decrease the gradients to avoid quenching due to fast changing fields the metastable atoms experience while entering and leaving the spin filter. Access to their windings is not needed, since their influence on the homogeneity of the central part is negligible.

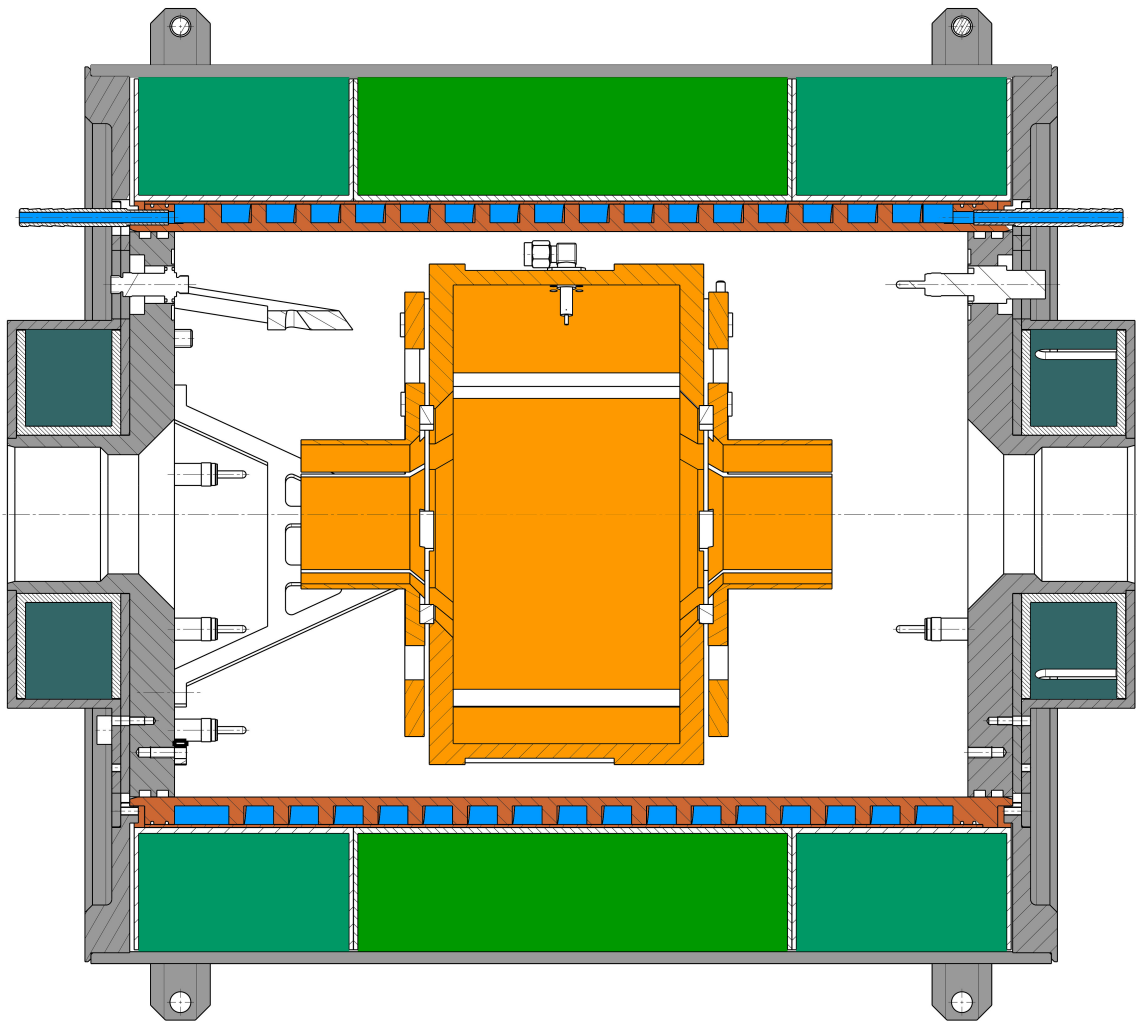Since each α state is transmitted, through the spin filter in a small magnetic field interval

Figure 3.10.: Schematics of a spin filter. The homogeneous magnetic field is primarily generated by the **main coil** and the two **secondary coils**, while the two **end coils** reduce the gradients at both ends of the spin filter. The main and secondary coils are cooled by a copper **heatsink** run through by **water**. The outer parts of the holding structure are made from materials with high permeability to also purpose as magnetic yock. The **cavity** and its holding structure are made from materials with low permeability to minimize their effect on the magnetic field.

only (see Sect. 2.4.4), the field obviously should vary less than the range of the interval over the length of the cavity at a fixed current through the coils. Thus, the homogeneity is an important factor for the transmittance of α states. Moreover, the transmittance should not vary for each individual α state as this would influence the transmission of

metastable atoms in this state and, therefore, the measured polarization. E.g., if the α1 state of hydrogen has a higher transmittance than the α2 state, the measured polarization would always tent more to "+1" compared to the real polarization. The homogeneity of the magnetic field, therefore, should be as good as possible throughout the whole range the spin filter is operating at and be the same for all five magnetic fields, at which the α states are transmitted. To tune the solenoid for maximum homogeneity, the magnetic field was measured along the axis. Then the mean value of the field spanning over the whole cavity plus some safety margins was calculated and the relative deviation of each data point from the mean was plotted. This was done for five currents, each producing a mean magnetic field close to one of the fields at which a α state is transmitted. If the relative deviation from the mean exceeded $\pm 10^{-3}$ anywhere in the region of the cavity windings were removed or added to the coils respectively at this position. Before any tuning, the solenoid of the spin filter for BINP was able to provide magnetic fields, with homogeneities in the order of 10^{-2}. After about two weeks of measurements and tuning the relative deviation was consistently lower then 10^{-3} in the critical region and for all fields, at which the α states are transmitted. A plot of the magnetic fields along the (whole) spin filter is shown in Fig. 3.11. In Fig. 3.12 the homogeneity after tuning is shown for a mean magnetic field of 53.5 mT as an example. Plots showing the final homogeneity for the four other magnetic fields of interest are provided in Appendix A.1.
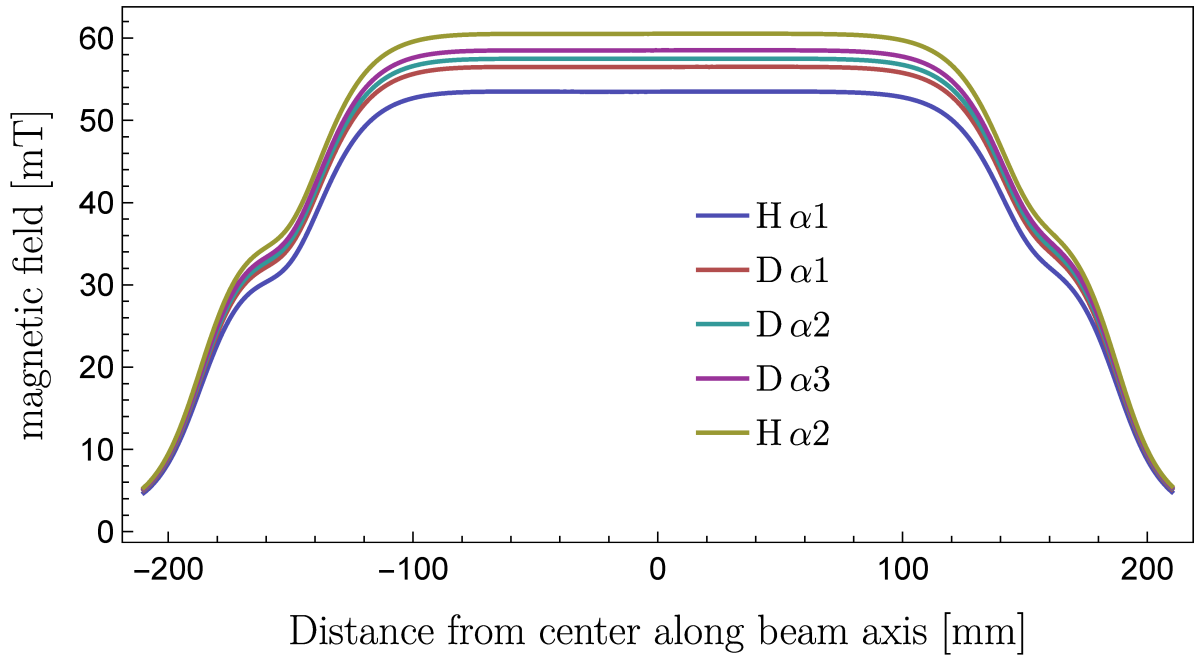
Figure 3.11.: Longitudinal magnetic field along the axis of the spin filter at five different currents, which produce the five magnetic fields – in the central region – at which the individual α states of hydrogen and deuterium are transmitted.

3.4.2. Cavity

The cavity, providing both, the perpendicular static electric and radio frequency electromagnetic fields, is located in the center of the solenoid. A picture of a cavity is shown in Fig. 3.13. The cavity is divided in three cylindrical sections along the beam axis, a central part, in which the radio frequency field is stored and two identical parts, with half the diameter of the central one, at both ends, to confine the radio frequency field to the central part. Each of those sections again is subdivided into quadrants. The outer quadrants are attached to the inner ones, building four units. Those four units are mounted on a holding structure, which allows for small and controlled changes of the radial position of all units individually.

Two opposing quadrants of the center part feature small antennas: One is connected to a frequency generator, supplying the radio frequency, and the other serves as pick up loop to measure the power inside the cavity, which is needed to tune the cavity's quality factor and resonance frequency. About 10% of the input power is extracted this way. The other two opposing quadrants are connected to high voltage power supplies
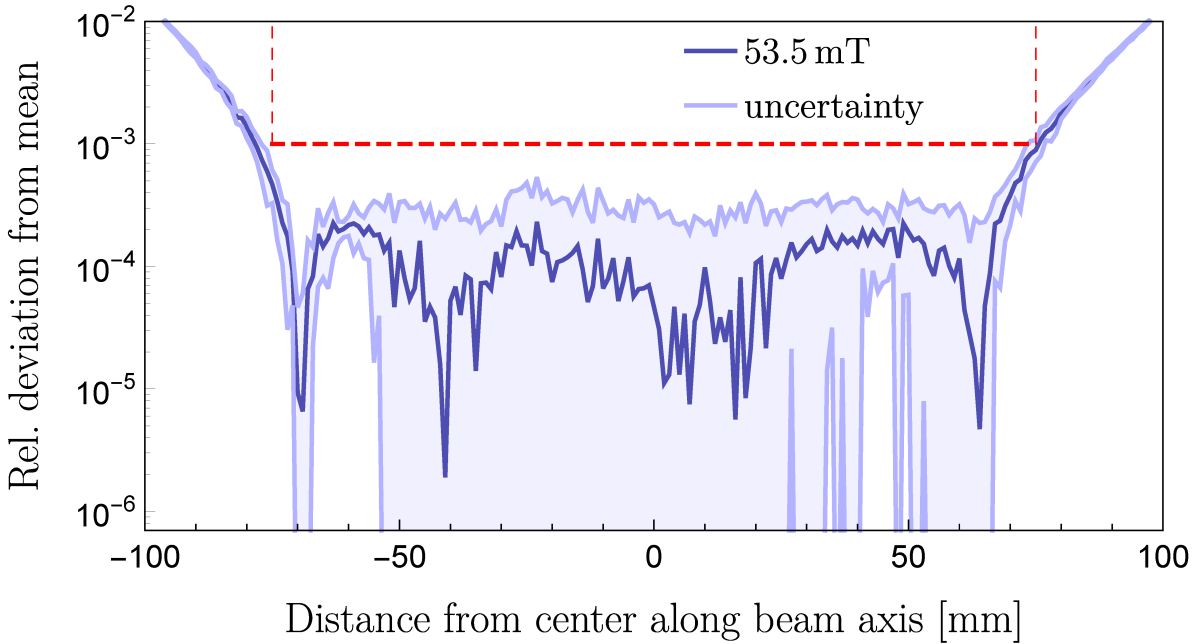
Figure 3.12.: Homogeneity of the magnetic field along the axis of the spin filter with a mean magnetic field of about $53.5\,\mathrm{mT}$ is better than 10^{-3} for a length of about $150\,\mathrm{mm}$. As measure for the homogeneity the absolute value of the relative deviation of the magnetic field at position z from the mean magnetic field $\overline{B} = \frac{1}{n} \sum\limits_{z=-75\,\mathrm{mm}}^{z=75\,\mathrm{mm}} B(z)$ is used: $\left| \frac{B(z) - \overline{B}}{\overline{B}} \right|$.

– one of positive and one of negative polarity – to provide an electric field in the order of $10\,\mathrm{V\,cm^{-1}}$. With an inner diameter of about $14.2\,\mathrm{cm}$ the voltages are around $\pm 70\,\mathrm{V}$. The smaller quadrants, mounted to the larger ones, which are connected to high voltage power supplies, are also connected to high voltage power supplies. This way the static electrical field extents to both ends of the cavity. The smaller quadrants, mounted to the larger ones, which are equipped with antennas, are electrically connected to those. All four central quadrants have an inner radius of $71\,\mathrm{mm}$, so that they enclose a cylinder with a diameter $d = 142\,\mathrm{mm}$. With $\lambda = \frac{c}{\nu} = \frac{2.99792}{1.60975} \frac{10^8}{10^9} \frac{\mathrm{m\,s^{-1}}}{\mathrm{s^{-1}}} = 186\,\mathrm{mm}$ and $d = \frac{\lambda}{1.31}$ for $\mathrm{TM_{010}}$-resonances ([MG86]), the enclosed cylinder fits the required frequency. In a $\mathrm{TM_{010}}$-resonance the electric field oscillates longitudinally in the cylinder, while the magnetic field oscillates radially, as sketched in Fig. 3.14. With this orientation, electric dipole transitions between the α states and the e states can be induced. The quadrants have an internal length $l = 76\,\mathrm{mm}$, and, thus, the quality factor of a perfect cylinder of

this dimensions would calculate to [MG86]:

$$Q = 0.38 \, \frac{\lambda}{\delta} \, \frac{1}{1 + 0.5 \, {}^{d}\!/_{l}} \approx 18000 \ , \tag{3.1}$$

with $\delta \approx 2 \, \mu\text{m}$ being the skin depth, which is a function of frequency and material. This quality factor is neither desired – it should be $Q \in [1000; 3000]$ (see Sect. 2.4.4) – nor achievable in practice, since the gab between the quadrants and inevitable inaccuracy in the manufacturing process will reduce the quality factor drastically. In fact, the cavity originally build for the Lamb-shift polarimeter in BINP could not reach the desired quality factor, even after minute tuning and applying several tricks, like: gold plating for better conductivity on the surface, optimization of the contact between the jacket and the base plates of the cylinder quadrants, wrapping with copper foil on the outside, and adjusting of the antenna size and orientation. The search for the reason of the bad quality factor of this cavity is still going on. Instead, a cavity of identical construction was taken from a different spin filter in Jülich. Despite no known or obvious differences this one works well and tuning to quality factors of $Q \approx 2500$ can be done consistently. It didn't even lose its setting after transporting from Jülich to BINP, which is surprising, since even minor changes in relative position of the quadrants to each other will change the quality factor significantly. A measurement of the resonance curve is shwon in Fig. 3.15.

It is worth noting, that the resonance frequency differs between operation in air and vacuum, since the resonance wavelength is defined by the diameter of the cavity and therefore is fixed, while the corresponding frequency is a function of the speed of light ($\nu = \frac{c}{\lambda}$), which is smaller in air by approximately 0.28‰. Furthermore the resonance frequency increase with temperature, due to the thermal expansion of the cavity. The quality factor, however, which is much more important than the exact resonance frequency, is not effected significantly by neither temperature nor difference in speed of light.
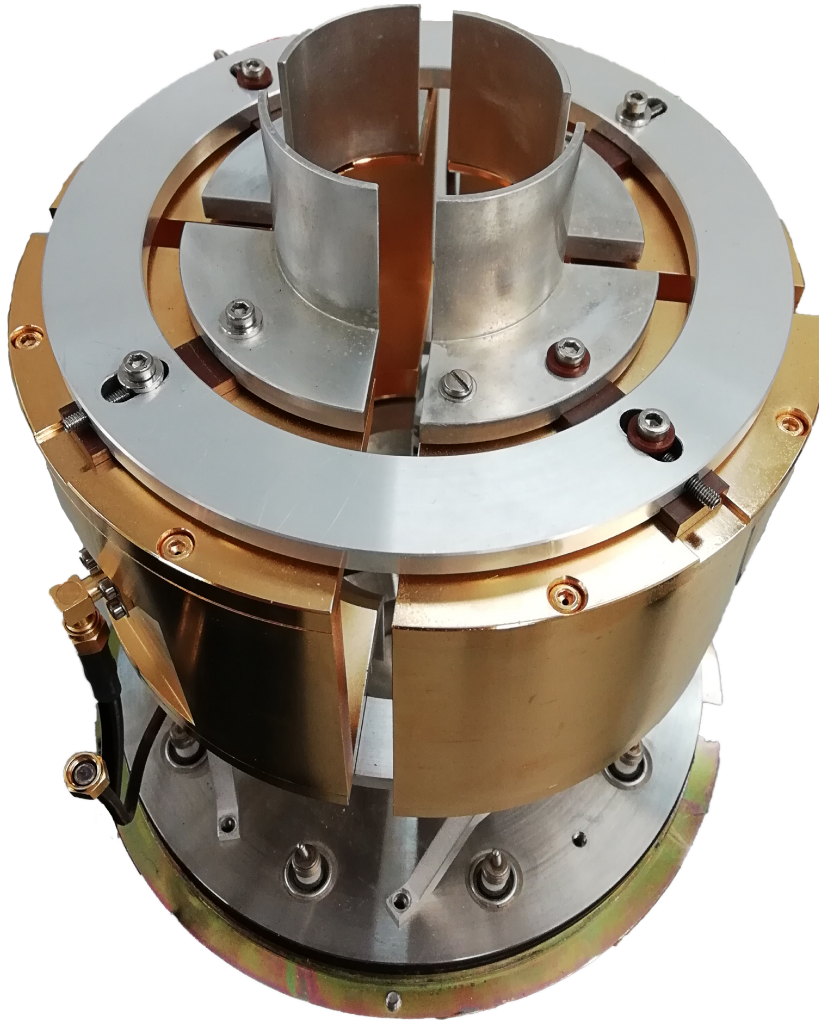
Figure 3.13.: A cavity as it is used in a spin filter. The four golden quadrants form the central part of the cavity. To each of them two smaller quadrants (silver colored) are attached, one visible on the top side and one hidden on the bottom side. At 8 o'clock in the picture a connection for the radio frequency signal can be found. Another one is positioned at the opposite side. The silver colored ring on the top is part of the holding structure. It includes four slotted holes and headless screws to set the relative positions of the quadrants.
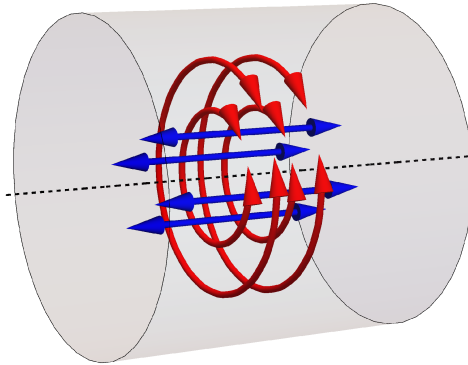
Figure 3.14.: Sketch of a TM$_{010}$-resonance. The electric field is indicated by blue arrows and the magnetic field by red arrows.
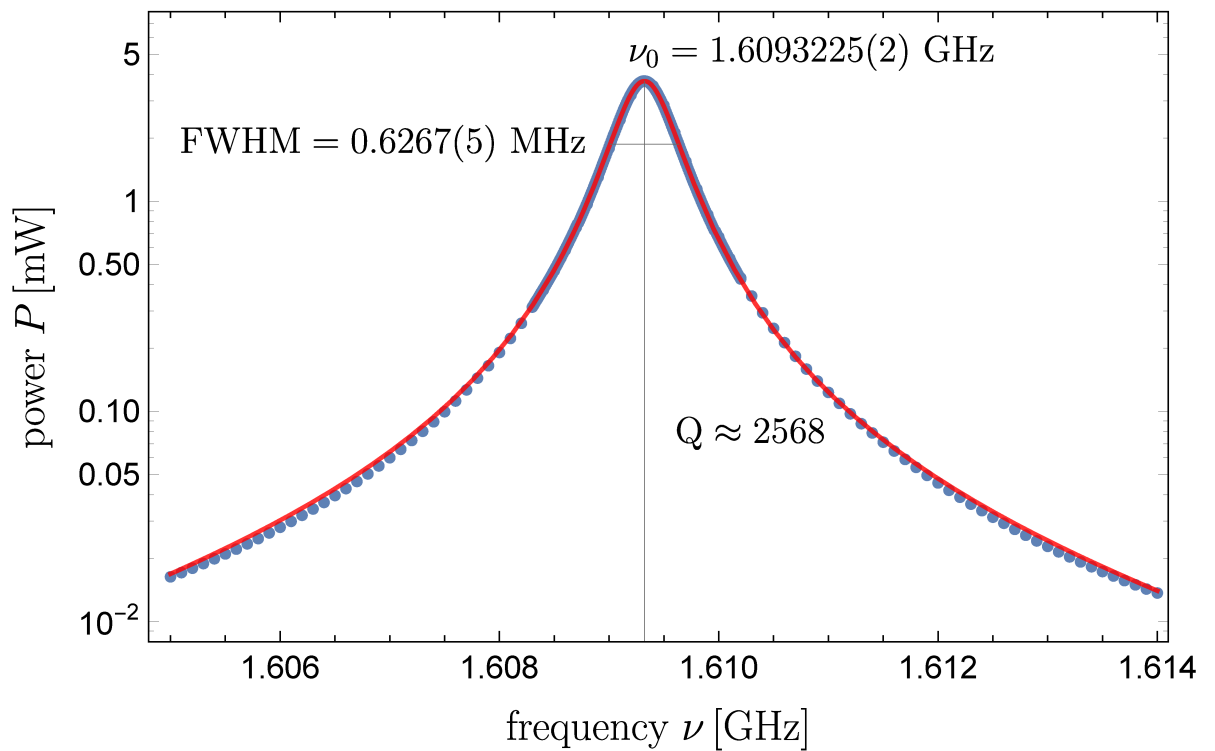
Figure 3.15.: Measured resonance curve of a cavity and a fit with a Lorentz-function.

3.5. Quenching Chamber

In the Quenching chamber, the stark effect is used to bring most of the remaining metastable atoms in the beam into the ground state. During this process Lyman-α photons ($\lambda_{\mathrm{Ly}} = 121\,\mathrm{nm}$) are emitted. These photons are detected by a photomultiplier. The beam enters the quenching chamber in a stainless steel tube, which reaches close to the center of the vacuum chamber. A second stainless steel tube is fixed to the end of the chamber. Between those, a third tube made from teflon is mounted. Inside the teflon piece, and isolated from the steel tubes, a ring-shaped electrode is positioned. It is connected to a high voltage vacuum feed-through, so an electrical field can be produced between the ring-electrode and the grounded stainless tubes. A large hole in the teflon is directed towards the photomultiplier, which is mounted in the top flange of the chamber. When the atoms exit the stainless steel tube, the strong electric field ($E \approx 200\,\mathrm{V\,cm^{-1}}$) acts on them, and metastable atoms will be quenched to the ground state, emitting Lyman-α photons. The photomultiplier covers a solid angle of about π/8. Thus, about ¹/30 of all photons will hit the window of the photomultiplier. The window is made from MgF, and the photo-cathode is made from KBr. MgF is transparent for photons with $\lambda > 110\,\mathrm{nm}$. With KBr photons with $\lambda < 165\,\mathrm{nm}$ can be detected with a quantum efficiency of about 10 %. Since only Lyman-α photons contribute to the signal, the small acceptance range ($165\,\mathrm{nm} > \lambda > 110\,\mathrm{nm}$) reduces the background.

3.6. Sona Transition Unit

The measurements with the Sona transition were performed in the IKP in Jülich and required a rearrangement of the existing Lamb-shift polarimeter. As beam source for this setup the ionizer, described in Sect. 3.1, was used by feeding it with (unpolarized) hydrogen gas. Like in the usual Lamb-shift polarimeter setup a Wienfilter was used to discard all ions except protons, from which metastable hydrogen was produced in the subsequent cesium cell. A first spin filter was used to quench both β states and one of the α state to the ground state. Usually the α1 state was allowed to pass, but some measurements were also performed with the α2 state. Positioned directly after the first

spin filter, two small solenoid coils were used to produce opposing longitudinal magnetic fields. A second spin filter behind these two Sona transition coils was then used to measure the occupation numbers of the two α states. To obtain a single magnetic field reversal, the first Sona coil was set up to produce a magnetic field in the same direction as the first spin filter, while the second Sona coil and the second spin filter produced fields in the opposite direction. Since the gradient around the zero crossing has to be fairly small (see Eq. (2.92)) the Sona coils are shielded with four layers of µ-metal against the stray fields of the spin filter and the earth's magnetic field. With a threaded nylon rod and nylon nuts the distance between the coils, and therefore, the wavelength λ (see Eq. (2.94)) can be adjusted. In the usual operation mode the current through the Sona coils was varied with sawtooth function. A schematic drawing of the Sona coils between the two spin filter is shown in Fig. 2.23 and the full setup for the measurements with the Sona transition is shown in Fig. 3.16 (taken from [Eng+20a]). The magnetic field profile
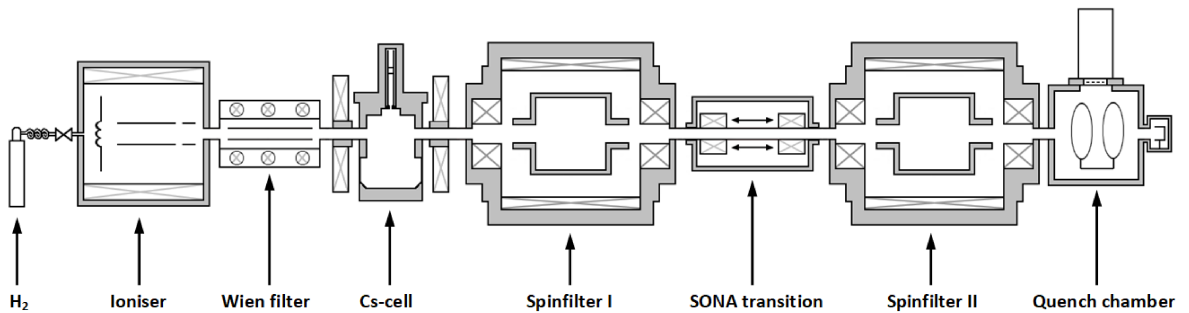
Figure 3.16.: The full setup used for the measurements with the Sona transition.

in the Sona setup was measured by means of a three axial Hall-probe, which was guided parallel to the beam axis – with an offset $\rho \approx 5\,\text{mm}$ – inside a plastic tube. In Fig. 3.17 the z-component of the magnetic field B_z along the beam axis is shown for four different currents through the Sona coils. At a distance between the coils of $60\,\text{mm}$ the wavelength – determined by a Fourier analysis – is $\lambda \approx 140\,\text{mm}$. For Fig. 3.18 the radial magnetic field B_{rad} was determined by the x- and y-components of the magnetic field measured by the Hall-probe and by the derivative of the z-component with $B_{\text{rad}}(z, \rho) = -\frac{\rho}{2}\frac{\partial B_z}{\partial z}$.
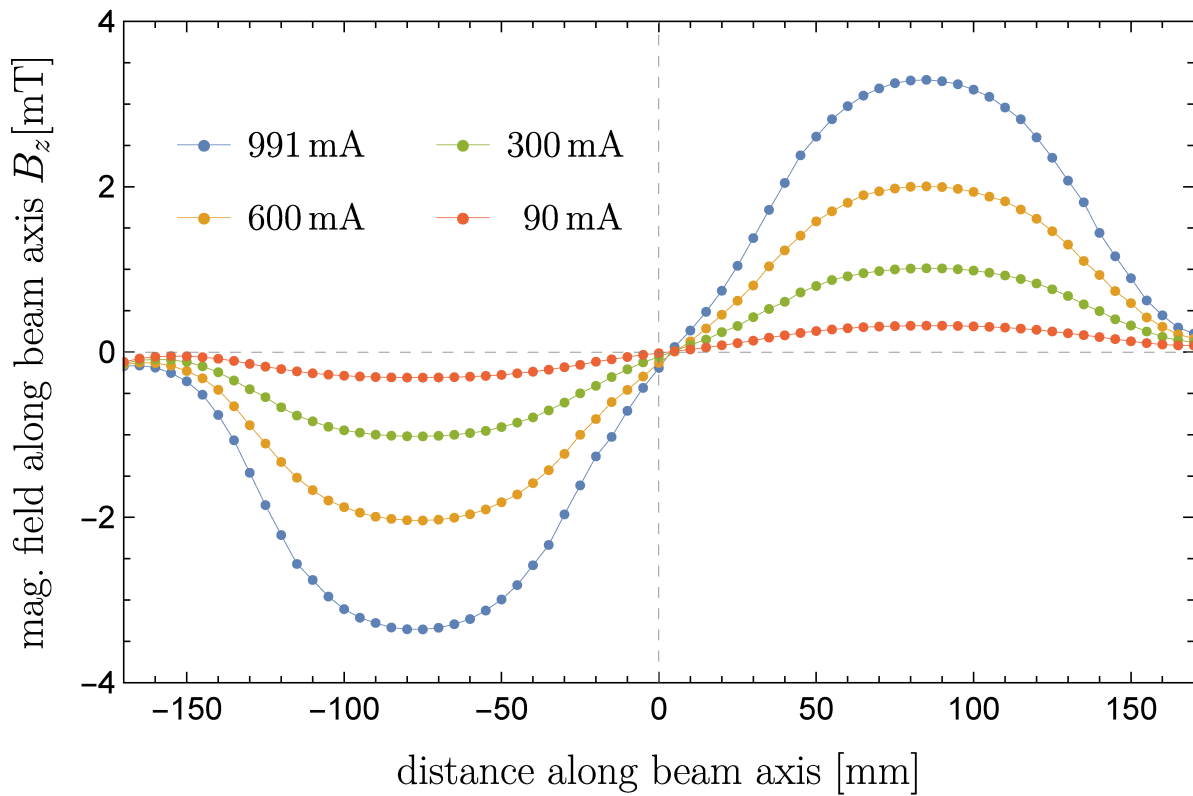
Figure 3.17.: The z-component of the magnetic field in the Sona setup at four different currents through the coils.
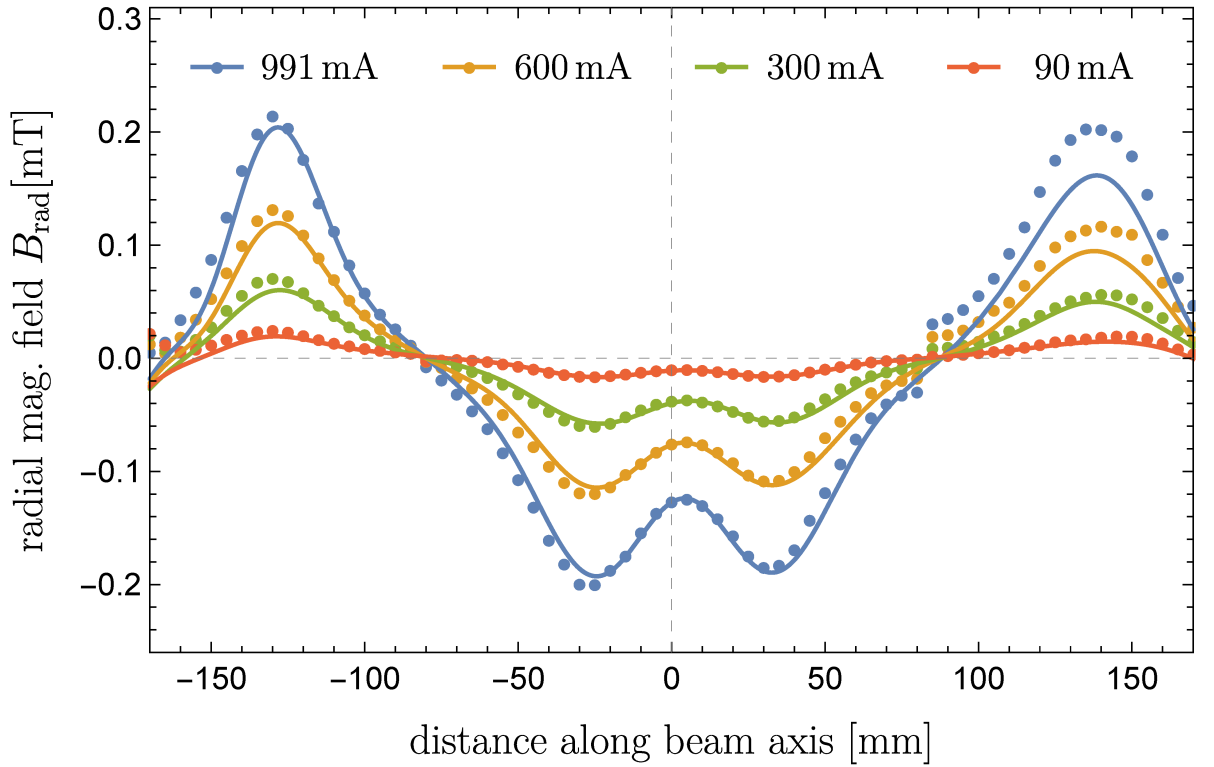
Figure 3.18.: The radial magnetic field in the Sona setup at four different currents through the coils determined by $B_{\mathrm{rad}}(z) = \sqrt{B_x(z)^2 + B_y(z)^2}$ (●) and $B_{\mathrm{rad}}(z, \rho) = -\frac{\rho}{2} \frac{\partial B_z}{\partial z}$ (─).

4. Measurements

4.1. Cesium Cell Optimization

As discussed in Sect. 2.4.3, it has been shown, that the production of metastable atoms from reactions of molecular ions (H_2^+, HD^+, D_2^+) is possible. However, in contrast to the production of metastable atoms from atomic ions (H^+, D^+), the optimal beam energies and areal number density of cesium atoms are still subject of investigation. Earlier measurements (see fig. 7 of Ref. [Eng+14]) indicate, that a slightly higher areal number density for the molecular ions at $1\,\mathrm{keV}$ is preferable compared to protons with the same energy. Since the expected beam intensity of the molecular beam source is fairly close to the detection limit of the Lamb-shift polarimeter, the optimal parameter of the cesium cell would help to ensure a successful polarization measurement of the molecular beams. Secondly, the parameters would provide advice, if the metastable atoms originate from a two step process (see Eq. (2.54)) or a single reaction (see Eq. (2.55)) with cesium atoms. Consequently, efforts to determine the optimal areal number density and beam energies have been made.

In the laboratory in Jülich, first, a beam of protons and H_2^+ ions was formed from unpolarized hydrogen with the help of an ECR ionizer. With the Wien filter, either protons or H_2^+ ions were selected from the beam. The beam intensity in front of the cesium cell was determined with a Faraday cup, which can be inserted into the beam. In the quenching chamber, the intensity of the metastable atoms was then measured using the intensity of the Lyman-α photons. A second Faraday cup behind the quenching chamber was used to measure the intensity of ions, which did not react with the cesium vapor. Both, the Lyman-α intensity and the ion intensity after the cesium cell, were normalized by the beam intensity before the cesium cell. At constant beam energy, measurements at cesium temperatures (measured at the bottom of the cell) between $120\,^{\circ}\mathrm{C}$ and $200\,^{\circ}\mathrm{C}$

were carried out with protons and H_2^+ ions – one after the other. Since the thermal equilibrium had to be waited for, a series of measurements took about 5 to 6 hours. Unfortunately it was not possible to keep the beam intensity and stability of the – old and delicate – ECR source at an acceptable level over this time. The ECR source was then exchanged for the Glavish ionizer described before, especially since this ionizer was also needed for another experiment in the laboratory. However, the improvement fell short of expectations, so that no reliable data could be obtained. Therefore, the control measurement with protons was omitted, in order to shorten the measurement time, and measurements were only made with H_2^+ ions. The results of these measurements are shown in Fig. 4.1. The measurements were carried out in series with fixed beam energy.
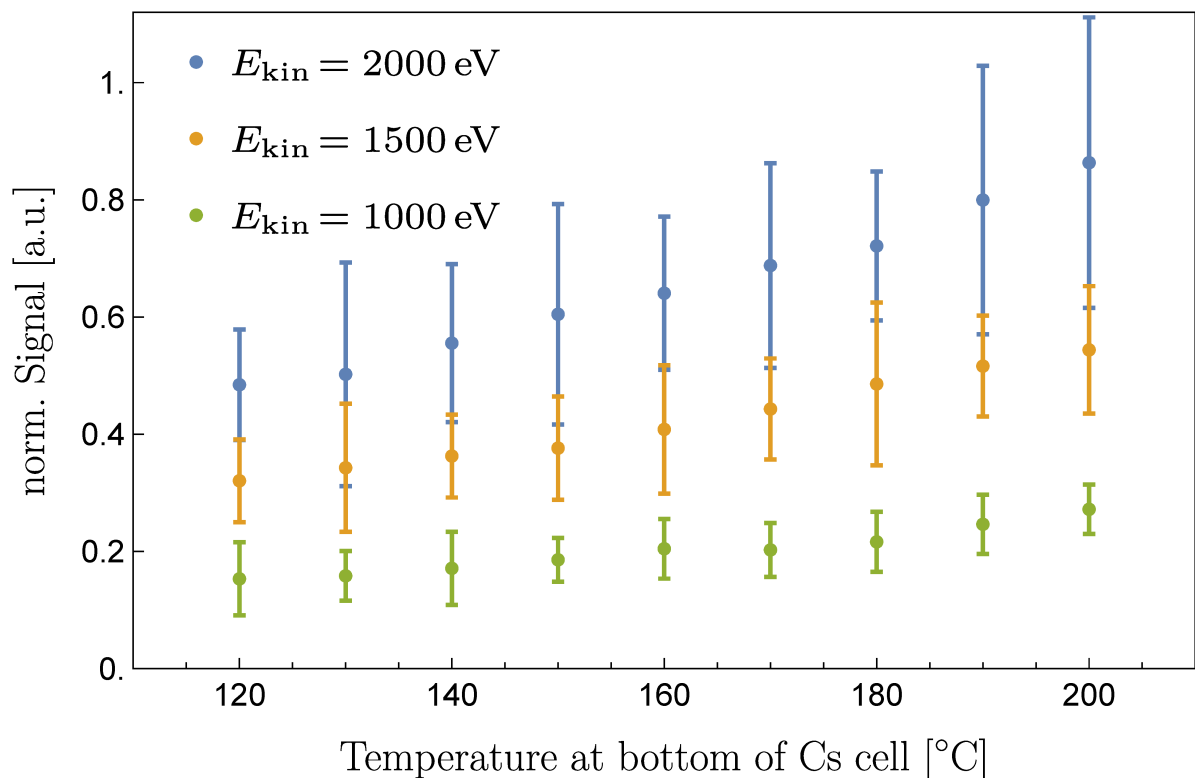
Figure 4.1.: Relative efficiency of metastable production from H_2^+ ions in the cesium cell, measured by the intensity of Lyman-α normalized to the ion current in front of the cesium cell, as function of the cesium temperature at different beam energies.

At each temperature, the ion current in front of the cesium cell was measured first, followed by the Lyman-α intensity and the ion current behind the quenching chamber

(with turned of electric fields in the quenching chamber). Then the ion current in front of the cesium cell was measured again. If the two measurements of the beam intensity in front of the cesium cell differed by more than 10% the data would be rejected, in order to reduce the uncertainty caused by the fluctuating beam intensity. At each temperature three valid data points were taken. For each energy, the measurement series were performed two times on different days. Thus, each data point in Fig. 4.1, is the mean value of two series with three single measurements each. The H_2^+-currents measured in the first Faraday cup varied between $2.5\,\mathrm{nA}$ and $7\,\mathrm{nA}$. This is equivalent to rates between $1.6 \cdot 10^{10}\,\frac{\mathrm{ions}}{\mathrm{s}}$ and $4.4 \cdot 10^{10}\,\frac{\mathrm{ions}}{\mathrm{s}}$ going into the cesium cell. The peak height of each α peak measured between $5\,\mathrm{mV}$ and $80\,\mathrm{mV}$. With a gain of the photomultiplier of about 10^7 this corresponds to registered Lyman-α photon rates between $3 \cdot 10^3\,\frac{\mathrm{ph}}{\mathrm{s}}$ and $5 \cdot 10^4\,\frac{\mathrm{ph}}{\mathrm{s}}$. The photomultiplier covers about $^1\!/_{30}$ of a sphere around the quenching region and has a quantum efficiency of about 10%, thus, between $9 \cdot 10^5\,\frac{\mathrm{atoms}}{\mathrm{s}}$ and $1.5 \cdot 10^7\,\frac{\mathrm{atoms}}{\mathrm{s}}$ are quenched in the quenching region. At the given beam energies and quenching fields in the quenching chamber more than 98% of all metastable atoms will be quenched. The transmission rate for each α state is less than $^1\!/_2$ at the resonant magnetic field, therefore, the amount of atoms quenched in the quenching chamber has to be multiplied by a factor of two to estimate the amount of atoms in these states before the spin filter. Since the H_2^+ beam is unpolarized each $2S_{1/2}$ substate after the cesium cell is equally populated, thus the amount of metastable atoms should be four times the amount of a single α state. By rounding the correction factors up, the rates of metastable atoms entering the spin filter are approximately between $9 \cdot 10^6\,\frac{\mathrm{atoms}}{\mathrm{s}}$ and $1.5 \cdot 10^8\,\frac{\mathrm{atoms}}{\mathrm{s}}$. With these estimations the ratio of metastable atoms (produced in the cesium cell and entering the spin filter) to H_2^+ ions was $\frac{N_\mathrm{meta}}{N_{H_2^+}} \approx 0.38\%$ at a beam energy of $2\,\mathrm{keV}$ and $200\,°\mathrm{C}$ at the bottom of the cesium cell and $\frac{N_\mathrm{meta}}{N_{H_2^+}} \approx 0.05\%$ at $1\,\mathrm{keV}$ and $120\,°\mathrm{C}$. This is in agreement with measurements of recombination experiments (see e.g. Ref. [Eng+14]), where the efficiency of metastable atom production from H_2^+ ions was estimated to be about a factor of 30 to 40 lower than the efficiency of metastable production from proton, which for this setup is estimated to be around 15%.

According to the measurements, the efficiency for the production of metastable hydrogen atoms from H_2^+ ions increases with temperature. Other than the earlier measurements (see fig. 7 of Ref. [Eng+14]), the present one indicates that the optimal temperature might even be higher than $200\,°\mathrm{C}$. Unfortunately, measurements with tem-

peratures above 200 °C cannot be carried out with this cesium cell design. As discussed in Sect. 2.4.3, higher cesium temperatures and, therefore, higher cesium vapor densities might indicate that the two step process (see Eq. (2.54)) dominates the production of metastable atoms from molecular ions. Furthermore, higher beam energies seem to favor the reaction, however, this can also be due to the focusing of the beam, which is usually better for higher energies. Concluding from these measurements, higher beam energies and cesium cell temperatures are preferable for measurements with polarized molecular ions compared to proton beams. This is especially important when the beam intensities are expected to be rather low like for the measurements at BINP.

4.2. Lamb-Shift Polarimeter at BINP

To confirm the functioning of the Lamb-shift polarimeter at the BINP measurements with the (unmodified) atomic beam source were performed. For these measurements atomic beam source was set up to produce a beam of hydrogen atom is a single hyperfine state, which was directed into the ionizer. In the ionizer proton beams of about $10\,\text{nA}$ or about $6 \cdot 10^{10}\,\frac{\text{ions}}{\text{s}}$ were formed and focused into the Lamb-shift polarimeter. As discussed in Sect. 2.4.2, the polarization vectors of protons (and deuterons) are rotated by the magnetic field of the Wienfilter, thus calibration measurements were made (see Fig. 3.6). One of these measurements is shown in Fig. 4.2. For this measurement the atomic beam source was set to produce a beam of hydrogen atoms in state $|F = 1, m_F = -1\rangle$, the Ionizer was set up to a beam energy of about $2\,\text{keV}$ and the current through the coils of the Wienfilter was $I_{\text{WF}} = 2.75\,\text{A}$. Looking at the complete set of measurements (see Fig. 3.6) the Wienfilter correction factor for this measurement is $C_{\text{WF}} \approx -1$. Ignoring the other correction factors the polarization of the beam, therefore, was about $-57.2\,\%$. It is noticeable that the background signal decreases linearly with the magnetic field. Although the polarization is easily determined with a linear fit to the background, it is desirable to eliminate this linear dependency. Usually, a linear background in the spectrum is due to residual protons in the beam, which are deflected in the spin filter depending on its magnetic field. This kind of background signal can be influenced by the electric fields in the spin filter and is beam energy dependent. Here, the linear background could be observed at all energies and could not be
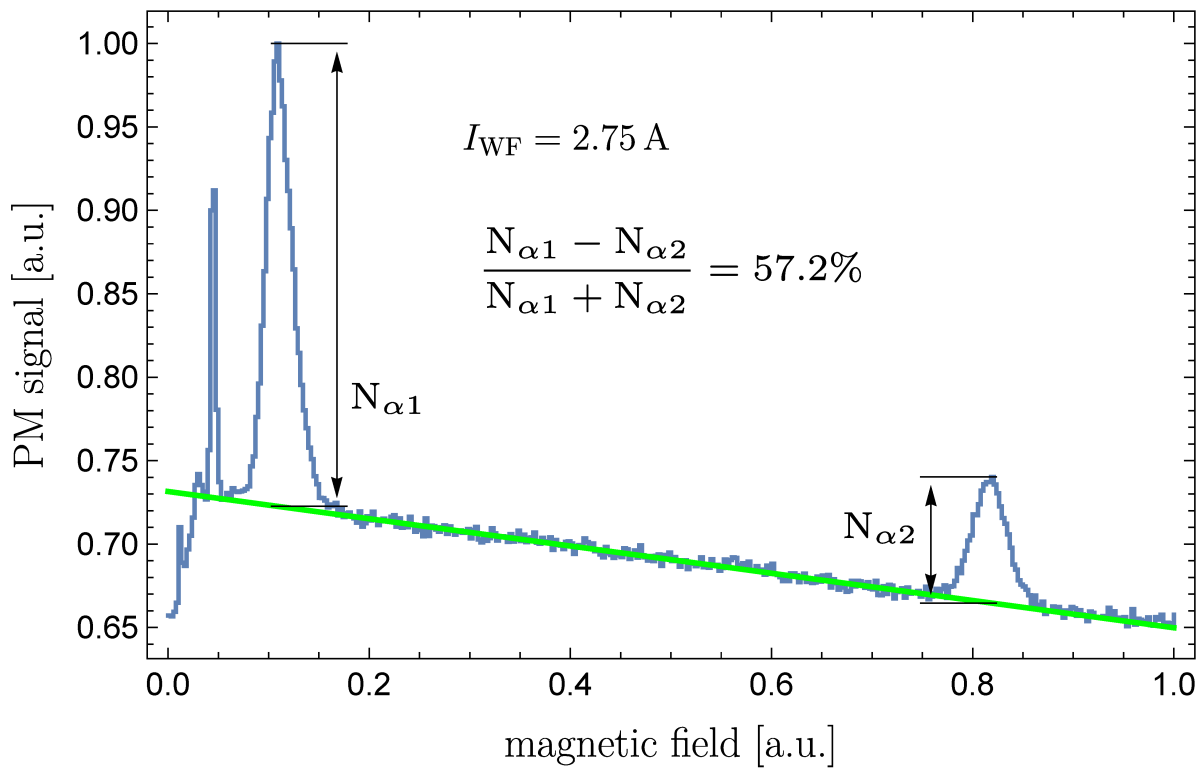
Figure 4.2.: A polarization measurement of an atomic hydrogen beam from the atomic beam source at the BINP. The ionizer was set to a beam energy of about 2 keV and the Wienfilter was set to rotate the polarization vector by 180°.
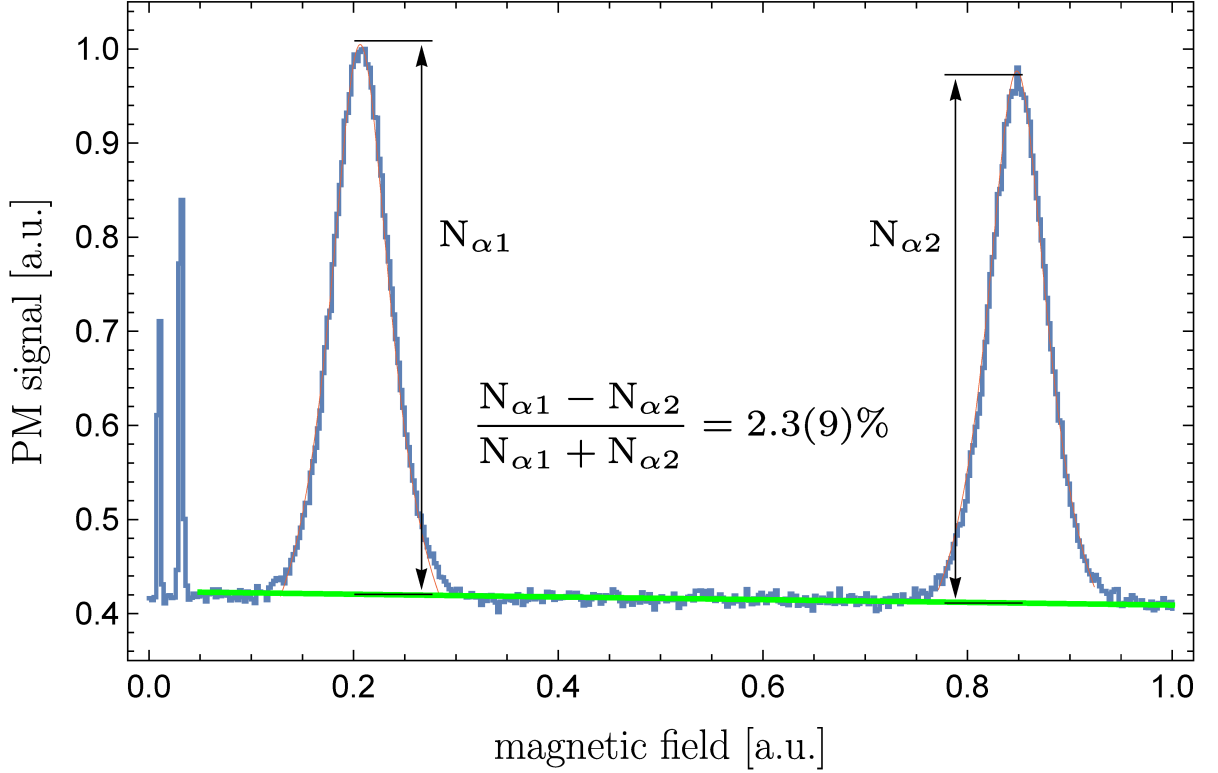
Figure 4.3.: A polarization measurement with an unpolarized hydrogen beam.

decreased with different setting of the electric potentials inside the spin filter. A further source was searched for and found in the insufficient shielding of the photomultiplier, i.e. the photomultiplier gain was influenced by the magnetic field of the spin filter nearby. By inserting an iron plate between the spin filter and the quenching chamber and an improvised coil around the housing of the photomultiplier, this background was reduced significantly [TS]. A measurement of an unpolarized beam, with this background reduction is shown in Fig. 4.3. The measured polarization is unusually high (2.3(9) %). Since the background is flat now it seems unlikely that this is due to a difference in gain of the photomultiplier for both peaks. Thus, this measurement might indicate a significant discrepancy between the transition probabilities for α1 and α2 of hydrogen in the spin filter, such that atoms in the α1 state are more likely to pass the spin filter than atoms in the α2 state at their respective resonance conditions. The resulting correction factor $C_{\mathrm{Sp,H}}$ for the spin filter (see Eq. (2.78)) and the difference between the measured (p_{m}) and corrected polarization ($p_{\mathrm{z}} = C_{\mathrm{Sp,H}} \cdot p_{\mathrm{m}}$) of the metastable atoms are shown in Fig. 4.4. This unexpectedly large discrepancy in the transition probabilities could be caused by
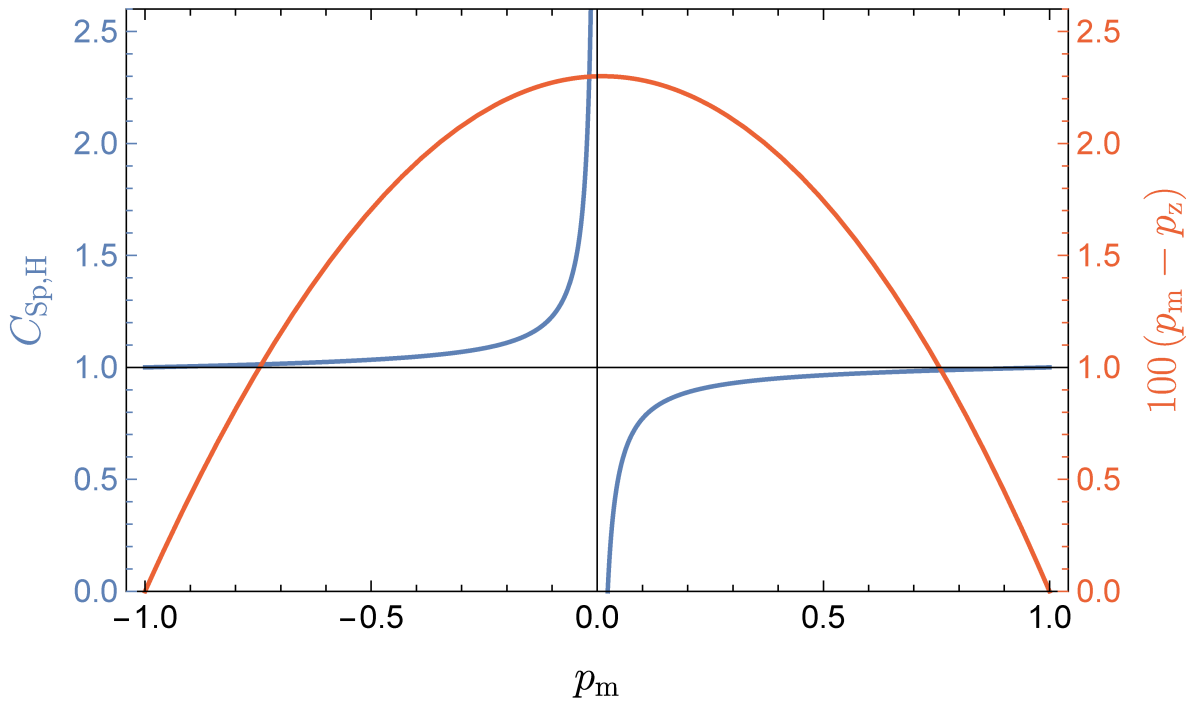
Figure 4.4.: The correction factor $C_{Sp,H}$ of the spin filter and the difference between measured (p_m) and corrected polarization (p_z) – scaled by a factor of 100 – as function of the measured polarization following from the "zero-measurement" shown in Fig. 4.3.
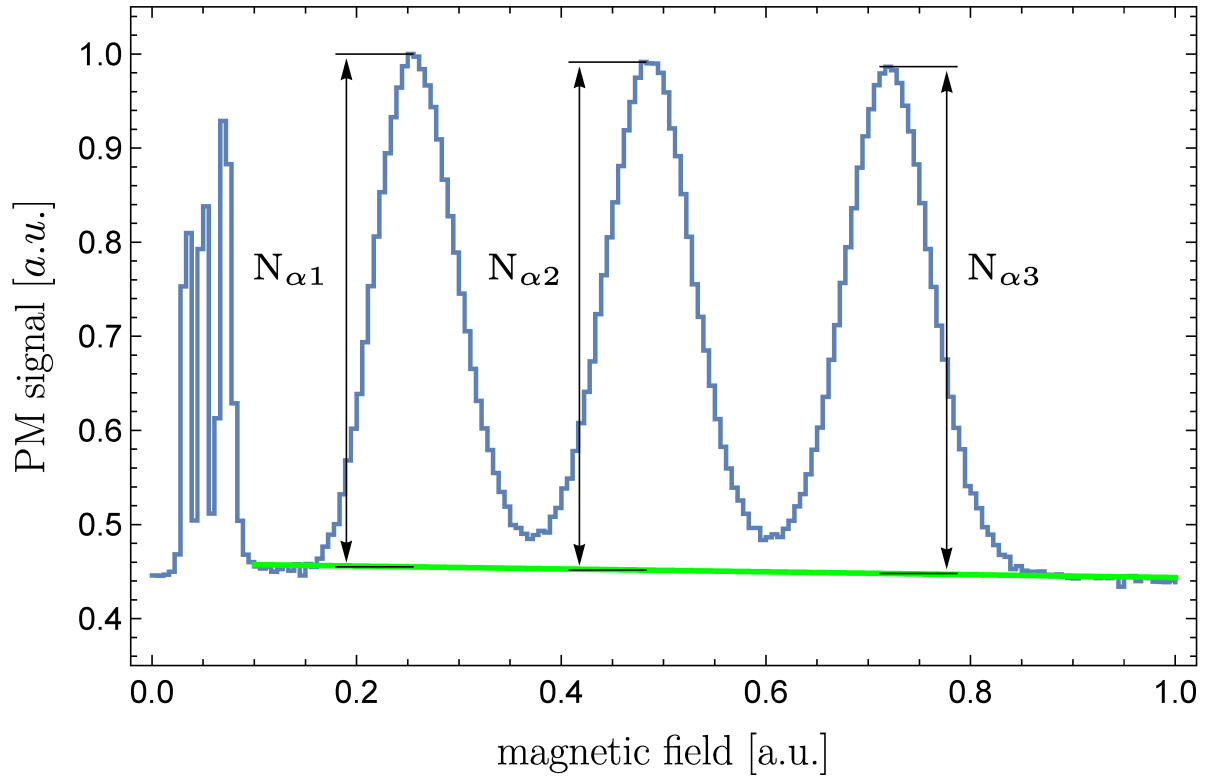
Figure 4.5.: A polarization measurement with an unpolarized deuterium beam. The measured vector- and tensor- polarizations are: $p_\mathrm{m} = 0.4(2)\,\%$ and $p_\mathrm{mm} = 0.2(1)\,\%$.

an accidental polarity reversal of the spin filter, which would have big influence on the homogeneity of the magnetic field, due to changes in the magnetization of the yock. Consequently, the correction factor of the spin filter cannot be neglected and therefore "zero-measurements" are mandatory before a precision measurement, to obtain a reliable correction factor. In Fig. 4.5 a measurement with unpolarized deuterium is shown. As expected, the difference of transition probabilities is smaller for the three α states of deuterium. The measured vector- and tensor- polarizations of the unpolarized deuterium beam are $p_\mathrm{m} = 0.4(2)\,\%$ and $p_\mathrm{mm} = 0.2(1)\,\%$, respectively.

While the magnetic field dependent part of the background was significantly suppressed, a huge constant background was observed, whenever the atomic beam source was running and all valves in the beam line were open. Since the background was also present when the ionizer was shut off or the ion beam was deflected by the Wienfilter, it was concluded that the background stemmed from Lyman-α photons, which are produced by the plasma

in the dissociator of the atomic beam source. Although, the photomultiplier is mounted perpendicular to the beam and most parts, which are exposed to the beam, are made from stainless steel, which is a poor reflector for Lyman-α photons, about $10^5 \frac{ph}{s}$ reach the photomultiplier. The rate of photons which are emitted through the nozzle of the atomic beam source is estimated to be in the order of $10^{18} \frac{ph}{s}$. This background was never observed during measurements with atomic beam sources in Jülich, since the atomic beams do not enter the Lamb shift polarimeter in a straight line from the atomic beam sources, but are deflected by 90°. Since the background can be subtracted easily, it is not a problem for measurements with the atomic beam source at BINP. For measurements with the molecular beam source this is irrelevant, since the dissociator and, therefore, the strong Lyman-α source is missing.

So far, a few attempts to measure the polarization of molecules from the molecular beam source have been made during a one-week experimental campaign. Unfortunately, the H_2^+ beam intensities after the ionizer were to low to detect metastable atoms in the quenching chamber, even if the rest of the Lamb-shift polarimeter is operating at ideal efficiency. One reason for this could be that the alignment of the molecular beam source and ionizer is not optimal, so that the molecular beam does not hit the ionization volume perfectly. Another reason could be insufficient ionization efficiency of the ionizer. If the gas density in the ionizer is too low, it will only work in the less efficient electron impact mode, thus, it might be reasonable add a suitable buffer gas. Since a getter pump is installed in the ionizer to reduce the background from scattered hydrogen molecules, a noble gas like argon should be preferred over other gases like nitrogen, so the getter pump will not fill up to fast.

4.3. Sona

The Sona transition setup discussed in Sect. 3.6 allows for several measurement modes. Each of the spin filters – the first one being the polarizer and the second one the analyzer – can be set up to either allow only one of the α-states (electrostatic field on, radio frequency on and magnetic field set to one of the "resonance" fields), both α-states (electrostatic field on, magnetic field around 55 mT and radio frequency off), or all

metastable states (all off) to pass. Measurements with Sona transitions where both α-states were allowed to pass the polarizer and the analyzer have been performed before [HRT77; HR78; GS81]. Therefore, the focus was on measurements in which only a single α-state was send through the Sona coils and a single α-state was analyzed. The current through the Sona coils can either be kept constant and the beam velocity changed to manipulate the frequency of the induced electromagnetic field, or the magnetic field can be increased to find the conditions where the energy difference between the hyperfine substates corresponds to integer multiples of the constantly induced radio frequency. For the measurements with hydrogen, presented below, the first spin filter was set that only the α1 state could pass and the current through the Sona coils was ramped with a sawtooth function from 0 A to 1.75 A. The photomultiplier signal, which is proportional to the rate of metastable atoms in the quenching chamber, was measured as function of time and, therefore, as function of the current through the Sona coils. A measurement, where only the α1 state could pass the second spin filter is shown in Fig. 4.6 and where only the α2 state was allowed to pass in Fig. 4.7. For both measurements, the "beam energy defining electrode" of the ionizer was set to 1500 V. However, the analysis showed a beam energy of 1.28 keV. This discrepancy can be explained by a plasma burning outside of the third electrode of the ionizer, which is further discussed in Sect. 3.1. The distance between the Sona coils was 60 mm, which results in a wavelength $\lambda \approx 140$ mm. To each peak a Lorentzian curve was fitted to determine the corresponding current through the Sona coils. Since the magnetic field in the coils is proportional to the current the photomultiplier signal can be plotted against a corresponding magnetic field instead. As discussed in Sect. 2.6, atoms flying through the Sona coils experience an electromagnetic field which can induce σ-transitions between $2S_{1/2}$ substates. For this the energy difference $\Delta E(B)$ between these stats, which is a function of the magnetic field and can be calculated by the Breit-Rabi theory, has to match the photon energy of the oscillating radial field: $\Delta E(B) = n\,h\nu = n\,h\frac{v_H}{\lambda}$ $(n \in \mathbb{N})$. The frequency ν of the electromagnetic field is independent of the magnetic field strength but is a function of the velocity of the atoms v_H and the wavelength λ which – in first order – is determined by the geometry of the setup. Notably, the magnetic fields at which the transitions are induced, and also the differences between those magnetic fields, are functions of the frequency ν. Thus, the pattern of the measured peak positions can be compared to calculations of the Breit-Rabi theory (with QED corrections) with different (second harmonic) frequencies ν (see Sect. 2.6). With the assumption that the relevant magnetic
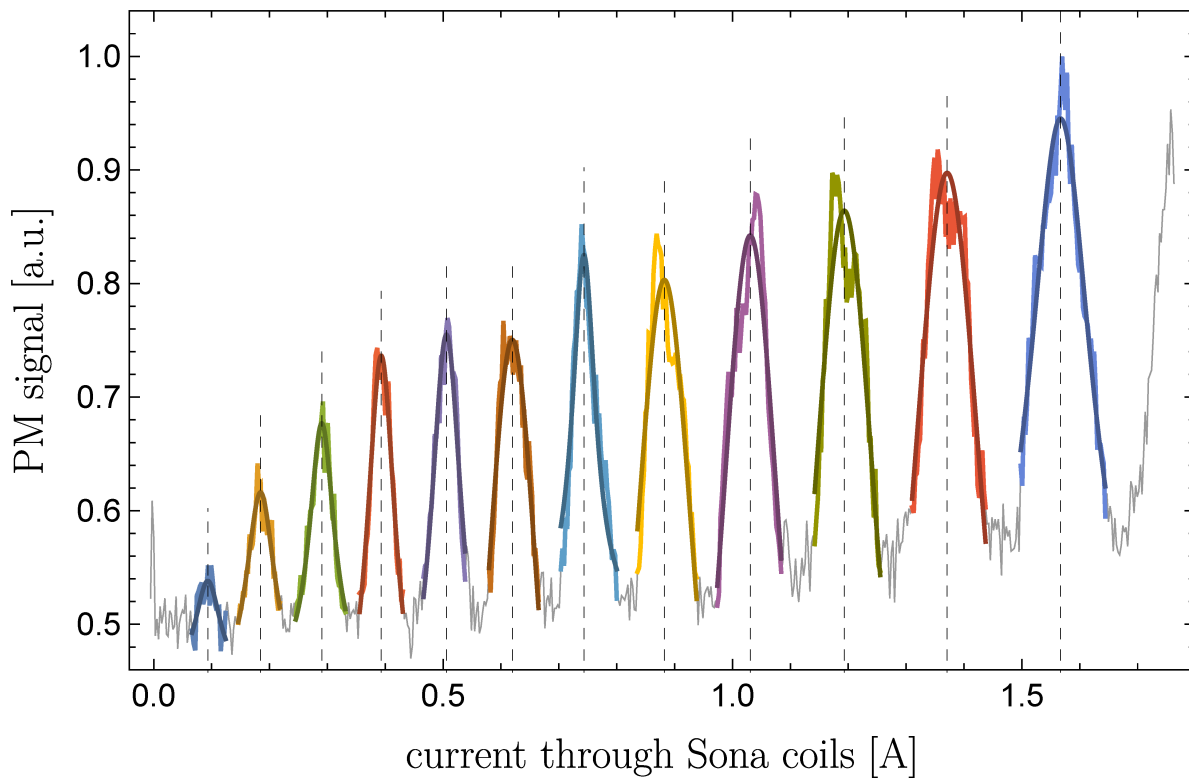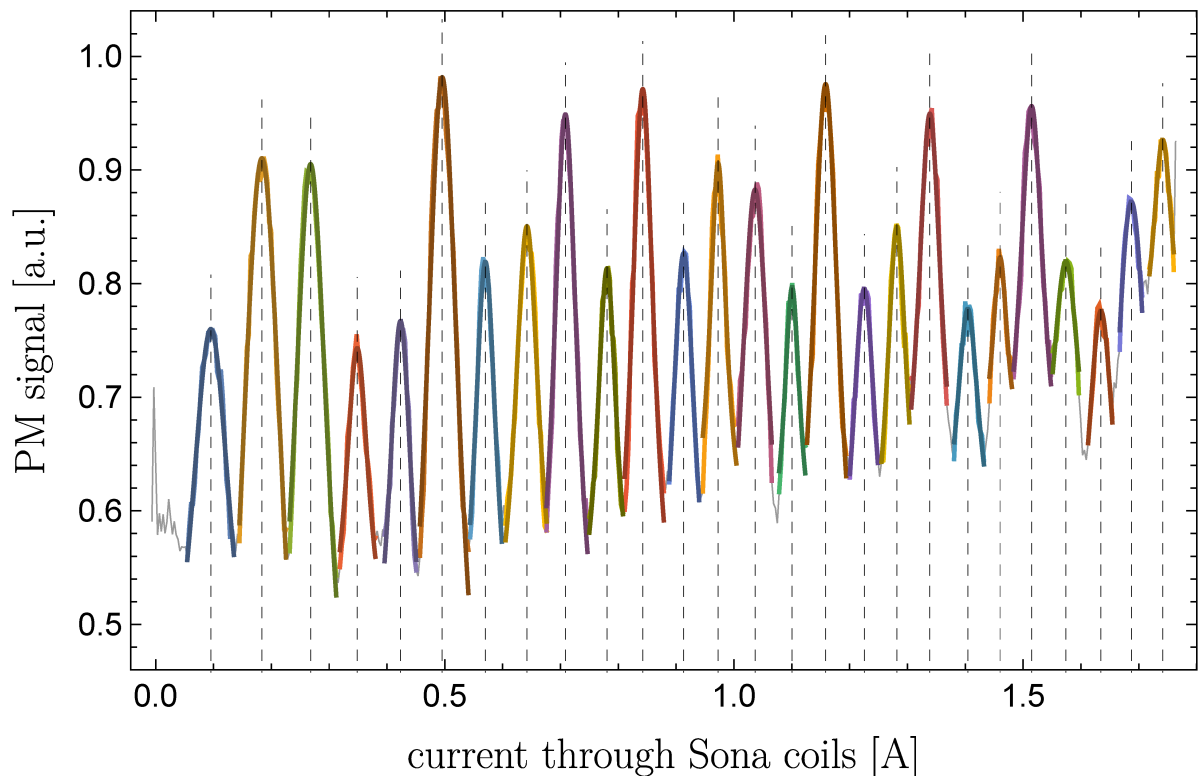
Figure 4.6.: Relative amount of hydrogen atoms in the α1 state after a beam of atoms starting in the α1 state passed the Sona coils, as function of the current through the coils. With fits of Lorentz functions to each colored peak the position was determined.

field B' is a linear function of the current through the coils a best fitting frequency for the measurements can be found. For this the magnetic fields $B'_i(\nu_0)$ at which the i-th peak appears was calculated for different frequencies ν_0. Then a quadratic calibration function $B'_i(\nu_0) = a \cdot I_i^2 + b \cdot I_i + c$, with I_i being the current through the Sona coils, at which the i-th peak was measured, was fitted to the data for each frequency ν_0. Now the frequency $\nu_{0,\text{fit}}$ at which the coefficient a of the quadratic term vanishes can be found. A plot of the coefficient a of the quadratic term as function of the frequency ν_0 (for the measurements presented in Fig. 4.6) is shown in Fig. 4.8. For the first measurement the best fitting frequency is 3.545(27) MHz and for the second measurement it is 3.518(30) MHz. The best fitting frequencies of both measurements agree within the uncertainties. A larger difference would indicate a change in the beam energy in between the measurements. A Breit-Rabi diagram, where the (multi-)photon transitions

Figure 4.7.: Relative amount of hydrogen atoms in the α2 state after a beam of atoms starting in the α1 state passed the Sona coils, as function of the current through the coils. With fits of Lorentz functions to each colored peak the position was determined.

corresponding to $\nu = 3.545\,\mathrm{MHz}$ are indicated, is shown in Fig. 4.9. Since the differences in the diagrams are almost not recognizable between $\nu = 3.545\,\mathrm{MHz}$ and $\nu = 3.518\,\mathrm{MHz}$ a second one is not shown here. The calibration function between the magnetic field B' and the current through the Sona coils is $B' = 2.83(3)\,\mathrm{mT} \cdot \frac{I}{\mathrm{A}} - 0.02(2)\,\mathrm{mT}$. Since the magnetic field was also directly measured with a Hall-probe at different currents through the Sona coils, B' can also be expressed by the maximum measured field B_{max} with: $B' \approx 0.73 \cdot B_{\mathrm{max}}$. In Figs. 4.10 and 4.11 the measurements are plotted against the magnetic field B' and the measured and calculated peak positions are shown for comparison.

In the following an approach for a simplified model explaining the measurements is outlined. A far more sophisticated theoretical treatment of the measurement results, using time-dependent Schrödinger equations, can be found in Ref. [Eng+20a].
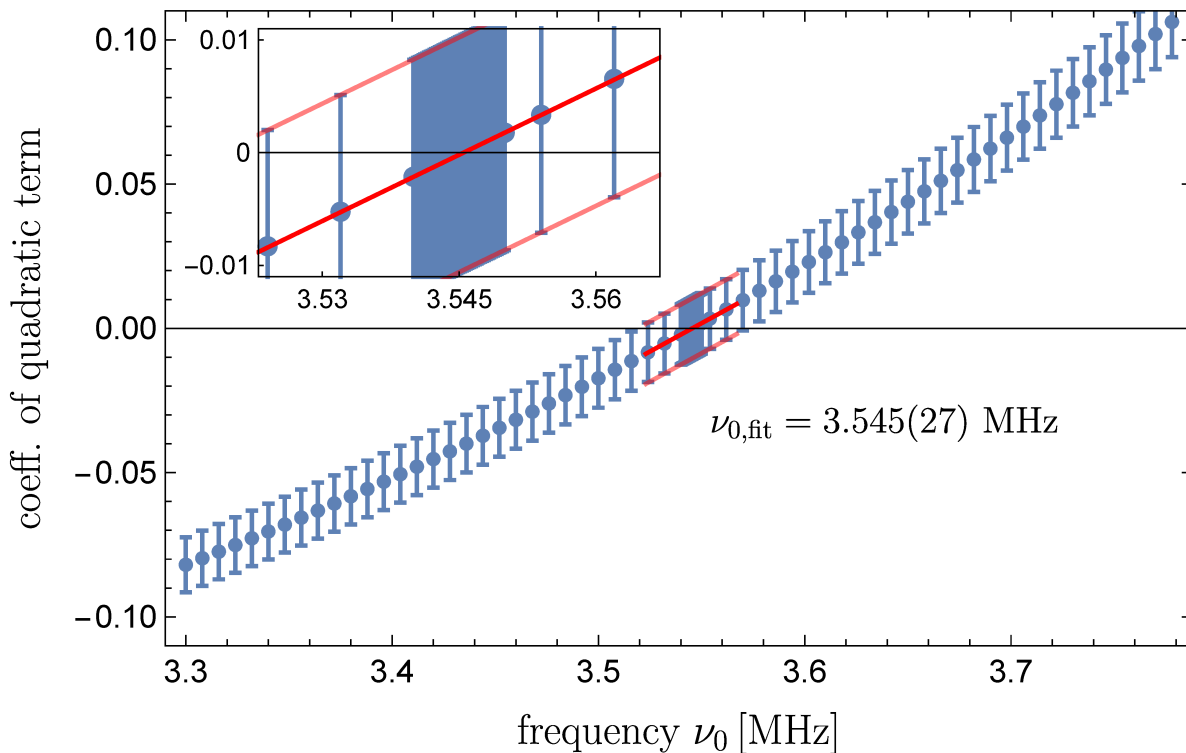
Figure 4.8.: Coefficient a of the quadratic term of the calibration function
$B_i'(\nu_0) = a \cdot I_i^2 + b \cdot I_i + c$ between the calculated magnetic field $B_i'(\nu_0)$
of the i-th peak and the peak position I_i found in the measurement as func-
tion of the frequency ν_0 with which $B_i'(\nu_0)$ was calculated. Since $B_i'(\nu_0)$ and
I_i should be proportional, the frequency $\nu_{0,\text{fit}}$ at which $a = 0$ is the best
estimate for the frequency, the atom experience during the flight through
the Sona coils.

In both measurements only metastable atoms in state α1 were allowed to enter the Sona
coils. Thus, in a naive picture, without any additional transitions, only the β3 state
would be populated after the reversal of the magnetic field. When transitions, induced
by the electromagnetic field, are considered, atoms in state α1 can only be observed (see
Fig. 4.10), if atoms went from α1 to α2, "before"[1] the reversal of the magnetic field, and
from α2 back to α1 "after" the reversal, or if atoms "after" the reversal change their
state from β3 to α2 and from α2 to α1. Direct transitions between α1 and β3 are not
allowed, since this would require $\Delta m_F = \pm 2$. Noteworthy, the α2 state is not effected
by the reversal of the magnetic field. Thus, atoms which change from α1 to α2, "before"

---

[1]Since the involved energy and time scales are close to the limit of the uncertainty principle there
is no well defined "before" or "after" the transition for the atoms.
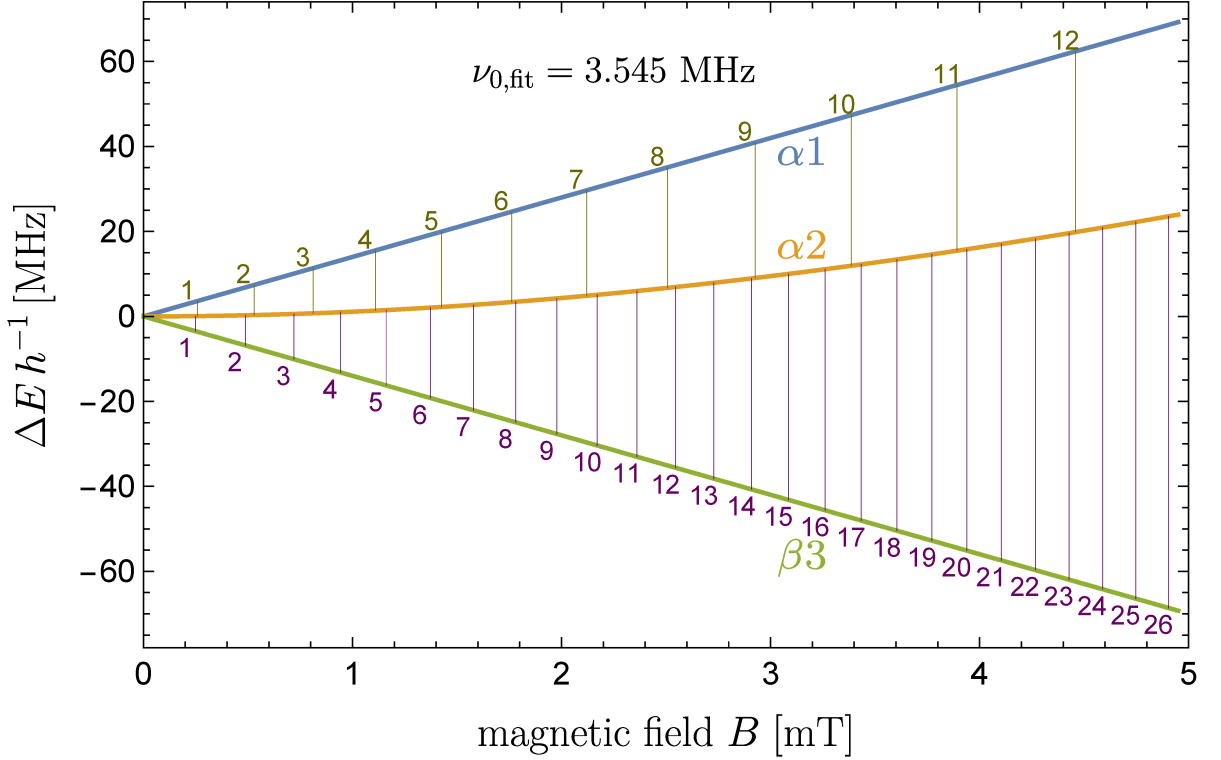
Figure 4.9.: Breit-Rabi diagram with transitions induced by a radial magnetic field $B_{\mathrm{rad}}(t)$ oscillating with a frequency $\nu = 3.545\,\mathrm{MHz}$.

the reversal of the magnetic field will still be in α2 "after" the reversal and, therefore, are available for transitions back to α1. Two-step transitions from β3 to α2 and from α2 to α1 are only possible, if there is a sufficient overlap of both transitions due to there linewidth. However, if there is such an overlap the transitions from β3 to α2 will also work in the other direction (from α2 to β3), which can reduce the amount of atoms in the α2 state. Looking at peak "8" (yellow) in Fig. 4.10 a deformation (reduction of the signal) on the right flank can be seen. A deformation (reduction of the signal) on the left flank can be observed for peak "9" (violet). From Fig. 4.9 it can be seen that the 12-photon transition between α2 and β3 follows directly after the 8-photon transition between α1 and α2, while the 14-photon transition between α2 and β3 appears directly before the 9-photon transition between α1 and α2. These deformations suggest that the dominant reason for finding atoms in the α1 state comes from the transitions between α1 and α2 "before" and "after" the magnetic field reversal, while the overlap with transitions between α2 and β3 causes a reduction in the signal. Similarly, atoms in state α2 can only
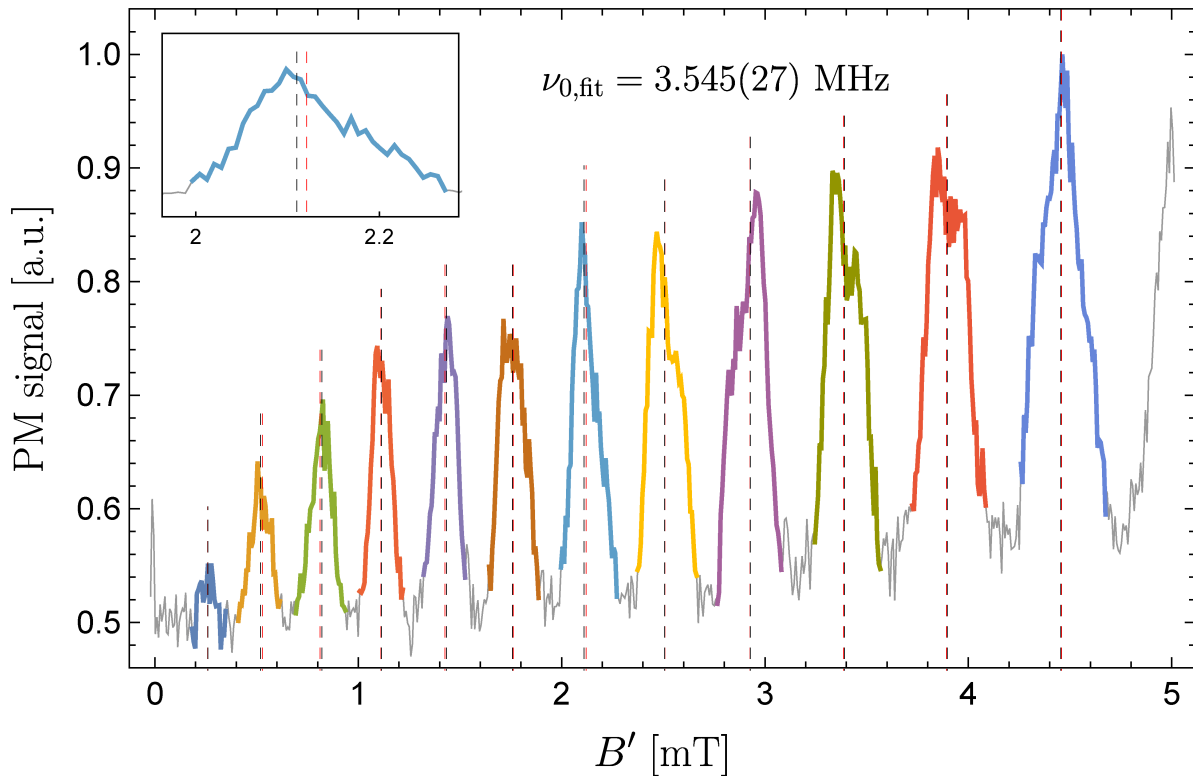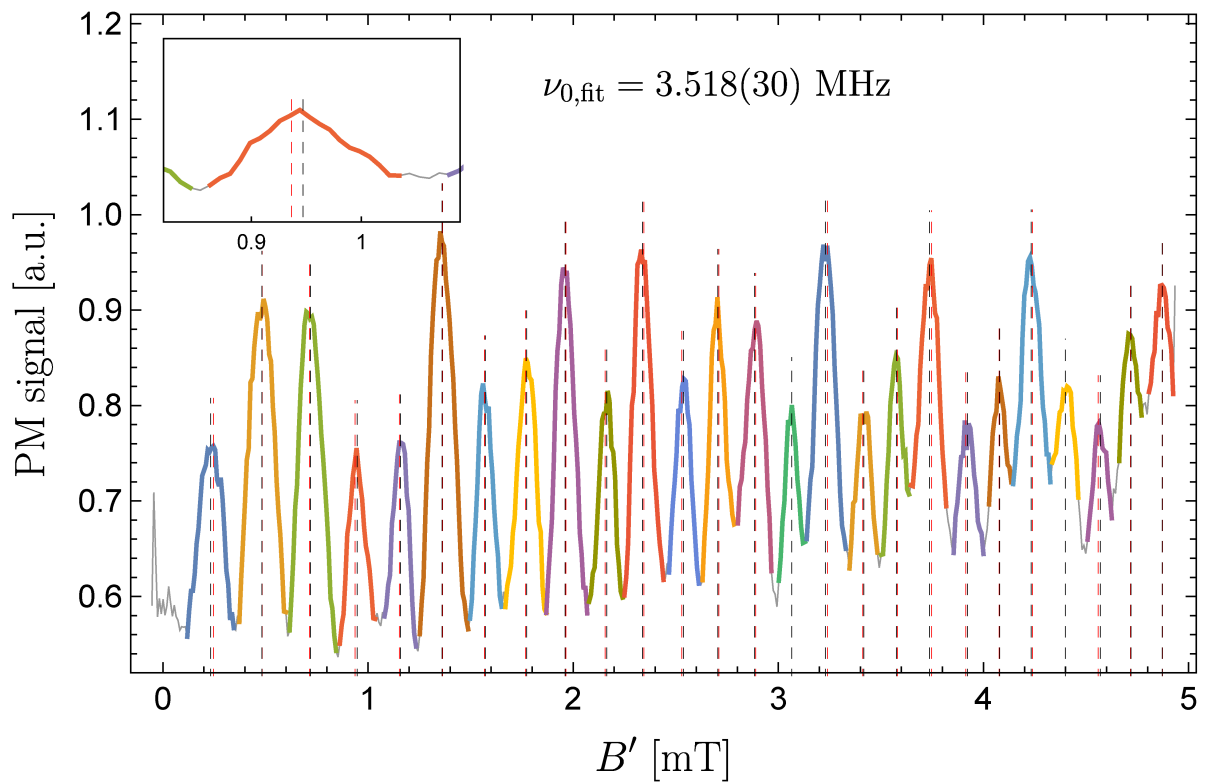
Figure 4.10.: Sona measurement as function of the magnetic field B'. The peak positions obtained from fits to the data (black dashed lines) and from Breit-Rabi calculations with the best fitting frequency for the second harmonic ($\nu = 3.545(27)\,\text{MHz}$) (red dashed lines) differ by less than $0.011\,\text{mT}$.

be observed (see Fig. 4.11), if atoms change from α1 to α2, "before" the reversal of the magnetic field, or if atoms change from β3 to α2 "after" the reversal. Again the peaks can be deformed, if transitions overlap, e.g. after a transition from β3 to α2, another transition from α2 to α1 would reduce the α2 population. These deformations seem to be less prominent. Although, these peak deformations change the position obtained by the fits, the calculated and measured peak positions are in good agreement. The Breit-Rabi calculations that were used here do not provide any quantitative information about the intensity of the peaks, but only about their position.

Figure 4.11.: Sona measurement as function of the magnetic field B'. The peak positions obtained from fits to the data (black dashed lines) and from Breit-Rabi calculations with the best fitting frequency for the second harmonic ($\nu = 3.518(30)\,\mathrm{MHz}$) (red dashed lines) differ by less than $0.014\,\mathrm{mT}$.

5. Conclusion and Outlook

A new Lamb-shift polarimeter for the molecular beam source in Novosibirsk has been
built at the research center Jülich. The most essential part of a Lamb-shift polarimeter
is the spin filter. Its two main components are a solenoid which needs to provide highly
homogeneous magnetic fields ranging between $53\,\text{mT}$ and $61\,\text{mT}$ and a cavity which
needs to provide an electromagnetic field with a resonance frequency of about $1.61\,\text{GHz}$
and a quality factor between 1000 and 3000. After carefully adjusting individual turns,
the solenoid provides magnetic fields with excellent homogeneity (see Fig. A.1). Since,
the required quality factor could not be achieved with the new cavity, an older one
which met the requirements (see Fig. 3.15) was used for the new polarimeter. For a
newly built cesium cell the magnetic fields at the center of the cell were measured for
different currents to obtain a magnetic field-to-current calibration (see Fig. 3.9). For
the restored Wienfilter such a calibration already existed (see Fig. 3.5). All components
were mounted on a bench such that transport as a whole was possible. After the transfer
to Novosibirsk only minor and uncritical damages were found.

In Novosibirsk the ionizer, which was built there, was mounted on the bench with the
other components of the Lamb-shift polarimeter and together they were connected to the
modifiable beam source. Polarization measurements of atomic beams from the atomic
beam source were carried out successfully (see Fig. 4.2), proving the functionality of
the new Lamb-shift polarimeter. An exemplary Wienfilter curve (see Fig. 3.6), which
is necessary for polarization measurements with atomic ions, and "zero-measurements"
for hydrogen and deuterium (see Figs. 4.3 and 4.5) from which the correction factors
of the spin filter are determined for precise absolute polarization measurements, were
recorded. During the first tests the ion beam intensity was too low to allow detection of
metastable atoms from hydrogen molecules from the prototype molecular beam source.
Further attempts to measure the polarization of the molecular beam were denied by the

schedule of the Vebb-3 accelerator, the unavailability of liquid helium[1] at BINP during summer and last but certainly not least the COVID-19 pandemic.

In the meantime the Lamb-shift polarimeter setup in Jülich was used to optimize the efficiency of the cesium cell when used with molecular ions. For the production of metastable atoms from protons absolute values of the production efficiency are available in literature [Pra+74]. The measurements, shown in Fig. 4.1, suggest that compared to proton beams, higher beam energies and higher cesium vapor densities are advantageous for H_2^+ ion beams. Absolute values of the metastable atoms production efficiency from H_2^+ ions can be obtained, if measurements with H_2^+ ions relative to protons can be made. Due to instabilities of the beam source, a direct comparison of measurements with proton and H_2^+ ion beams was not possible. Since the polarization measurement of molecules from the prototype molecular beam source failed because the rate of Lyman-α photons was too low, each improvement in sensitivity of the Lamb-shift polarimeter is highly desirable. To obtain more reliable measurements, which also allow for direct comparisons of proton beams and H_2^+ ion beams, a commercial ion source has been ordered. It should be capable to provide stable H_2^+/D_2^+ beams of up to $2\,\mu A$ at a kinetic energy of $1\,keV$ and up to $20\,\mu A$ at $5\,keV$ [Eng; Pan20].

Moreover, the Lamb-shift polarimeter in Jülich was modified to perform measurements with a Sona transition unit. The experiments showed that this setup can be used as a new spectroscopy method [Eng+20a]. When atoms are traveling through the static magnetic fields of the two Sona coils with opposite direction they experience an oscillating electromagnetic field. The frequency of this field is determined by the geometry of the setup and the atoms' velocity. Since these velocities can be several orders of magnitude lower than the speed of light, extremely low frequencies are possible without the need of a large cavity. With this setup the photon energy, with which transitions are induced in the atoms, was in the order of $10\,neV$. This enables high precision measurements of QED corrections of Breit-Rabi calculations. Absolute uncertainties in the order of $10^{-11}\,eV$ were already achieved and with further improvements a reduction by another order of magnitude is expected. While the measurements presented here were performed with hydrogen in the $2S_{1/2}$ state only, in principle, the method can be applied to all kinds of particle beams. With a different orientation of the magnetic field π-transitions can be induced, too. Thus, the method is not restricted to σ-transitions

---

[1]for cooling of the nozzle and superconducting magnets of the molecular beam source

either.

The measurements with the Sona setup showed that the expected complete exchange of the occupation numbers of the α1 and the β3 hyperfine states cannot be ensured with certainty, but depends very sensitive on external magnetic fields. Especially for the BoB experiment, in which extremely low rates of β3 compared to both α states are expected, the background caused by transitions would probably prevent a reliable detection of β3. In order to find a different approach for the detection of β3 atoms for the BoB experiment, considerations were made to design a spin filter that can separate not only the α states but also the β states. Since, as mentioned in Sect. 2.4.4, it is not necessary to operate the spin filter at the magnetic fields of the intersections between the β and the e states, significantly lower magnetic fields and frequencies can also be used. At low magnetic fields and without static electric fields, the lifetime of the β states is significantly longer (see Figs. 2.10 and 2.11). If the α states are coupled to the e states in the same fashion as with the current version of the spin filter, the β states can pass the spin filter. This would cause a signal, which is independent of the magnetic field. If, however, a second radio frequency is introduced, the β states can also be coupled to $2P_{1/2}$ states. By choosing suitable frequencies and orientations of the electromagnetic field (electric field parallel or perpendicular to quantization axis (= beam axis)) for the couplings between the $2S_{1/2}$ and $2P_{1/2}$ states, the resonance conditions, which allow the states to pass the spin filter will occur at different magnetic fields. In Tab. 5.1 the couplings between $2S_{1/2}$ and $2P_{1/2}$ substates of hydrogen for the two possible orientations of the electric component of the electromagnetic field in respect to the quantization axis are shown. A Breit-Rabi diagram of hydrogen, with some exemplary transition frequencies is shown in Fig. 5.1. By choosing two electromagnetic fields, one with $\boldsymbol{E} \perp z$ and

Table 5.1.: Coupling of $2S_{1/2}$ and $2P_{1/2}$ substates of hydrogen with the electric component of the electromagnetic field being either parallel ($\parallel$) or perpendicular ($\perp$) to the quantization axis.

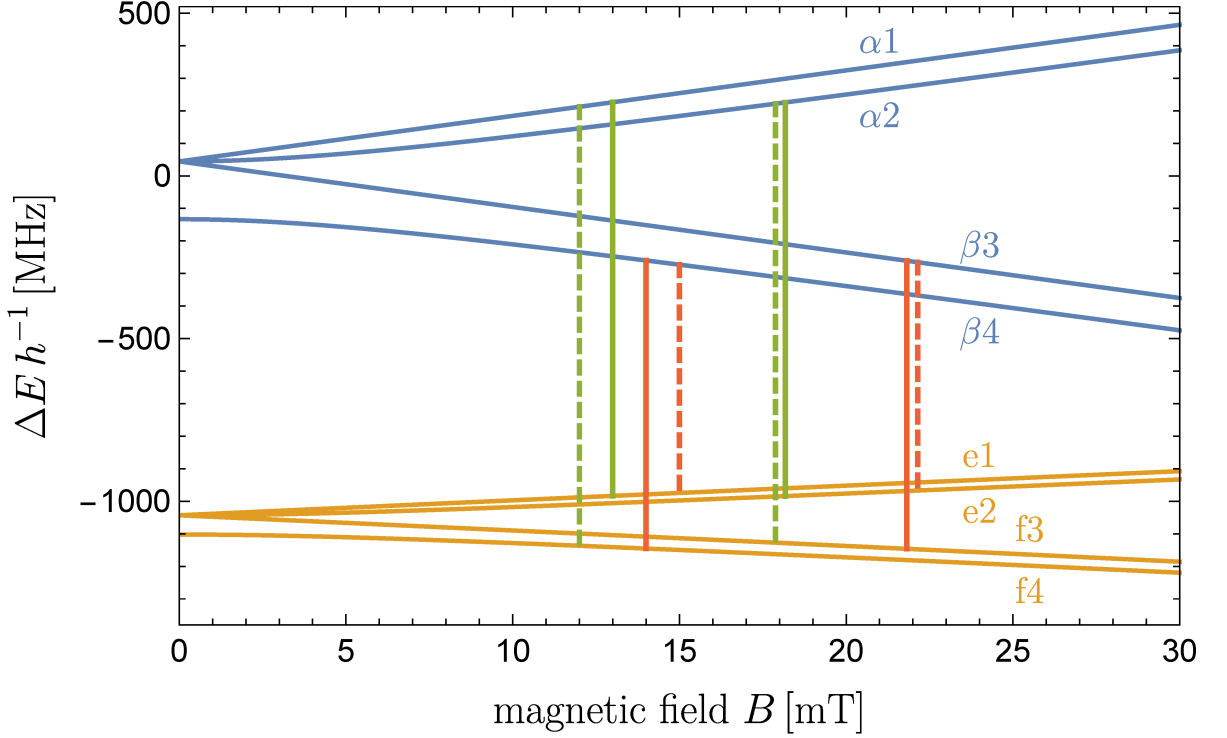| $\parallel$	$\perp$
α1 ↔ e1	α1 ↔ f4
α2 ↔ e2	α2 ↔ f3
β3 ↔ f3	β3 ↔ e2
β4 ↔ f4	β4 ↔ e1

Figure 5.1.: Breit-Rabi diagram of hydrogen for a new type of spin filter. Two couplings between the α states are marked in green: one for $\boldsymbol{E} \perp z$ at $B_{\alpha 1} = 12\,\text{mT}$ and $B_{\alpha 2} \approx 17.9\,\text{mT}$ with a frequency $\nu_1 \approx 1348.9\,\text{MHz}$ (dashed) and one for $\boldsymbol{E} \parallel z$ at $B_{\alpha 1} = 13\,\text{mT}$ and $B_{\alpha 2} \approx 18.2\,\text{mT}$ with a frequency $\nu_2 \approx 1209.7\,\text{MHz}$ (solid). Two couplings between the β states are marked in red: one for $\boldsymbol{E} \parallel z$ at $B_{\beta 4} = 14\,\text{mT}$ and $B_{\beta 3} \approx 21.8\,\text{mT}$ with a frequency $\nu_3 \approx 885.3\,\text{MHz}$ (solid) and one for $\boldsymbol{E} \perp z$ at $B_{\beta 4} = 15\,\text{mT}$ and $B_{\beta 3} \approx 22.1\,\text{mT}$ with a frequency $\nu_4 \approx 701.5\,\text{MHz}$ (dashed).

$\nu = 1348.9\,\text{MHz}$, and one with $\boldsymbol{E} \parallel z$ and $\nu = 885.3\,\text{MHz}$, four peaks should be observable at $B_{\alpha 1} \approx 12\,\text{mT}$, $B_{\beta 4} \approx 14\,\text{mT}$, $B_{\alpha 2} \approx 17.9\,\text{mT}$, and $B_{\beta 3} \approx 21.8\,\text{mT}$. A spin filter which is capable of detecting β states additionally to the α states could be used not only in the BoB experiment, but also in further experiments with the Sona transition unit. With a new detection method, which utilizes a MCP (see Sect. 2.4.5), the sensitivity of Lamb-shift polarimeters could potentially be increased by one to two orders of magnitude. In particular, it must be examined whether ground state atoms will create a substantial background signal or not. A background signal from ions should be easy to prevent by deflecting them. Such a detector is currently developed and tested in Munich in context of the BoB experiment. If the tests are successful, the new detector would

also be a great improvement for measurements with the molecular beam source at BINP. During the measurements with the atomic beam source at BINP an unexpected high background was observed which could be traced back to Lyman-α radiation, created in the dissociator of the source. This intense Lyman-α radiation had not jet been considered in recombination experiments and storage cell gas targets. With an energy of about 10.2 eV Lyman-α photons can break up molecular bounds between hydrogen atoms and atoms of the storage cell surface (e.g. carbon), allowing neighboring hydrogen atoms to recombine [Sie+10]. So far, the Eley-Rideal and Langmuir-Hinschelwood mechanisms have been used to explain the recombination in storage cells. The light induced recombination, however, might explain why lower recombination rates have been observed with aluminum and teflon surfaces: Both materials absorb Lyman-α poorly, so that the photon energy cannot contribute well to breaking the molecular bonds. In order to gain further insights, it is planned to (periodically) block the incidence of Lyman-α photons into the storage cell of the recombination experiment setup and measure the presumed change of the recombination rate. The findings may influence the future choice of storage cell materials to either increase or reduce the recombination rate depending on the application.

With this recombination setup it is also planed to freeze out polarized D_2 and HD molecules in order to find out whether the polarization is conserved during the process. For this the molecules could either be evaporated again to build a beam that can be measured with the Lamb-shift polarimeter or the polarization of the solid could be measured directly using nuclear magnetic resonance methods. Currently a chamber for the freezing of the molecules is being designed in a collaboration of the PGI and IKP in Jülich, and the Laboratory of Cryogenic and Superconductive Techniques at the Petersburg Nuclear Physics Institute. Solid, polarized D_2, HD, and TD could then be used as fuel for polarized fusion, polarized external targets in accelerator experiments and as proton-/deuteron- source for laser-driven acceleration of protons and deuterons [Ciu+16]. The planed, dedicated molecular beam source should increase the production rate of these polarized solids. The Lamb-shift polarimeter at BINP will hopefully help to make the development of this source a success.

Bibliography

[Alt+00]   M. Altmeier et al. "Excitation Functions of the Analyzing Power in $p\,\overrightarrow{p}$ Scattering from 0.45 to 2.5 GeV". In: *Physical Review Letters* 85.9 (Aug. 2000), pp. 1819–1822. DOI: `10.1103/physrevlett.85.1819`.

[Bel13]   A. S. Belov. "Polarized ion sources: Status and perspectives". In: *Physics of Particles and Nuclei* 44.6 (Nov. 2013), pp. 873–877. DOI: `10.1134/s1063779613060038`.

[BH98]   B. Braun and HERMES Collaboration. "The HERMES polarimeter". In: vol. 421. API Conference Proceedings. AIP, 1998, p. 156. DOI: `10.1063/1.54998`.

[Boh13]   N. Bohr. "I. On the constitution of atoms and molecules". In: *The London, Edinburgh, and Dublin Philosophical Magazine and Journal of Science* 26.151 (July 1913), pp. 1–25. DOI: `10.1080/14786441308634955`.

[BR31]   G. Breit and I. I. Rabi. "Measurement of Nuclear Spin". In: *Physical Review* 38.11 (Dec. 1931), pp. 2082–2083. DOI: `10.1103/physrev.38.2082.2`.

[Bro24]   Louis De Broglie. "Recherches sur la théorie des Quanta". Theses. Migration - université en cours d'affectation, Nov. 1924. URL: `https://tel.archives-ouvertes.fr/tel-00006807`.

[Bro28]   Robert Brown. "XXVII. A brief account of microscopical observations made in the months of June, July and August 1827, on the particles contained in the pollen of plants, and on the general existence of active molecules in organic and inorganic bodies". In: *The Philosophical Magazine* 4.21 (Sept. 1828), pp. 161–173. DOI: `10.1080/14786442808674769`.

[CFS56]   G. Clausnitzer, R. Fleischmann, and H. Schopper. "Erzeugung eines Wasser-
            stoffatomstrahles mit gleichgerichteten Kernspins". In: *Zeitschrift für Physik*
            144.4 (Aug. 1956), pp. 336–342. DOI: `10.1007/bf01340806`.

[Ciu+11]   G Ciullo et al. "The polarised internal target for the PAX experiment".
            In: *Journal of Physics: Conference Series* 295 (May 2011), p. 012150. DOI:
            `10.1088/1742-6596/295/1/012150`.

[Ciu+16]   Giuseppe Ciullo et al. *Nuclear Fusion with Polarized Fuel*. Springer Inter-
            national Publishing, 2016. DOI: `10.1007/978-3-319-39471-8`.

[Don+64]   Bailey L. Donnally et al. "Metastable Hydrogen Atoms Produced in Charge
            Exchange". In: *Physical Review Letters* 12.18 (May 1964), pp. 502–503. DOI:
            `10.1103/physrevlett.12.502`.

[Eng]   R. Engels. private communication.

[Eng+02]   R. Engels et al. "A Lamb-shift polarimeter for the polarized target at
            ANKE". In: *Polarized Sources and Targets*. World Scientific, May 2002.
            DOI: `10.1142/9789812777683_0008`.

[Eng+03]   R. Engels et al. "Precision Lamb-shift polarimeter for polarized atomic
            and ion beams". In: *Review of Scientific Instruments* 74.11 (Nov. 2003),
            pp. 4607–4615. DOI: `10.1063/1.1619550`.

[Eng+05]   R. Engels et al. "Background reduction by a getter pump around the ioniza-
            tion volume of a Lamb-shift polarimeter and possible improvements of po-
            larized ion sources". In: *Review of Scientific Instruments* 76.5 (May 2005),
            p. 053305. DOI: `10.1063/1.1898923`.

[Eng+14]   Ralf Engels et al. "Measurement of the nuclear polarization of hydrogen
            and deuterium molecules using a Lamb-shift polarimeter". In: *Review of
            Scientific Instruments* 85.10 (Oct. 2014), p. 103505. DOI: `10.1063/1.
            4897479`.

[Eng+15]   R. Engels et al. "Production of Hyperpolarized H_2 Molecules from $\vec{H}$ Atoms
            in Gas-Storage Cells". In: *Physical Review Letters* 115.11 (Sept. 2015). DOI:
            `10.1103/physrevlett.115.113007`.

[Eng+20a]   R. Engels et al. "Exploiting the Planck-Einstein Relation". In: (Oct. 26,
            2020). arXiv: `2010.13690v1` `[physics.atom-ph]`.

[Eng+20b] R. Engels et al. "Production of HD Molecules in Definite Hyperfine Substates". In: *Physical Review Letters* 124.11 (Mar. 2020). DOI: 10.1103/physrevlett.124.113003.

[Eng02] Ralf Engels. "Entwicklung eines universellen Lambshift-Polarimeters für polarisierte Atomstrahltargets wie an ANKE/COSY". German. PhD thesis. Univ. Köln, Feb. 15, 2002. URL: https://juser.fz-juelich.de/record/23573.

[Fel+13] O. Felden et al. "Negative ion source development at the cooler synchrotron COSY/Jülich". In: AIP, 2013. DOI: 10.1063/1.4792800.

[Fey48] R. P. Feynman. "Space-Time Approach to Non-Relativistic Quantum Mechanics". In: *Reviews of Modern Physics* 20.2 (Apr. 1948), pp. 367–387. DOI: 10.1103/revmodphys.20.367.

[FS33] R. Frisch and O. Stern. "Über die magnetische Ablenkung von Wasserstoffmolekülen und das magnetische Moment des Protons. I". In: *Zeitschrift für Physik* 85.1-2 (Jan. 1933), pp. 4–16. DOI: 10.1007/bf01330773.

[Gar58] R. L. Garwin. "Production of Beams of Polarized Protons by the Acceleration of Protons Derived from Polarized Hydrogen Molecules". In: *Review of Scientific Instruments* 29.5 (May 1958), pp. 374–376. DOI: 10.1063/1.1716200.

[Gla68] H.F. Glavish. "A strong field ionizer for an atomic beam polarized ion source". In: *Nuclear Instruments and Methods* 65.1 (Oct. 1968), pp. 1–7. DOI: 10.1016/0029-554x(68)90002-5.

[GS22] Walther Gerlach and Otto Stern. "Der experimentelle Nachweis der Richtungsquantelung im Magnetfeld". In: *Zeitschrift für Physik* 9.1 (Dec. 1922), pp. 349–352. DOI: 10.1007/bf01326983.

[GS81] Frank Garisto and B. C. Sanctuary. "Spin transitions in time-dependent magnetic fields". In: *Physical Review A* 23.3 (Mar. 1981), pp. 1234–1242. DOI: 10.1103/physreva.23.1234.

[Hae67] W Haeberli. "Sources of Polarized Ions". In: *Annual Review of Nuclear Science* 17.1 (Dec. 1967), pp. 373–426. DOI: 10.1146/annurev.ns.17.120167.002105.

[Hou37]   W. V. Houston. "A New Method of Analysis of the Structure of Hα and Dα". In: *Physical Review* 51.6 (Mar. 1937), pp. 446–449. DOI: 10.1103/physrev.51.446.

[HR00]   F. Hinterberger and H. Rohdjeß. "Proton-proton elastic scattering excitation functions at intermediate energies: Cross sections and analyzing powers". In: *Nuclear Physics A* 663-664 (Jan. 2000), pp. 533c–536c. DOI: 10.1016/s0375-9474(99)00649-1.

[HR78]   R. D. Hight and R. T. Robiscoe. "Nonadiabatic transition in $n = 2$ atomic hydrogen". In: *Physical Review A* 17.2 (Feb. 1978), pp. 561–565. DOI: 10.1103/physreva.17.561.

[HRT77]   R. D. Hight, R. T. Robiscoe, and W. R. Thorson. "Nonadiabatic spin transitions in an inhomogeneous magnetic field". In: *Physical Review A* 15.3 (Mar. 1977), pp. 1079–1087. DOI: 10.1103/physreva.15.1079.

[Isa+98]   L.G. Isaeva et al. "High field superconducting sextupole magnets". In: *Nuclear Instruments and Methods in Physics Research Section A: Accelerators, Spectrometers, Detectors and Associated Equipment* 411.2-3 (July 1998), pp. 201–204. DOI: 10.1016/s0168-9002(98)00352-0.

[Kan+19]   Chr. Kannis et al. "A new type of laser-induced polarized proton source". en. In: (2019). DOI: 10.13140/RG.2.2.35007.02720.

[Lam52]   Willis E. Lamb. "Fine Structure of the Hydrogen Atom. III". In: *Physical Review* 85.2 (Jan. 1952), pp. 259–276. DOI: 10.1103/physrev.85.259.

[Lem+93]   S.K. Lemieux et al. "A spin-filter polarimeter for low energy hydrogen and deuterium ion beams". In: *Nuclear Instruments and Methods in Physics Research Section A: Accelerators, Spectrometers, Detectors and Associated Equipment* 333.2-3 (Sept. 1993), pp. 434–442. DOI: 10.1016/0168-9002(93)91188-s.

[Lor99]   H. A. Lorentz. "Considerations Concerning the Influence of a Magnetic Field on the Radiation of Light". In: *The Astrophysical Journal* 9 (Jan. 1899), p. 37. DOI: 10.1086/140547.

[LR47]   Willis E. Lamb and Robert C. Retherford. "Fine Structure of the Hydrogen Atom by a Microwave Method". In: *Physical Review* 72.3 (Aug. 1947), pp. 241–243. DOI: 10.1103/physrev.72.241.

[LR50]   Willis E. Lamb and Robert C. Retherford. "Fine Structure of the Hydrogen Atom. Part I". In: *Physical Review* 79.4 (Aug. 1950), pp. 549–572. DOI: 10.1103/physrev.79.549.

[LR51]   Willis E. Lamb and Robert C. Retherford. "Fine Structure of the Hydrogen Atom. Part II". In: *Physical Review* 81.2 (Jan. 1951), pp. 222–232. DOI: 10.1103/physrev.81.222.

[MG86]   H. Meinke and Friedrich-Wilhelm Gundlach. *Taschenbuch der Hochfrequenztechnik*. Ed. by Klaus Lange and Karl-Heinz Löcherer. Springer Berlin Heidelberg, 1986. DOI: 10.1007/978-3-642-96894-5.

[MLO68]   Joseph L. McKibben, George P. Lawrence, and Gerald G. Ohlsen. "Nuclear Spin Filter". In: *Physical Review Letters* 20.21 (May 1968), pp. 1180–1182. DOI: 10.1103/physrevlett.20.1180.

[MM87]   A.A. Michelson and E.W. Morley. "On a Mehtod of making the Wavelemgth of Sodium Light the actual and practical standard of length". In: *The American Journal of Science*. 3rd ser. 34 (1887), p. 427. URL: https://archive.org/details/americanjourna3341887newh/page/427/mode/2up.

[MO59]   L. Madansky and G. E. Owen. "Production of Polarized Proton Beams". In: *Physical Review Letters* 2.5 (Mar. 1959), pp. 209–211. DOI: 10.1103/physrevlett.2.209.

[MS06]   D. L. Moskovkin and V. M. Shabaev. "Zeeman effect of the hyperfine-structure levels in hydrogenlike ions". In: *Physical Review A* 73.5 (May 2006). DOI: 10.1103/physreva.73.052506.

[Nem80]   L L Nemenov. "Decay of the neutron into a hydrogen atom and an antineutrino". In: *Sov. J. Nucl. Phys. (Engl. Transl.); (United States)* 31:1 (Jan. 1980). URL: https://www.osti.gov/biblio/6780445.

[NIS94]   NIST. *Standard Reference Database 121*. 1994. URL: https://physics.nist.gov/cuu/Constants/index.html (visited on 03/25/2020).

[NO80]   L Nemenov and A Ovchinnikova. "Effects of scalar and tensor interactions on the atomic decay of the neutron, n→H+$\overline{\nu}$". In: *Soviet Journal of Nuclear Physics* 5 (1980), pp. 659–660.

[Pan20] Pantechnik. *OFFER: M100 ECRIS system*. Ed. by Matthieu Cavellier. Aug. 4, 2020.

[Pas38] Simon Pasternack. "Note on the Fine Structure of Hα and Dα". In: *Physical Review* 54.12 (Dec. 1938), pp. 1113–1113. DOI: 10.1103/physrev.54.1113.

[PB21] F. Paschen and E. Back. "Liniengruppen magnetisch vervollständigt". In: *Physica* 1 (1921), pp. 261–273.

[Pra+74] P. Pradel et al. "Formation ofH(n=2)atoms by the nearly resonant processH+in Cs. Multiple collision processes". In: *Physical Review A* 10.3 (Sept. 1974), pp. 797–812. DOI: 10.1103/physreva.10.797.

[PT27] T. E. Phipps and J. B. Taylor. "The Magnetic Moment of the Hydrogen Atom". In: *Physical Review* 29.2 (Feb. 1927), pp. 309–320. DOI: 10.1103/physrev.29.309.

[Ram52] Norman F. Ramsey. "Theory of Molecular Hydrogen and Deuterium in Magnetic Fields". In: *Physical Review* 85 (1 Jan. 1952), pp. 60–65. DOI: 10.1103/PhysRev.85.60. URL: https://link.aps.org/doi/10.1103/PhysRev.85.60.

[Rut11] E. Rutherford. "LXXIX. The scattering of α and β particles by matter and the structure of the atom". In: *The London, Edinburgh, and Dublin Philosophical Magazine and Journal of Science* 21.125 (May 1911), pp. 669–688. DOI: 10.1080/14786440508637080.

[Sch+06] W. Schott et al. "An experiment for the measurement of the bound- β-decay of the free neutron". In: *The European Physical Journal A* 30.3 (Dec. 2006), pp. 603–611. DOI: 10.1140/epja/i2006-10136-3.

[Sch+19] Wolfgang Schott et al. "Towards a first measurement of the free neutron bound beta decay detecting hydrogen atoms at a throughgoing beamtube in a high flux reactor". In: *EPJ Web of Conferences* 219 (2019). Ed. by T. Jenke et al., p. 04006. DOI: 10.1051/epjconf/201921904006.

[Sch+99] C. Schwob et al. "Optical Frequency Measurement of the2S-12DTransitions in Hydrogen and Deuterium: Rydberg Constant and Lamb Shift Determinations". In: *Physical Review Letters* 82.25 (June 1999), pp. 4960–4963. DOI: 10.1103/physrevlett.82.4960.

[Sch26]   E. Schrödinger. "Quantisierung als Eigenwertproblem". In: *Annalen der Physik* 385.13 (1926), pp. 437–490. DOI: 10.1002/andp.19263851302.

[She+19]   Yu. V. Shestakov et al. "Nuclear-Polarized Hydrogen/Deuterium Molecular Source". In: *Physics of Particles and Nuclei* 50.5 (Sept. 2019), pp. 513–519. DOI: 10.1134/s1063779619050204.

[She+98]   Yu. V. Shestakov et al. In: *13th Intern. Symosion on High Energy Spin Phys.* 13th Intern. Symp. on High Energy Spin Phys. (1998). 13. Protvino, Russia, 1998, p. 415.

[Sie+10]   B. Siemer et al. "Desorption of H atoms from graphite (0001) using XUV free electron laser pulses". In: *Chemical Physics Letters* 500.4-6 (Nov. 2010), pp. 291–294. DOI: 10.1016/j.cplett.2010.10.040.

[Som16]   A. Sommerfeld. "Zur Quantentheorie der Spektrallinien". In: *Annalen der Physik* 356.17 (1916), pp. 1–94. DOI: 10.1002/andp.19163561702.

[Son67]   P. G. Sona. In: *Energia Nucleare* 14 (1967), p. 295.

[Tho97]   J. J. Thomson. "XL. Cathode Rays". In: *The London, Edinburgh, and Dublin Philosophical Magazine and Journal of Science* 44.269 (Oct. 1897), pp. 293–316. DOI: 10.1080/14786449708621070.

[TL37]   John Bradshaw Taylor and Irving Langmuir. "Vapor Pressure of Caesium by the Positive Ion Method". In: *Physical Review* 51.9 (May 1937), pp. 753–760. DOI: 10.1103/physrev.51.753.

[Top+17]   D.K. Toporkov et al. "Source of polarized hydrogen molecules". In: *Nuclear Instruments and Methods in Physics Research Section A: Accelerators, Spectrometers, Detectors and Associated Equipment* 868 (Oct. 2017), pp. 15–18. DOI: 10.1016/j.nima.2017.06.038.

[TS]   D. K. Toporkov and Yu. V. Shestakov. private communication.

[UG26]   G. E. Uhlenbeck and S. Goudsmit. "Spinning Electrons and the Structure of Spectra". In: *Nature* 117.2938 (Feb. 1926), pp. 264–265. DOI: 10.1038/117264a0.

[Wie98]   Willy Wien. "Untersuchungen über die electrische Entladung in verdünnten Gasen". In: *Annalen der Physik* 301.6 (1898), pp. 440–452. DOI: 10.1002/andp.18983010618.

[Wig97]   E. P. Wigner. "Über die paramagnetische Umwandlung von Para-Ortho-wasserstoff. III". In: *Part I: Physical Chemistry. Part II: Solid State Physics.* Springer Berlin Heidelberg, 1997, pp. 126–130. DOI: `10.1007/978-3-642-59033-7_11`.

[Wil38]   Robley C. Williams. "The Fine Structures ofHα and Dα Under Varying Discharge Conditions". In: *Physical Review* 54.8 (Oct. 1938), pp. 558–567. DOI: `10.1103/physrev.54.558`.

[Yur+17]   A V Yurchenko et al. "Design of magnetic system to produce intense beam of polarized molecules of H2and D2". In: *Journal of Physics: Conference Series* 938 (Dec. 2017), p. 012023. DOI: `10.1088/1742-6596/938/1/012023`.

[Zee97]   P. Zeemann. "The Effect of Magnetisation on the Nature of Light Emitted by a Substance". In: *Nature* 55.1424 (Feb. 1897), pp. 347–347. DOI: `10.1038/055347a0`.

[Zel+02]   A. Zelenski et al. "Optically pumped polarized H- ion source for RHIC spin physics". In: *Review of Scientific Instruments* 73.2 (Feb. 2002), pp. 888–891. DOI: `10.1063/1.1427669`.

[Zel+05]   A. Zelenski et al. "Absolute polarized H-jet polarimeter development, for RHIC". In: *Nuclear Instruments and Methods in Physics Research Section A: Accelerators, Spectrometers, Detectors and Associated Equipment* 536.3 (Jan. 2005), pp. 248–254. DOI: `10.1016/j.nima.2004.08.080`.

[Zyl+20]   P. A. Zyla et al. "Review of Particle Physics". In: *Progress of Theoretical and Experimental Physics* 2020.8 (Aug. 2020). DOI: `10.1093/ptep/ptaa104`.

A. Appendix

A.1. Magnetic field homogeneity of spin filter
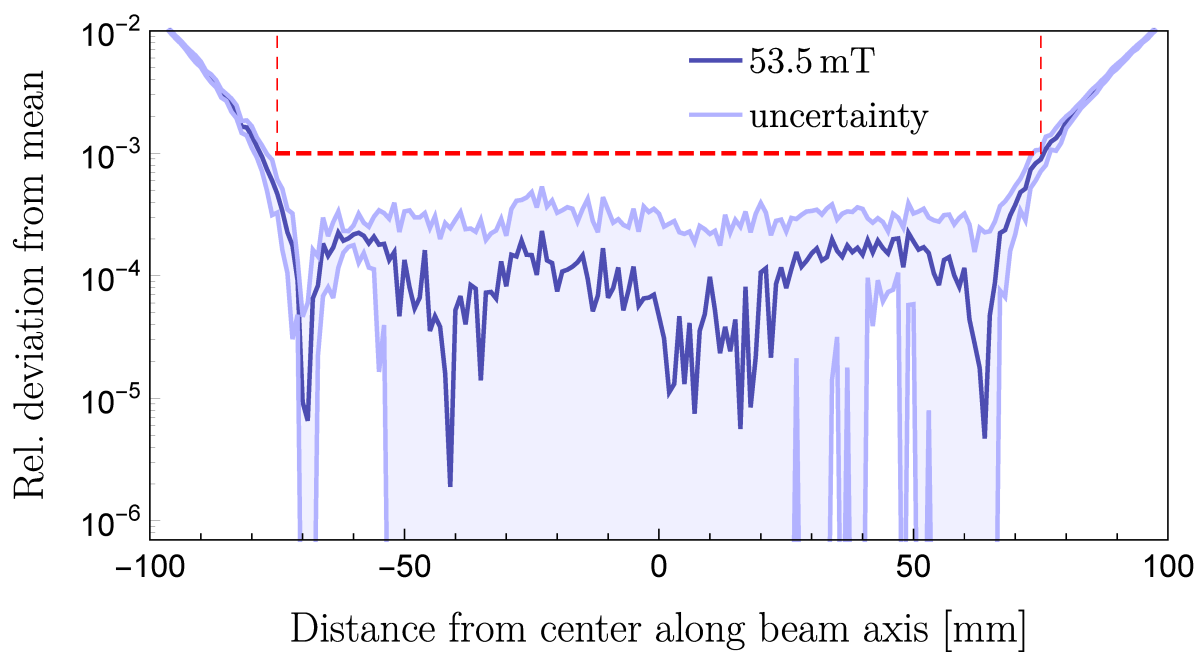
(a) At the magnetic field corresponding to α1 of hydrogen.
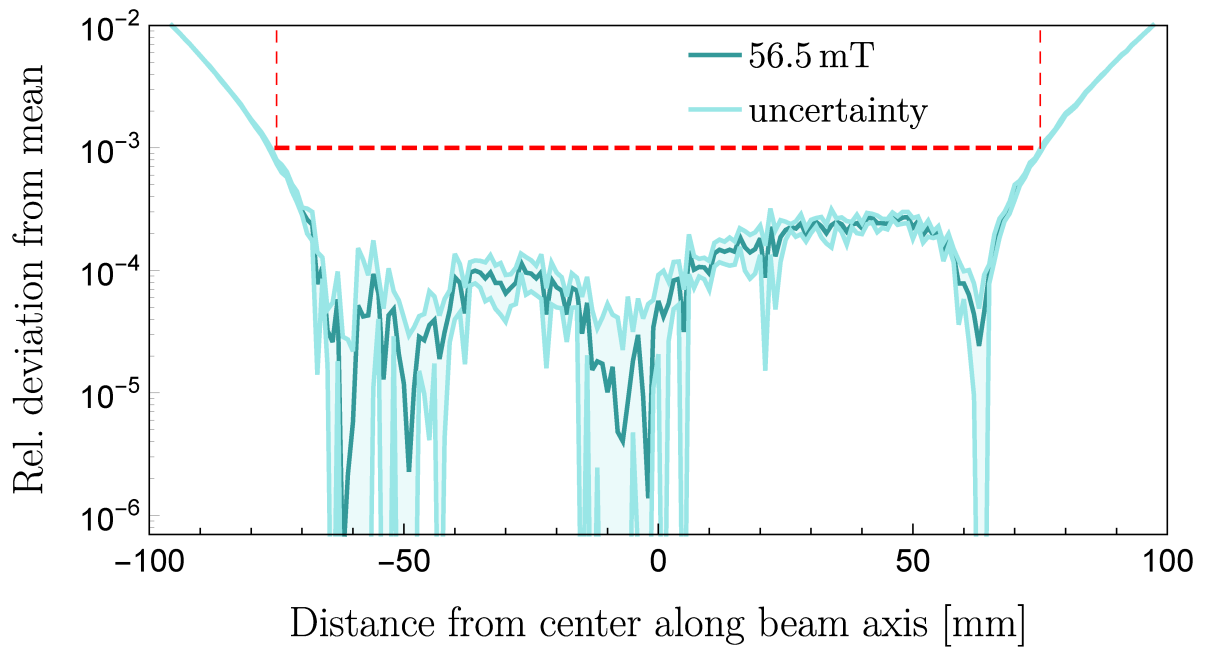
(b) At the magnetic field corresponding to α1 of deuterium.
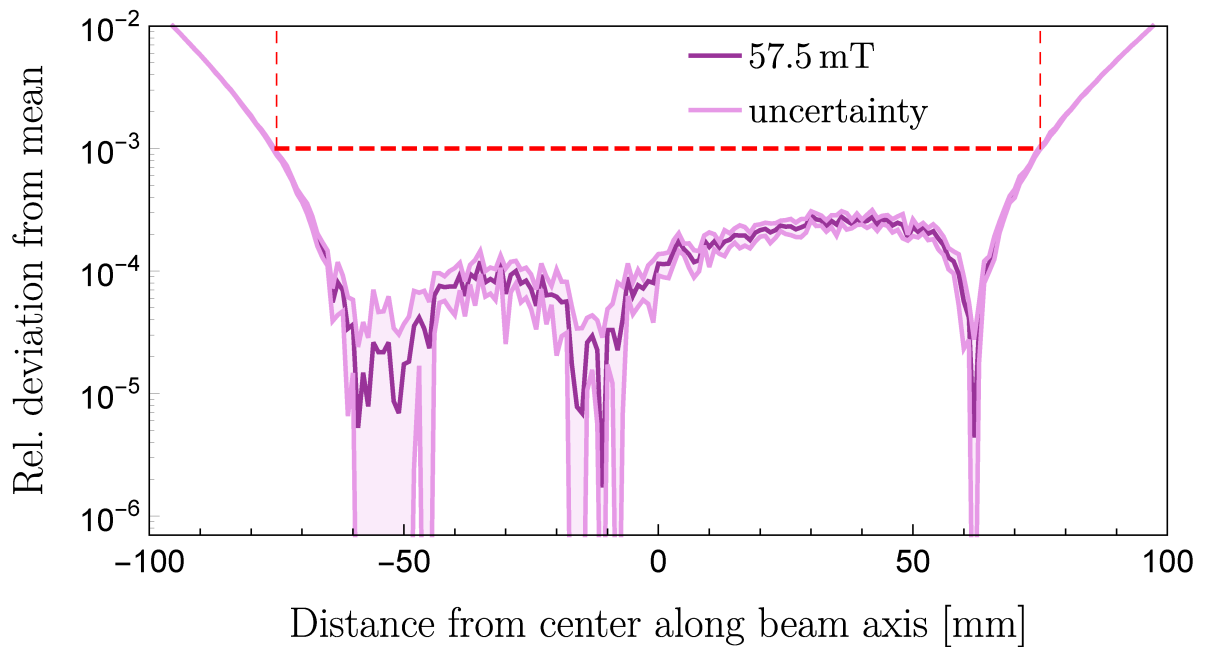
(c) At the magnetic field corresponding to α2 of deuterium.
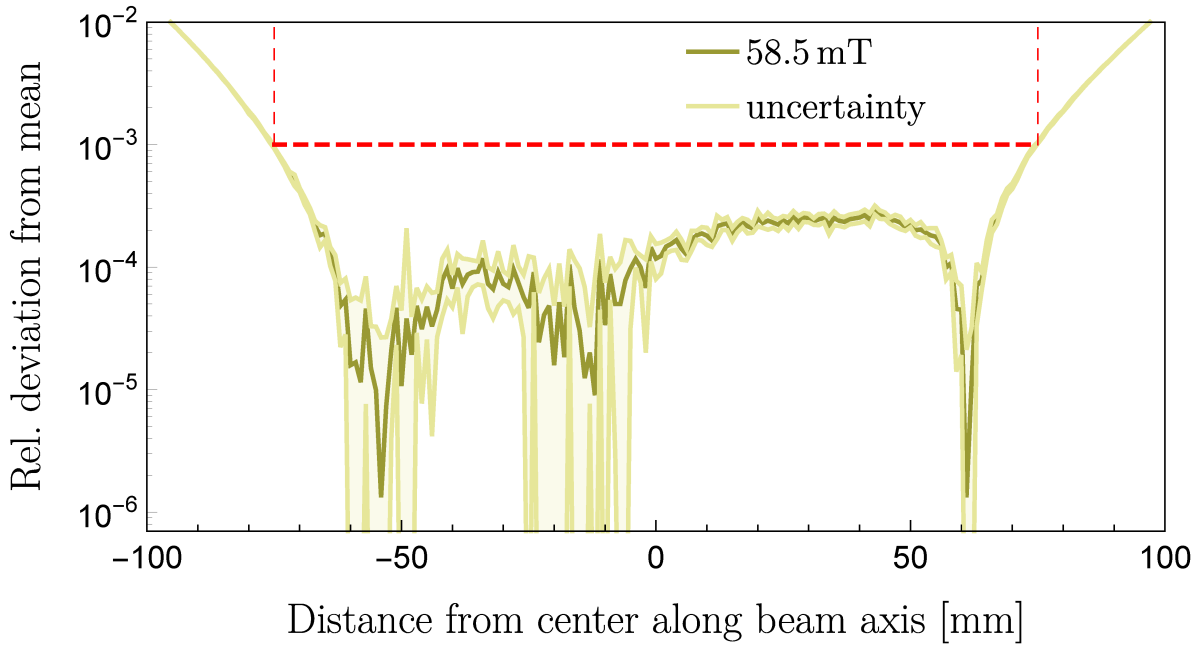
(d) At the magnetic field corresponding to α3 of deuterium.
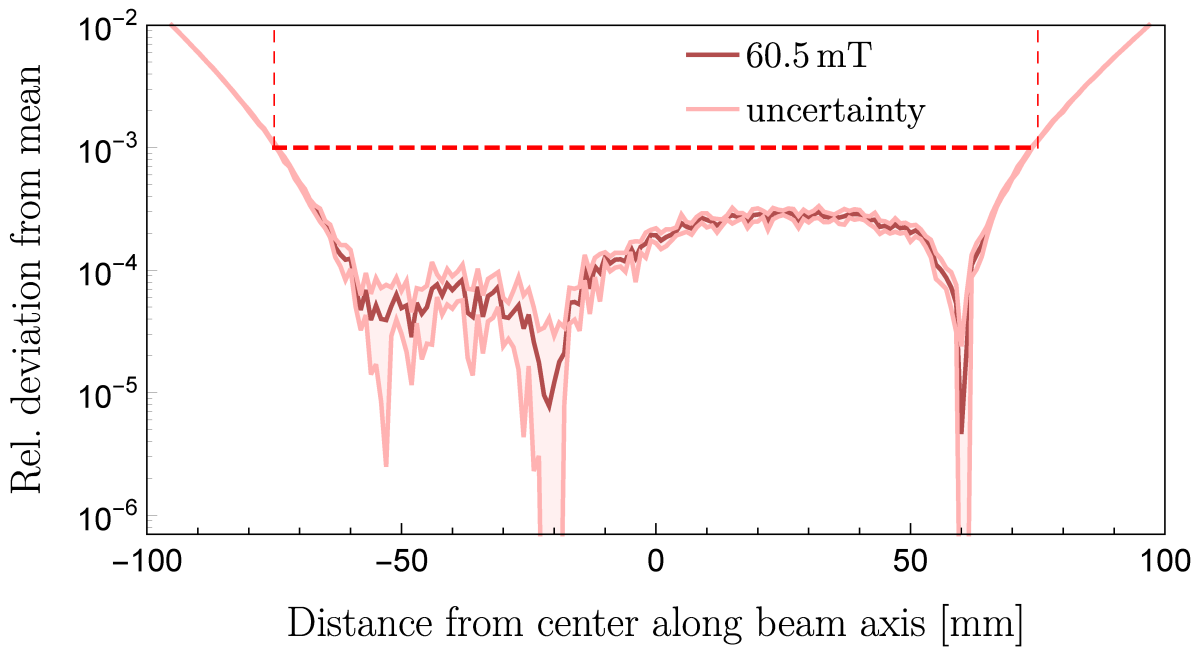
(e) At the magnetic field corresponding to α2 of hydrogen.

Figure A.1.: Magnetic field homogeneity of spin filter at different mean magnetic fields.

Acknowledgments

Last but not least, I would like to express my greatest gratitude to my whole family. Laura, in all the ups and downs that this thesis brought with it, you were the greatest emotional support I could ever imagine. Thank you for enduring this grumpy guy I have often been in this last pandemic and thesis-writing dominated months. I am so unbelievably happy to be married to such an empathetic, cheerful and overall wonderful woman. I love you!

Mum and Dad, you are great parents and huge role models for me as a future father. Thank you for all your love and support throughout my life.